New Materials and Device Designs for Organic Light-Emitting Diodes

by

Barry Patrick O'Brien

A Dissertation Presented in Partial Fulfillment
of the Requirements for the Degree
Doctor of Philosophy

Approved April 2017 by the
Graduate Supervisory Committee:

Jian Li, Chair
James Adams
Terry Alford

ARIZONA STATE UNIVERSITY

May 2017

ABSTRACT

Research and development of organic materials and devices for electronic applications has become an increasingly active area. Display and solid-state lighting are the most mature applications and, and products have been commercially available for several years as of this writing. Significant efforts also focus on materials for organic photovoltaic applications. Some of the newest work is in devices for medical, sensor and prosthetic applications.

Worldwide energy demand is increasing as the population grows and the standard of living in developing countries improves. Some studies estimate as much as 20% of annual energy usage is consumed by lighting. Improvements are being made in lightweight, flexible, rugged panels that use organic light emitting diodes (OLEDs), which are particularly useful in developing regions with limited energy availability and harsh environments.

Displays also benefit from more efficient materials as well as the lighter weight and ruggedness enabled by flexible substrates. Displays may require different emission characteristics compared with solid-state lighting. Some display technologies use a white OLED (WOLED) backlight with a color filter, but these are more complex and less efficient than displays that use separate emissive materials that produce the saturated colors needed to reproduce the entire color gamut. Saturated colors require narrow-band emitters. Full-color OLED displays up to and including television size are now commercially available from several suppliers, but research continues to develop more efficient and more stable materials.

This research program investigates several topics relevant to solid-state lighting and display applications. One project is development of a device structure to optimize performance of a new stable Pt-based red emitter developed in Prof Jian Li's group. Another project investigates new Pt-based red, green and blue emitters for lighting applications and compares a red/blue structure with a red/green/blue structure to produce light with high color rendering index. Another part of this work describes the fabrication of a 14.7" diagonal full color active-matrix OLED display on plastic substrate. The backplanes were designed and fabricated in the ASU Flexible Display Center and required significant engineering to develop; a discussion of that process is also included.

To my family

ACKNOWLEDGEMENTS

Most of the research detailed in this dissertation was conducted in Professor Jian Li's Applied Advanced Materials Lab and would not have been possible without his support. Numerous past and present members of the AAML provided invaluable training and assistance, most notably Dr. Tyler Fleetham, Kody Klimes, and Dr. Jeremy Ecton. All errors in this document are the responsibility of the writer.

Professors James Adams and Terry Alford served on my committee, but most importantly, they provided the encouragement needed to convince an old dog to learn some new tricks.

Active-matrix displays require thin-film transistor arrays, and the fabrication could not have been accomplished without the team of experienced engineers and technicians at the ASU Flexible Display Center. Significant engineering efforts were required to develop a suitable flexible substrate/adhesive/carrier system as well as processes suitable for fabricating high-quality TFT arrays necessary for displays. Of the numerous people comprising this group, Dr. Edward Bawolek and Curt Moyer provided invaluable insight into TFT characterization, and Scott Ageno, Dr. Michael Marrs and Dirk Bottesch provided significant process insights and support. Their contributions to humor in a sometimes-challenging environment cannot be understated, either. Dr Yong-Kyun Lee was a great asset to help in developing an understanding of organic electronics, particularly for display applications. This writer's contributions consisted of developing numerous dielectric and active layer films (not discussed in this dissertation), as well as material selection and structure optimization of the organic materials used for the emissive elements.

Chapter 4 is adapted from a previously published paper by O'Brien et al.[164]. This writer's contributions consisted of selecting the materials for the various functional layers, fabricating the devices by vacuum deposition, assisting in opto-electrical testing of the devices, and writing the bulk of the paper. Dr. Guijie Li fabricated the emitter materials, and Dr. Tyler Fleetham provided invaluable discussions related to interpreting the data.

Chapter 5 is adapted from a previously published paper by O'Brien et al.[184]. This writer's contributions consisted of devising the experiment to test the effect of emitter order on device efficiency and electroluminescence spectra, assisting with opto-electronic testing, jointly discussing data interpretation, and writing the detailed discussion of the effect of emitter order on device efficiency and electroluminescence spectra.

Chapter 6 is adapted from a previously published paper by Norby et al.[208]. This writer's contribution consisted of working with Greg Norby on: i) the design of device architecture; ii) device fabrication and testing; and iii) writing part of the results and discussion section. Dr. Timo Park assisted with interpretation of the results and edited the paper to its final form. Dr. Guijie Li designed the emitter materials, and Liang Huang performed the synthesis of the emitter materials.

Chapter 7 is adapted from a previously published paper by O'Brien et al.[230]. This writer's contributions consisted of screening suitable red, green and blue emissive materials; and electrical and optical characterization of test structures used to optimize the OLED device performance. The research was sponsored by the Army Research Laboratory (ARL) and was accomplished under Cooperative Agreement 911NG-04-2-005. The views and conclusions contained in this document are those of the authors and

should not be interpreted as representing the official policies, either expressed or implied, of the ARL or the U.S. Government.

Most of all, and most important, I could not have done this without the love, support and (especially) the patience, of my family. Now, back to the important things in life!

TABLE OF CONTENTS

Page

LIST OF FIGURES

LIST OF FIGURES

Figure Page

LIST OF FIGURES

LIST OF FIGURES

LIST OF FIGURES

LIST OF FIGURES

LIST OF TABLES

Table Page

LIST OF TABLES

Table Page

1. INTRODUCTION

1.1 Organic Electronic Materials Applications

Electronic devices based on organic materials are being used in an ever-increasing number of applications[1,2,3,4]. Organic light-emitting diode (OLED)-based displays are quickly becoming the preferred technology in applications such as television, cellular phones and tablet computers[5]. Their advantages over liquid crystal displays (LCDs) include simpler structure, lighter weight, better color saturation and reduced power consumption. Figure 1 shows a comparison between displays based on LCD and OLED structures[6].

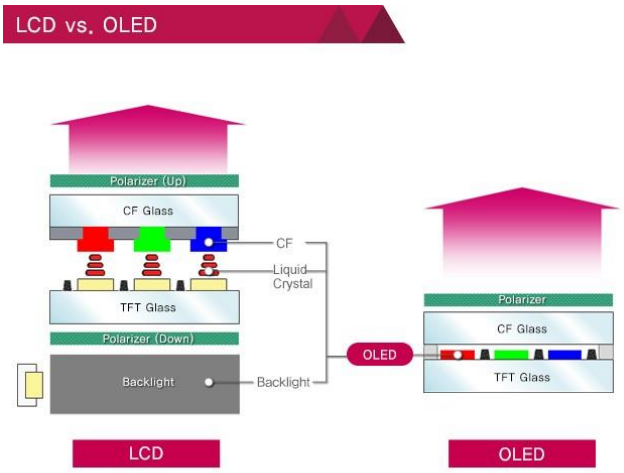

Figure 1: Comparison of liquid crystal display and organic light-emitting display construction.

Displays are the most common application of OLEDs at this time. They can leverage the huge infrastructure already in place from LCD manufacturing, and prices for

OLED televisions have decreased to the point where they are competitive with LCD, while producing superior images.

Organic electronic devices are made using low-temperature fabrication processes, which enables the use of flexible plastic or metal foil substrates that yield more rugged displays than the current standard LCDs. The use of flexible plastic or metal foil substrates makes roll-to-roll fabrication a possibility, with the potential for inexpensive, high production processing[7].

Organic photovoltaics (OPV) are one area of intense research. The earliest devices consisted of a single organic layer sandwiched between two electrodes and had low power conversion efficiencies of 0.1% or less[8]. A substantial improvement was demonstrated in 1986 by Tang, who made a vacuum-deposited 2-layer device that had power conversion efficiency of approximately 1%[9]. Photovoltaic research continues to be a major focus of organic electronics, and organic cells with power conversion efficiencies of over 10% have been reported, making organic photovoltaic efficiencies competitive with amorphous silicon devices[10,11,12,13,14,15,16,17]. Processing of large-area substrates 370mm x 470mm and larger has been demonstrated on glass panels using cluster-type process systems similar to those used for high-volume semiconductor manufacturing[18,19]. The possibility of roll-to-roll production of OPVs would enable fabrication of large area, lightweight and rugged cells, suitable for installation in remote areas. At least one group has demonstrated transparent organic photovoltaic cells, which would be well-suited for building-integrated photovoltaic (BIPV) and energy-scavenging applications[20].

Stability of organic materials under atmospheric and solar exposure has been a long-standing challenge, but Hauch et al. reported P3HT:PCBM polymer cells with degradation in efficiency of approximately 3% after 1000 hours exposure to the sun, although they did not report actual efficiency values[21]**.** Encapsulation remains a crucial element to the successful adoption of organic electronic devices.

Emerging applications for organic electronic devices include lightweight, rugged photodiodes and phototransistors[22, 23]. Organic photodiodes with multi-color response have been fabricated, with applications in machine vision and possibly even artificial eyes[24, 25]. At least one company is producing organic photodiodes and image sensors on large-area, lightweight, rugged flexible substrates with performance comparable to silicon-based detectors. These devices can be used for a variety of applications, such as medical imaging, non-destructive examination, industrial sensors and smart lighting[26]**.**

Organic-based devices have also been used in various sensor applications. Someya et al., (and references therein) have fabricated organic thin-film transistors that were able to detect numerous chemical species, such as oxygen, ammonia, carbon monoxide, hydrogen sulfide and simulated nerve agents[1]. Such devices would be extremely valuable as compact, low-cost, single-use sensors that could provide real-time monitoring for persons exposed to hazardous environment. Kraker et al. reported oxygen sensors with integrated OLED excitation source and organic photodiode detector (OPD)[27]**.**

Fluorescence is a common analytical and diagnostic technique used in biotechnology[28]**.** However, standard instrumentation requires a laser and other expensive

and delicate components and must be maintained in a clean environment. Pais et al. and Banerjee at al. fabricated microfluidic-based fluorescence detectors for lab-on-chip applications using an OLED excitation source and OPD, with crossed polarizers to reduce the excitation light source contribution to the detected signal[29, 30]. However, the OLED was a relatively inefficient NPB/Alq device, and they used a lock-in amplifier to improve the signal to noise ratio; this approach adds cost and complexity to the device. Smith et al. demonstrated an improved device for point-of-care (POC) device on a flexible substrate that used a more efficient phosphorescent OLED emitter, a charge integrating readout circuit and optical filters rather than crossed polarizers to eliminate interference of the excitation source with the fluorescence signal[31]. Using this approach, they achieved a lower detection limit of 10 pg/ml or below, with no lock-in amplifiers, yielding a cheaper, simpler device. Devices with this design have successfully detected cancer cells and human papilloma virus cells. Ongoing research may lead to many other POC test capabilities for drinking water pathogens, human immunodeficiency virus, chemical or biological agents or exceptionally dangerous diseases such as Ebola. Researchers are working on self-powered OLED systems that would eliminate the need for an external energy source, with potential applications including self-contained disposable POC devices, energy harvesting touch-screen displays and supplementary energy sources for sensor systems[32].

OLEDs and OPDs are being tested for application in optogenetics. Optogenetics combines genetics and optics to control events within living tissue that has been genetically modified to be sensitive to light[33, 34]. Optogenetics has potential in treatment of

disorders such as depression, post-traumatic stress disorder, and Parkinson's disease, as well as new methods of drug delivery, and restoring eyesight to those who are visually impaired. Many other applications are under investigation as well[35]. A common optogenetic technique uses an external laser light source and an implanted optical fiber to address the desired region of the brain[36]. However, this approach has several disadvantages, namely: i) the implanted fiber penetrates the skull, thus leaving a possible route for infection; ii) due to the fiber's relatively large size, it is difficult to activate small regions of the brain; iii) the discrete laser/fiber approach creates another potential failure point. An integrated approach proposed by Smith et al. uses an active matrix array of OLEDs on a conformable substrate such as thin polyimide with a wireless inductive power transfer and telemetry link[37]. Using a full-color pixel with subpixel pixel size of ~ 312x104μm enables addressing of small regions of neurons. Only 64 connections are required for the 32x32 pixel array reported in their paper. Using a simple interconnect approach would require x times y individual connections; the 32x32 array in this case would require 1024 separate connections[38].

Solid-state lighting (SSL) is a fast-growing application that is well-suited for OLED-based sources. World energy demand is increasing as the population grows and standards of living increase. Electrical consumption for 2014 was ~20 petawatt-hours (PWh) according to some studies[39, 40]. Energy conservation is crucial to reduce the demand on power generation and infrastructure development, particularly in developing countries. One US Department of Energy report estimates that by 2030, solid-state lighting could potentially save up to 395 terawatt-hours (TWh) annually, approximately

equal to $40 billion in today's dollars and nearly 20 times the expected electricity generation of solar by then[46]**.** Luminaires based on white OLEDs (WOLEDs) are available commercially, although present costs preclude them from widespread adoption. To be competitive with existing lighting sources, costs for WOLEDs must decrease substantially. Table 1 summarizes typical costs of lighting sources as of this writing. Representative costs for LED and OLED sources were estimated based on retail prices of commercially available units.

Table 1: Cost per kilolumen for various lighting sources[46]

Lighting Source	Approximate Cost/klm
Incandescent	$0.63
Compact Fluorescent	$2-10
Inorganic LED	$10-30
Organic LED	> $800

Some cost reductions can be achieved by converting depreciated earlier generation OLED fabrication lines previously used for display products to WOLED lighting products. Roll-to-roll manufacturing has the potential to increase production capacity due to its faster cycle time compared with the common method of using separate vacuum chambers to deposit the different films required in the structure. Other opportunities for improvement include more-efficient materials, improved device structures, and methods to increase light outcoupling of the devices. Solution coating methods such as inkjet printing or slot die coating generally have simpler structures and eliminate the need for vacuum deposition of some layers, but still require vacuum

deposition for the electrodes and possibly other layers. Solution-coated device performance is, in general, inferior to devices made using vacuum-deposited small molecule material, so more research is needed to make polymer-based devices competitive with those made from small molecules.

1.2 Outline of Dissertation

This dissertation describes development of structures for lighting applications using platinum-based phosphorescent emitters, and the engineering and process development necessary for fabrication of a full-color, 14.7" diagonal OLED display on a flexible plastic substrate. Chapter 2 discusses lighting sources and the potential for OLED luminaire lighting as well as a brief discussion of some lighting metrics. Chapter 3 discusses organic optical materials, photophysics, OLED operation and OLED device structures. Chapter 4 describes the fabrication of efficient white OLEDs made using red, green and blue Pt-based emitters and is one of the earliest reports using platinum-based red, green and blue emitters for lighting applications. Chapter 5 investigates the use of a new, more efficient red and deeper-blue platinum-based emitters for an efficient 2-layer white OLED. Chapter 6 describes white OLEDs made with the red and blue emitters used in chapter 5, with an added green layer to achieve a better white balance with high efficiency. Chapter 7 describes the design and fabrication of a full-color OLED display on a flexible PEN substrate in the Flexible Electronics and Display Center at Arizona State University.

2. LIGHTING SOURCES

2.1 Existing Technologies

Lighting, which by some estimates accounts for ~10-20% of electrical energy consumption, is one major field targeted for improved energy efficiency[41,42]. The global general market as of 2011 was >$90 billion, so improvements in lighting efficiency can have an enormous financial benefit[43]. One United States Department of Energy (USDOE) estimate predicts that increased use of solid-state lighting could halve the domestic lighting energy demand by 2030, saving up to 395 terawatt-hours (TWh) of energy[46]. In addition, conditions in developing countries can be harsh, so more rugged lighting sources are desirable as well.

The incandescent bulb was the main light source for many years. It has an emission spectrum similar to that of the sun and thus provides a nearly ideal spectrum. It does not contain hazardous materials, but it is only about 5% efficient; most of the energy is lost as heat. Higher efficiency lighting sources have been developed, but each has its disadvantages as well. Fluorescent lights have been used for commercial and residential lighting for many years; compact fluorescent bulbs which are compatible with existing incandescent sockets were developed some time after the common straight tube sources. While more efficient than incandescent sources, fluorescent lights contain hazardous materials such as mercury and present health hazards and disposal problems. Sodium vapor lamps, although very efficient, emit a strong yellow light which makes them undesirable for most common lighting applications.

Light emitting diodes (LEDs) are another approach to provide high efficiency lighting. Inorganic light emitting diode-based light sources are available commercially; see for example[44,45]. Since inorganic LEDs are monochromatic, they require some method of emitting different wavelengths to make a white OLED suitable for lighting applications. These typically use a blue-emitting LED and a yellow phosphor. Part of the emitted blue light is down-converted by the phosphor to produce high-quality white light. However, this leads to a loss of efficiency of approximately 20%. Adding other red, green and amber LEDs can produce a warmer light, but these devices have efficiencies as low as 20%, which further reduces efficiency Tyan notes that there is a significant difference in specified inorganic LED efficiency compared with real-world performance. Specification efficacies are measured using a short pulse at relatively low current density, while the LEDs are on continuously in actual use conditions and usually much higher current densities. Thus, the efficacy of an LED luminaire may be as little as ~32% of the efficacy of the LED package alone[43].

Inorganic LEDs are long-lasting as well, but require expensive single-crystal substrates and high temperature film deposition processes such as molecular beam epitaxy to produce the device quality crystals needed. In addition, these devices are point sources which emit very bright light, so they need reflectors, diffusers and other hardware to make them useful, which further reduces efficiency and adds to the cost. Achieving uniform illumination in a room- or office-sized area requires many LEDs, adding to the expense.

2.2 Opportunities for OLED Lighting

A comparison of efficiency for some different light sources is, shown in Table 2 below.

Table 2: Lighting Performance for Different Sources[46]

2015 Product Type	Luminous Efficacy (lm/W)	Correlated Color Temperature (K)	Color Rendering Index (CRI)	Usable Life (hours)*
Incandescent	10-17	2,700-2,800	98-100	750-2,500
Linear Fluorescent	65-110	2,700-6,500	70s to 90s	24,000-80,000
Compact Fluorescent	60-80	2,700-6,500	77-88	10,000
High-Pressure Sodium	50-140	2,100	20	16,000-40,000
LED	70-130	2,700-6,500	70s to 90s	25,000-50,000
OLED, LG Display N65 series	55	3000	90	40,000
OLED, OLEDWorks FL300	42	2500	80	50,000
OLED, Kaneka Corporation	40	3000	86-92	50,000

*Usable life for OLED lighting product type is defined as the time at which luminance decays to 70% of the initial luminance, denoted LT_{70}. Usable lifetime for other product types is defined as the time to failure for 50% of samples of that particular type.

As seen in Table 2, inorganic LEDs had the best overall performance as of 2015. However, US Department of Energy tests as recent as 2014 found that many commercially available LEDs failed to meet the performance specified by the manufacturer[47]. There were problems with large variability within a manufacturer and with tested performance parameters failing to meet the manufacturer's specified values.

Although the quoted OLED efficiency is significantly less than that for LEDs, OLEDs have several advantages over inorganic LEDs. OLEDs are distributed light

sources and so need no additional diffusers, reflectors or other similar hardware. They can be made on inexpensive substrates which are more suitable for high-volume production. They can be made on large-area substrates, including flexible substrates, that enable more versatile applications[48]. Some OLEDs can be color-tuned by the end user for use as mood lighting. Transparent OLEDs have been reported that can be used for window or signage applications[49, 50, 51, 52].

Kido and co-workers were the first to report a white organic light emitting diode (WOLED) using all small-molecule materials[53]. They used a 3-emitter structure that used Nile Red, Alq and TPD as the red, green and blue fluorescent emitters, respectively. Although the efficiency and stability were not commercially acceptable, this demonstrated that OLEDs had great potential for solid-state lighting.

A significant advance in WOLEDs for SSL came in 2009, when Reineke et al. reported white OLEDs with power efficiency of 90 lm/W, equivalent to fluorescent lighting sources[54]. More recently, Yamae et al. reported efficiencies of up to 114 lm/W [55] However, both groups used a combination of high refractive index substrates and an additional periodic light outcoupling layer to achieve these results. Both approaches add complexity and cost to the manufacturing process and are undesirable. Research into organic materials[41,56,57] and device structures[58,59,60] for lighting and display applications continues to attract much attention, focusing on color purity, color temperature, stability and efficiency.

2.3 Lighting Metrics

This section gives an overview of photometry, beginning with definitions of some lighting terms and concluding with a discussion of figures of merit used to compare different lighting systems.

The human eye is sensitive to that part of the electromagnetic spectrum between approximately 400 and 750nm. The eye contains two types of receptors, namely rods and cones. The rods are very sensitive to light and are responsible for night vision, also referred to as scotopic vision. Cones enable us to perceive colors and are responsible for daylight, or photopic, vision. Cones are divided into three classes and are color-specific, with peak sensitivities in the blue, green and red portions of the visible spectrum at 445nm, 535nm and 575nm, respectively[61]. Peak sensitivity under photopic conditions is 683 lm/W at ~ 555nm, while peak scotopic sensitivity is 1700 lm/W and occurs at ~ 507nm. Figure 2 shows a plot of the eye's scotopic and photopic response[62].

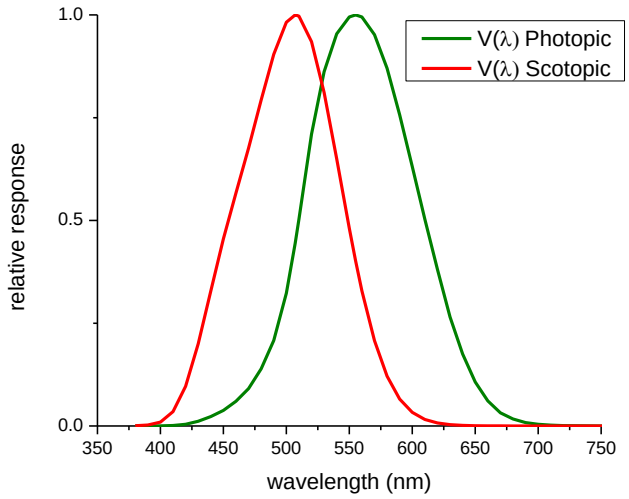

Figure 2: Normalized Photopic and Scotopic Luminous Efficacy of the Human Eye.

Note that photons with wavelengths below ~380nm and above ~700nm are not detected by the human eye, so they are not included in many lighting metrics.

There are numerous terms used for characterizing and quantifying electromagnetic radiation in the visible spectrum. Only some of these will be discussed here. The *luminous flux, Φ*, is defined as the wavelength-weighted power emitted in a given direction per unit solid angle weighted by the eye's photopic or scotopic response:

$$\Phi = Km \int \varphi \, V(\lambda) d\lambda \quad (1)$$

Where Φ is in lumens, φ is the radiant power in W/nm, λ is the wavelength in nm, V(λ) is the photopic or scotopic response, and K_m is the maximum spectral luminous efficacy, which is 683 lm/W for photopic vision and 1700 lm/W for scotopic vision.

The SI unit for luminous intensity is the *candela* (cd), The candela was originally defined as the optical power output of one candle, but is now quantitatively defined as the luminous intensity in a given direction of a source that emits monochromatic radiation of 540 x 10^{12} Hz and that has a radiant intensity in that direction of 1/683 W/steradian [63]. A *steradian* (sr) is the SI unit of solid angle. One *lumen* is defined as the luminous flux emitted into a unit solid angle (sr) by an isotropic point source having a luminous intensity of 1 candela (cd) [64]. *Luminance* is defined as the power per unit area per unit solid angle, with units of cd/m^2. Luminance is one factor in determining the brightness of a source, although brightness is a sensation that also depends on the eye's response (for example, a dark-adapted eye vs one that is adapted to bright sunshine). A *Lambertian source* is one whose luminous intensity in any direction varies as a function of the cosine

of the angle of that direction with respect to the line normal to the surface element of the source:

$$I(\theta) = I_0 \cos(\theta) \quad (2)$$

Where $I(\theta)$ is the intensity when viewed at angle θ and I_0 is the intensity when viewed at normal incidence to the source. A Lambertian source has the same luminance when viewed from any angle. OLED sources are typically assumed to be Lambertian for characterization purposes.

There are several methods used to quantify the efficiency of a light source. *Current efficiency* is defined as the ratio of the luminance in the forward direction divided by the measured current density, with units of cd/A:

$$\eta_C = L_{0°}/j_{meas} \text{ [cd/A]} \quad (3)$$

Luminous efficacy, or power efficiency, is the ratio of the luminous flux to the electrical power input, with units of lm/W:

$$\eta_L = (\pi L) / (jV) \quad (4)$$

where L is the luminance [cd/m^2], j is the current density [A/m^2] and V is the voltage required to obtain the luminance.

Internal quantum efficiency (IQE) is the ratio of the total number of photons generated within a device to the number of electrons injected. IQE can be up to 100% for some materials, for reasons discussed in Chapter 3.

External quantum efficiency (EQE) is the ratio of total photons emitted from the device into the viewing direction to the number of charge carriers injected. It is not a

function of the eye's response. The EQE is reported as a percentage and contains several factors:

$$EQE = \gamma * X * \varphi_{PL} * \eta_{outcoupling} = (\eta_{IQE}) * \eta_{outcoupling} \quad (5)$$

where γ is the charge balance factor, X is the fraction of excitons which can decay radiatively, φ_{PL} is the photoluminescence quantum efficiency and $\eta_{outcoupling}$ is the outcoupling efficiency. The charge balance factor represents the ratio of injected minority carriers which undergo recombination to total number of charges injected. Charge balance is achieved through material selection and/or device structure. Use of ambipolar host materials, charge blocking layers, and materials with suitable HOMO and LUMO levels are common approaches to achieving charge balance. The photoluminescence quantum efficiency is the ratio of the number of photons emitted to the number of photons incident on the sample. Note that the current efficiency and luminous efficacy incorporate the spectral sensitivity of the human eye, while the external quantum efficiency is a measure of all photons emitted from the device to air. Outcoupling efficiency is a function of several loss mechanisms, depicted in Figure 3. Far-field, substrate and organic modes result of the difference in refractive indices at the air/substrate substrate/organic interfaces[65], which produce total internal reflection (TIR) losses. Surface plasmon losses increase exponentially as the distance between the EML and cathode metal decrease. Combined, these losses limit the EQE of a conventional bottom-emitting OLED to approximately 20-25% of the IQE of the emitter[66,67]. Thus, conventional devices based on fluorescent emitters which are limited to 25% IQE can yield ~5% EQE at best, while devices based on phosphorescent emitters with 100% IQE

can yield ~25% EQE. Various outcoupling methods have been used to increase EQE, but add complexity to the fabrication sequence.

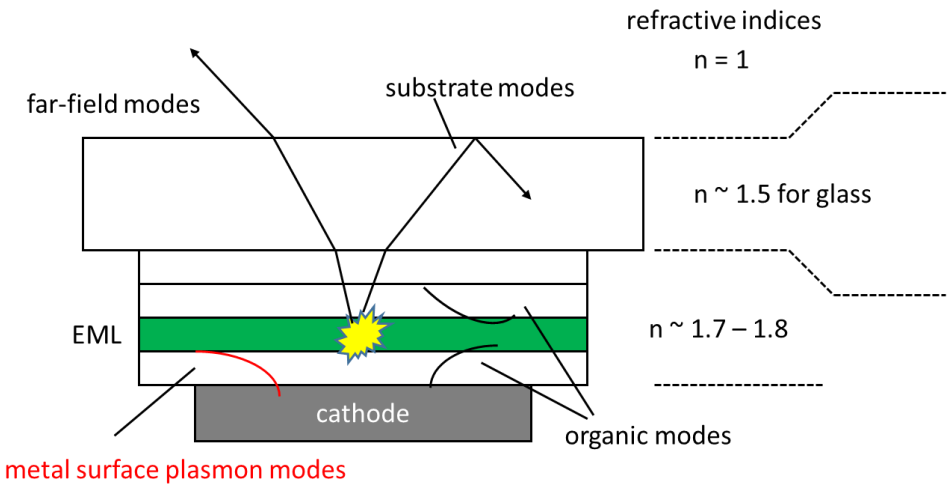

Figure 3: Different light modes in a conventional bottom-emitting OLED. Typical refractive indices of the different OLED components are given. In this configuration, only far-field modes reach the observer. Substrate and organic modes are trapped in the device. Surface plasmon modes occur when the emitting dipoles couple to the metal cathode. Surface plasmon modes decrease exponentially with distance.

Chromaticity of a lighting source is most commonly described using the 1931 Commission Internationale de l'Eclairage (CIE) system, which consists of a horseshoe-shaped diagram that contains all the colors perceptible to the human eye. An example of the CIE diagram is shown in Figure 4[68]. The outer border contains all monochromatic colors detectable by the human eye. The curved line in the interior of the CIE diagram is the Planckian locus, which denotes the observed color of a blackbody radiator at the indicated temperature. The significance of the Planckian locus is discussed later in this section.

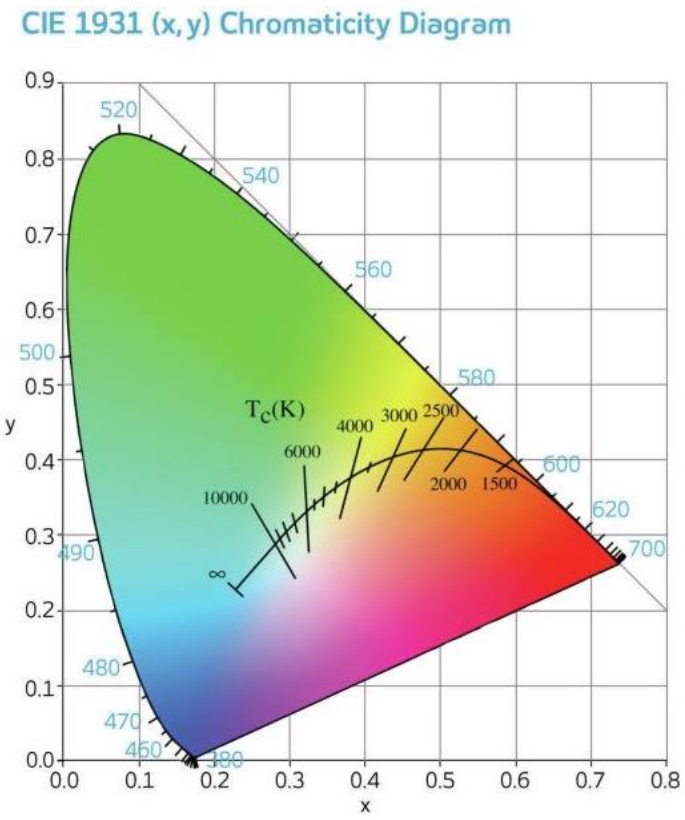

Figure 4: CIE 1931 (x,y) Chromaticity Diagram showing the Planckian locus.

Any color within the CIE diagram can be reproduced using an appropriate combination of the CIE primary colors. The amounts of each primary color required to reproduce a particular color are called the tristimulus values and are determined using the spectral power distribution, S(λ), and the color matching functions, denoted x-bar, y-bar and z-bar, by the following equations:

$$X = \int S(\lambda)\bar{x}(\lambda)d(\lambda) \tag{6a}$$

$$Y = \int S(\lambda)\,\bar{y}(\lambda)d(\lambda) \tag{6b}$$

$$Z = \int S(\lambda)\bar{z}(\lambda)d(\lambda) \tag{6c}$$

A plot of the CIE color matching functions is shown in Figure 5.

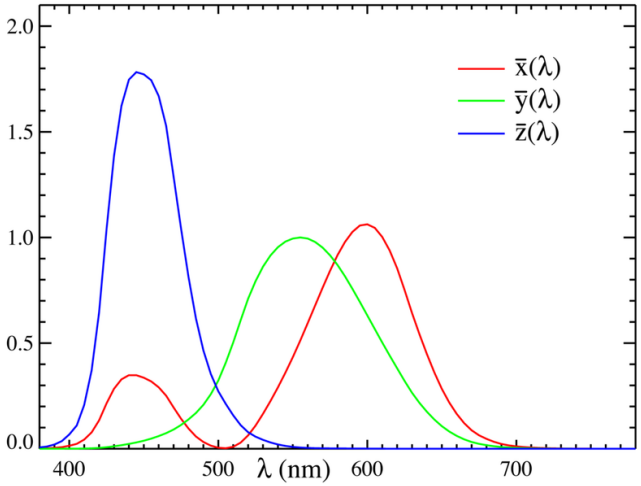

Figure 5: CIE Color matching functions x-bar, y-bar and z-bar versus wavelength

The CIE x, y and z values are obtained by normalizing the tristimulus values as shown in equation 7:

$$X = \frac{X}{X+Y+Z} \tag{7a}$$

$$Y = \frac{Y}{X+Y+Z} \tag{7b}$$

$$Z = \frac{Z}{X+Y+Z} \tag{7c}$$

By convention, only the x and y values are used to specify the chromaticity; z is not an independent variable since z = 1-x-y. Colors not on the boundary of the CIE diagram may be produced using combinations of light sources with different spectral responses, a phenomenon known as metamerism. When viewed directly, the colors will appear identical. However, differences in reflection spectra of the object(s) under illumination can cause the color of the object(s) to differ significantly, depending on the illumination source.

Additional lighting standards have been deve, loped based on blackbody emission sources[69]. The spectral distribution of a blackbody source follows Planck's equation [70]:

$$\rho(\omega) = \frac{h\omega^3}{\pi^2 c^3 (e^{h\omega/k_B T} - 1)} \quad (8)$$

where ρ is the energy density per unit frequency, h is Planck's constant, c is the velocity of light, k_B is the Boltzmann constant, ω is the angular frequency, and T is the Kelvin temperature.

As seen in Figure 4 above, the spectrum of a blackbody source depends only on its temperature. Although the solar spectrum is not a true blackbody spectrum (due to atmospheric scattering and absorption), it is normally used as the reference for evaluating lighting sources. The Planckian locus, shown as a curved line on the CIE diagram, indicates the colors of a Planckian radiator as it is heated from <2000K to ~10,000K[60]. Light sources intended for illumination should emit light that falls on or close to the Planckian locus. The *color temperature* (CT) of a light source refers to the temperature to which a Planckian, or blackbody, radiator would have to be heated to produce light of a specific color. For example, an incandescent bulb will produce light of different colors as the filament is heated. CT is used to characterize the spectral properties of a near-white light source. The *Correlated Color Temperature* (CCT) describes the emission of a non-blackbody source to temperature of a blackbody radiator emitting light of the same color as the source, and is used to describe the chromaticity of a spectrum that is off of the Planckian locus. The *Color Rendering Index* (CRI) describes how well a light source reproduces the colors it illuminates when compared to a blackbody radiation source. It was first introduced by the Commission Internationale de l'Eclairage in 1965 to provide a

quantitative measure of the accuracy of color reproduction and subsequently updated in 1995[71]. The CRI ranges from 0 to 100 and is only defined in the proximity of the Planckian locus. A CRI of 80 or greater is considered suitable as a lighting source. The solar spectrum has a CRI of 100. A tungsten incandescent lamp produces a continuous spectrum and is typically considered the most comfortable artificial lighting source. It has CIE coordinates (0.448, 0.408) at a color temperature of 2856K with a CRI of 100[69]. Table 2 compares power efficiency, CCT, CRI and lifetime values for different sources.

3: ORGANIC SEMICONDUCTORS

Until the 1970's, organic materials were used primarily as insulators or in applications where high electrical conductivity was not needed. Organic materials with alternating single and multiple bonds are termed conjugated; benzene is an example of a cyclic conjugated molecule because the electron wave functions have cyclic periodicity around the closed ring structure of the molecule.

Work by Shirakawa et al. in the 1970's showed that useful levels of electrical conductivity could be achieved if the polymeric materials could be formed in linear chains[72]. These linearly conjugated molecules allowed the π electrons to delocalize along the chains, which greatly increased the conductivity. Shirakawa et al. could vary the conductivity over seven orders of magnitude by doping with halogen materials and were awarded the Nobel Prize in Chemistry in 2000 for this work.

Pfeiffer et al. subsequently showed that evaporated small molecule organic materials could also be effectively doped[73]. The term "small molecule" refers to the well-defined structure and definite molecular weight of this class of materials. The experiments described in this dissertation used only small-molecule materials.

3.1 Organic Electronic Materials

The optoelectronic properties of organic materials are primarily a result of the intra-molecular structure rather than the inter-molecular structure. In contrast to inorganic materials which are held together by strong covalent bonds, organic materials are held together with each other by van der Waals forces, while the atoms within a particular molecule are held together by strong σ bonds. Thus, the electronic and optical properties

of organic molecules are dominated by those of the individual molecule. The highest filled energy level is designated the highest occupied molecular orbital (HOMO) of the constituent molecule. The HOMO level in organic materials is analogous to the valence band in inorganic materials. The first excited state above the HOMO is termed the lowest unoccupied molecular orbital (LUMO), analogous to the conduction band in inorganic molecules. Electrons fill the available orbitals per the Aufbau principle[74]

3.2 Photophysics of Organic Optical Materials

3.2.1 Exciton Formation

Most organic molecules have filled HOMO levels and empty LUMO levels in the ground state. In the case of an OLED under forward bias conditions, holes injected from the anode move through the HOMO of adjacent molecules, while electrons injected from the cathode move through the LUMO. The uncorrelated charge carriers move toward the opposite electrode due to the applied field. Often, one charge carrier (for example, hole) will be trapped at an organic-organic interface. An electron is attracted to the hole; when the electron and hole are close enough to each other, typically 10-15nm, they are attracted to each other by coulombic forces and form a neutral pair called an exciton. Exciton binding energy is given by[75]:

$$\Delta E(e-h) = \frac{e^2}{4\pi\varepsilon_0\varepsilon R_C} = k_B T \quad (9)$$

Where $\Delta E(e - h)$ is the electron-hole binding energy, e is the electron charge, ε_0 and ε are the respective vacuum and host permittivities, R_C is the critical radius where the Coulomb attraction energy is roughly equal to the thermal energy, k_B is Boltzmann's constant and T is absolute temperature.

Typical values of dielectric constant for organic materials are approximately 3, compared with ~12 for inorganic materials such as Si[76]. The resulting exciton binding energies are in the range of 0.1 to 1 eV for organics, compared to ~0.03 to 0.1 for inorganics[77]. Tightly bound excitons in organics, called Frenkel excitons, are localized on the same molecule, while those of inorganics are called Wannier excitons and are delocalized. Due to the high Frenkel exciton binding energy, the localized π electrons are much less mobile than those in inorganic semiconductors. The result is that carriers in organic materials move via a hopping mechanism, which results in very low electrical conductivities of organic materials compared with inorganic materials. Charge transfer excitons describe states where the electron and hole are on separate nearby molecules, rather than the same one.

Since the electron and hole are fermions with spins of ±1/2, there are four possible configurations of exciton, illustrated in Figure 6.

$$\Psi_s = \frac{1}{\sqrt{2}}[X_1(\uparrow)X_2(\downarrow) - X_1(\downarrow)X_2(\uparrow)] \qquad \text{singlet}$$

$$\left.\begin{aligned} \Psi_s &= X_1(\uparrow)X_2(\uparrow) \\ \Psi_s &= X_1(\downarrow)X_2(\downarrow) \\ \Psi_s &= \frac{1}{\sqrt{2}}[X_1(\uparrow)X_2(\downarrow) + X_1(\downarrow)X_2(\uparrow)] \end{aligned}\right\} \text{triplet}$$

Figure 6: Anti-symmetric and symmetric wave functions illustrating singlet and singlet exciton configurations.

3.2.2 Intramolecular Energy Transfer

Various photophysical transitions occur when a molecule experiences electronic excitation. The energy levels of species experiencing these transitions occur at discrete

values per quantum mechanical principles[81]. A Jablonski diagram, shown in Figure 7, shows the relative positions of electronic energy levels of a molecule as well as the various intramolecular energy transitions which occur[74] . Absorption, represented on the Jablonski diagram as $S_0 \rightarrow S_1$ and $S_0 \rightarrow S_2$ transitions, results from excitation by species with energies higher than that of the bandgap energy $E_g = hc/\lambda$, where h is Planck's constant, c is the speed of light, and λ is the wavelength of a photon emitted upon decay from the lowest excited state to the ground state. Absorption can occur over a range of energies; as a result, the absorption spectrum consists of a broad peak. Absorption is the fastest of the various transitions, occurring in roughly 10^{-15} s The excited species release energy through several mechanisms, namely vibrational relaxation, internal conversion, intersystem crossing, fluorescence and phosphorescence. These processes occur at different rates, indicated in Table 3. Vibrational relaxation and internal conversion are non-radiative transitions that occur as result of nuclear interactions, and occur in the 10^{-14} to 10^{-11} s time range. Transitions from S_1 singlet states to the S_0 ground state are allowed by quantum mechanics and thus occur relatively rapidly. These transitions are emissive and are denoted as fluorescence. Kasha's rule states that these transitions occur from the lowest excited state, represented by the vertical lines originating at the heavy line of the S_1 state, to the ground state[78]. Intersystem crossing (ISC) between a singlet state and a triplet state, or between a triplet state and ground state, is forbidden by quantum mechanics. ISC requires spin flip, which does not occur unless there is some degree of spin-orbit interaction, denoted spin-orbit coupling (SOC)[79]. SOC is strongly dependent on

atomic number, and so occurs much more rapidly in molecules containing heavy metals such as iridium or platinum compared with purely organic molecules[80,114].

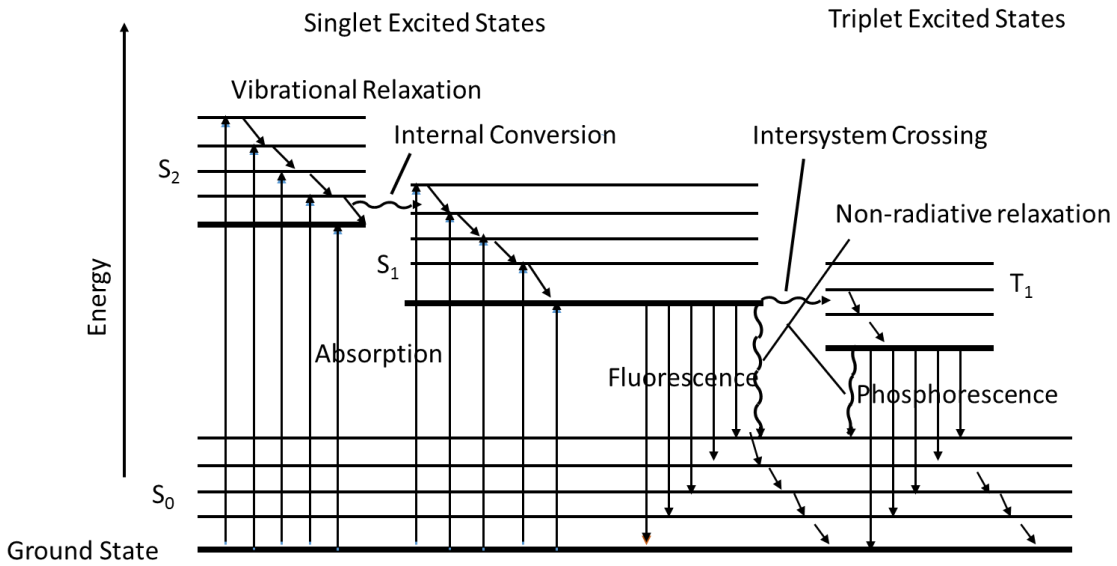

Figure 7: Jablonski diagram illustrating relative positions of electron energy levels and various energy transfer processes.

Table 3: Approximate times for intramolecular energy transfer processes [81]

Process	Time, sec
Excitation/absorption	10^{-15}
Internal conversion/vibrational relaxation	10^{-14} - 10^{-11}
Fluorescence	10^{-10} - 10^{-8}
Phosphorescence	10^{-6} – 10^{2}

The potential energy of a molecule is a function of its nuclear coordinates. A polydimensional plot is required to describe the potential energy of a polyatomic molecule. By substituting a diatomic molecule model and its center of mass for a polyatomic molecule and its associated group of neutrons, the potential energy surface

can be reduced to a two-dimensional diagram. Excitation of the molecule usually results in an increase in nuclear coordinates. Since the electronic excitation occurs on a much faster time scale than the vibrational relaxation, the Born-Oppenheimer approximation, which states that the electronic motion, spin contribution and nuclear motion can be treated separately when calculating the potential energy of the molecule, can be applied[82]. The molecular wave function, Ψ, is thus approximated as

$$\Psi \cong \psi_0 \chi \zeta \tag{10}$$

where ψ_0 represents the electronic wave function, χ represents the nuclear wave function, and ζ represents the spin wave function. The nuclear coordinates can be assumed to be stationary during the electronic excitation process, since the nuclear mass is much greater than that of an electron. This change in electron distribution causes a change in the nuclear coordinates. The nuclear coordinates must then return to the equilibrium value, so the vibrational relaxations that occur during the change in nuclear coordinates are the rate limiting step for energy transitions. The Franck-Condon principle states that these transitions are most favorable when the nuclear coordinates of the ground state and the excited state are most similar[83]. Transitions with no change in nuclear coordinates are known as vertical transitions and are the most favorable.

3.2.3 Intermolecular Energy Transfer

Energy transfer between excitons can occur by three processes: light mediated (LM), dipole mediated (or Förster) transfer, and electron exchange (or Dexter) transfer. LM transfer occurs when an exciton decays radiatively and emits a photon, which is then absorbed by another molecule[84]. This requires overlap of the emission spectrum of the

exciton and the absorption spectrum of the acceptor molecule, with the rate depending on the emission efficiency of the exciton and the concentration and light absorbing ability of acceptor molecules[81]. The Förster process is a non-radiative resonant transfer process which occurs by a dipole-dipole coupling mechanism and does not require collisions between molecules. The Förster energy transfer rate is a function of the dipole moments of the donor and acceptor molecules, the separation between donor and acceptor molecules, and the electronic overlap integral between the excited donor molecule and the ground state acceptor[85]. The energy transition rate between donor and acceptor species, K_{DA}, can be written in simplified form as

$$K_{DA}(R) = (1/\tau_D)(R_0/R)^6 \quad (11)$$

Where R_0 is the Förster transfer radius, R is the radius between species, and τ_D is average donor lifetime in the absence of energy transfer. The Förster transfer radius is the critical distance between the donor and acceptor where the probability of energy transfer between donor and acceptor is equal to the probability of emission by the donor. The critical distance varies as R^{-6}, where R is the radius between species, with typical values in the 10-100nm range, depending on the materials involved. Förster energy transfer dominates when $R < R_0$ and is the dominant energy transfer mechanism between singlet states[81].

Energy transfer can also occur by electron exchange between adjacent molecules. This mechanism, known as Dexter transfer, requires overlap of the molecular orbitals and occurs over a distance up to ~1nm[87]. It is also a non-radiative process. Triplet-triplet energy transfer occurs by the Dexter process, which is the primary energy transfer

mechanism in phosphorescent devices[86]. Electron exchange rate in Dexter transfer decreases exponentially with donor-acceptor separation, as shown in equation 12[87]:

$$k_{ET}(Dexter) = KJe^{(-2R_{DA}/L)} \quad (12)$$

Where K is related to specific orbital interactions, J is a spectral overlap integral normalized for the acceptor absorption coefficient, and R_{DA} is the donor-acceptor separation relative to their van der Waals radii, L. A schematic depicting the Förster and Dexter processes is shown in Figure 8

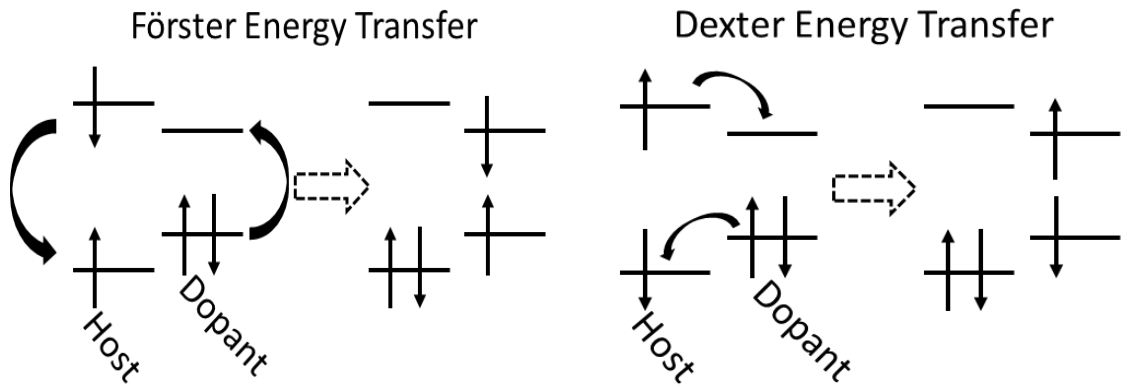

Figure 8: Schematic representation of Förster energy transfer (left) and Dexter energy transfer (right).

3.2.4 Exciton Relaxation Processes

Excitons can relax by non-radiative or radiative processes. Non-radiative processes include internal conversion, vibrational relaxation and intersystem crossing, and are illustrated in the Jablonski diagram in Figure 7. The electronic energy released from these processes is converted into heat[81].

Radiative recombination occurs when an excited species relaxes to the ground state. As discussed previously, emission occurs from the $S_1 \rightarrow S_0$ transition in purely

organic molecules. The $T_1 \rightarrow S_0$ transition rate is very slow in these materials, so this transition normally occurs non-radiatively. However, this transition occurs much more rapidly in organometallic materials, and triplet excitons can contribute to electroluminescent emission. Creation of the excited species can occur by energy transfer from an excited host molecule to a guest, or dopant, molecule. It can also occur when an exciton is formed directly on a dopant molecule. Direct trapping on the dopant is preferred to trapping on the host, since it avoids the losses due to energy transfer processes that can reduce efficiency [88, 89, 90].

Excitons tend to accumulate at the hole transporting layer (HTL) and electron transporting layer (ETL) interface with the emissive layer (EML) where charges tend to accumulate due to the LUMO and HOMO energy offsets of these materials, so the emissive layer (EML) is usually located at this interface[91,92].

3.2.5 Loss Mechanisms

There are several loss mechanisms that can result in reduced device efficiency by reducing the number of excitons which can decay radiatively. Triplet-triplet annihilation, triplet-polaron annihilation, singlet-polaron annihilation, singlet-triplet annihilation and singlet-singlet annihilation are potential mechanisms; however, triplet-triplet and triplet-polaron annihilation are the dominant ones[93,94,95]. Triplet-triplet annihilation occurs by the following reaction:

$$T_1 + T_1 \rightarrow S_n + S_0 \rightarrow S_1 + S_0 \qquad (13)$$

Triplet-polaron annihilation proceeds according to equation 14 for electrons or equation 15 for holes[95]:

$$T_1 + e^- \rightarrow S_0 + e^{-*} \quad (14)$$

$$T_1 + h^+ \rightarrow S_0 + h^{+*} \quad (15)$$

Where e^- and h^+ represent electrons and holes in the LUMO and HOMO, respectively. The asterisk denotes a charge carrier in an excited state. Triplet-triplet annihilation increases as triplet exciton concentration increases and can be reduced by increasing the width of the emissive zone, which reduces the triplet concentration. Triplet-polaron annihilation can be reduced through optimal device design and careful charge balance. Both annihilation processes contribute to the efficiency droop commonly observed in OLEDs containing phosphorescent emitters.

3.3 Electroluminescence in Organic Optical Materials

Electroluminescence in organic materials was reported by Bernanose as early as the 1950's[96] Helfrich and Schneider subsequently demonstrated electroluminescence in single-crystal anthracene in 1965[97]. They used crystals of 1-5mm thickness, and had to apply voltages in the 10s to 1000s of volts via liquid electrolytes to induce fluorescence. They were only able to produce fluorescence if appropriate charge-injecting materials were used for each electrode. The high operating voltages and liquid electrolytes required for operation precluded practical application, however.

In 1982, Vincett et al. reported electroluminescence in thin films of vacuum-deposited anthracene with bias as low as 30V[98]. They used various thin-film layers for the electrodes and found that current injection, rather than field-dependent bulk charge generation was responsible for charge generation. This showed efficient device operation required choosing a contact layer with the appropriate work function for the anode and

cathode contacts. However, their films were deposited at temperatures from 0º to -150ºC, making these devices interesting for scientific study but not of practical use.

A significant improvement was reported in 1987 when Tang and VanSlyke demonstrated devices which operated at relatively low voltage[99] They used a heterostructure consisting of an indium-tin oxide (ITO) anode for hole injection, 75nm diamine as a hole transporter, 60nm Alq_3, where Alq_3 is tris(8-quinolinolato)aluminum(III), as the emissive layer/electron transporter, and a cathode of MgAg alloy as the electron injecting layer. A schematic of their device is shown in Figure 9.

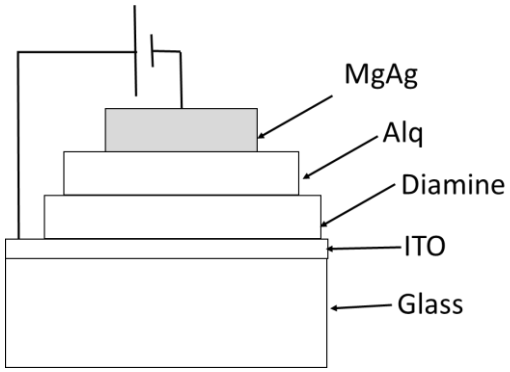

Figure 9: Schematic of OLED device reported by Tang and VanSlyke. Drawing not to scale.

These devices began emitting light at as low as 2.5V due to the thinness of the organic layers. However, they emitted only in the green portion of the spectrum due to the Alq emitter. The devices showed poor electron injection and large transport barriers arising from the difference in LUMO levels between the diamine hole transport layer and Al. The charge transport imbalance between holes and electrons resulted in hole recombination at the cathode. Although these devices were not very efficient at ~1%

photon/electron external quantum efficiency (EQE), they demonstrated the feasibility of organic materials for practical emissive applications. The organic layers in these devices were deposited at ambient temperature and were amorphous, which allowed them to be made on relatively low-cost substrates such as glass, and potentially on more temperature-sensitive substrates such as plastics. Tang et al. subsequently made devices which emitted in other parts of the spectrum by sandwiching an Alq_3 host layer which had been doped with fluorescent dye in between neat layers of Alq[100]. This separated the charge transport and emissive layers and allowed the use of emissive materials that produced the desired colors. Excitons which had formed in the host material could transfer their energy via dipole coupling mechanism (Förster transfer), or by direct electron exchange (Dexter transfer) to the emissive dopant molecules[85,87]. The doped devices were more efficient than the undoped, but the EQE was still low at about 2.5% photon/electron due to inefficient charge transport through the device.

Since then, researchers have developed materials specialized for hole transport, electron transport, emissive layer host, and hole- or electron-blocking to manage charge transport between the adjacent layers. Appropriate HOMOs and LUMOs are needed to minimize injection barriers as well as prevent charge carriers and excitons from recombining non-radiatively at the electrodes. A review by Shirota and Kageyama discusses principles of charge transport in molecular materials and the material properties needed for efficient charge transport and confinement, and provides an extensive listing of charge carrier transport materials[56].

Electroluminescence in polymeric materials was initially reported by Burroughes et al. in 1990 using poly(p-phenylene vinylene) films[101]. The reported quantum efficiency was approximately 0.05%, much lower than the Tang and VanSlyke device. Polymeric materials are better suited to solution processing methods compared with small-molecule materials, making them a potentially lower-cost approach to emissive devices. However, polymer-based OLED performance is typically inferior to that of small-molecule devices and will not be discussed further in this work.

3.4 OLED Emission Mechanism

A typical heterostructure OLED is shown in Figure 10.

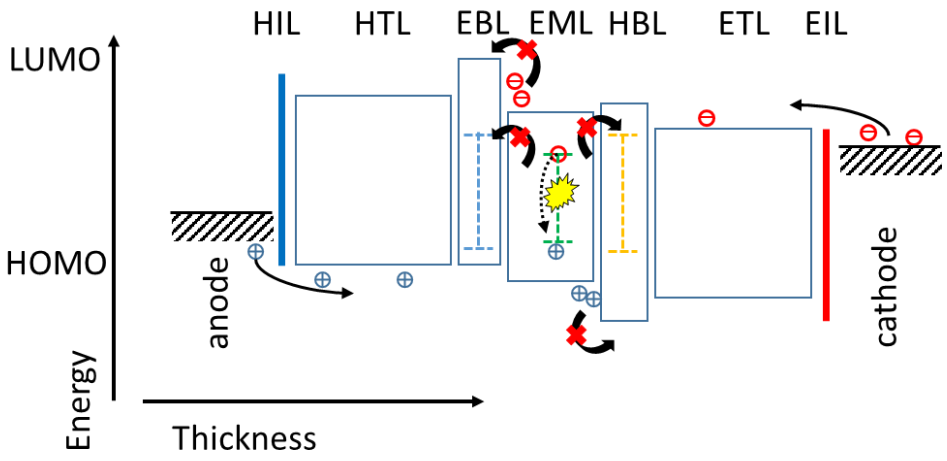

Figure 10: Energy diagram of a typical multilayer OLED. From anode to cathode there are: hole injection layer (HIL), hole transport layer (HTL), electron blocking layer (EBL), emission layer (EML), hole blocking layer (HBL), and electron injection layer (EIL). Boxes indicate HOMO and LUMO levels of the materials. The dashed lines in the EBL, EML and HBL are the desired triplet energies of the materials in case of phosphorescent OLEDs. The red crosses indicate energetically unfavorable charge transfers.

Applying a positive bias to the anode injects holes at the anode and electrons at the cathode. Hole transport and electron transport facilitate the movement of the carriers toward the oppositely charged electrodes. Electron blocking and hole blocking layers confine the respective carriers to the emissive region due to the barriers created by the energy offset between the blocking layer and the corresponding charge carrier. Energy levels for some common charge injection, transport and blocking materials are listed in Table 4.

Table 4: Energy levels for some common injection, transport, host and blocking materials used for fabrication of organic light-emitting diodes. Energies are given in eV

Material	Function	HOMO, eV	LUMO, eV	E_T, eV	Reference
ITO	Anode	4.7-5.1	n/a	n/a	[102]
HAT-CN	Hole Injection	9.5	5.7	n/a	[103]
NPD	Hole Transport	5.2	2.4	2.3	[104]
TAPC	Electron Blocker	5.5	2	2.5	104
CBP	Host	6.3	2.8	2.5	104
26mCPy	Host	6	2.3	2.9	[105]
BCP	Hole Blocker	6.5	3.0	2.6	104
Alq_3	Electron Transport	5.8	3.0	2.2	86
LiF	Electron Injection	n/a	3.6	n/a	[106]
MgAg	Cathode	3.7	n/a	n/a	[107]

Where ITO is indium-tin oxide, HAT-CN is Dipyrazino[2,3-f:2',3'-h]quinoxaline-2,3,6,7,10,11-hexacarbonitrile, NPD is N,N'-Bis(naphthalen-1-yl)-N,N'-bis(phenyl)-benzidine, TAPC is Di-[4-(N,N-ditolyl-amino)-phenyl]cyclohexane, CBP is N,N'-

dicarbazolyl-4–4'-biphenyl, 26mCPy is 2,6-bis(N-carbazolyl) pyridine, BCP is 2,9-dimethyl-4,7-diphenyl-1,10-phenanthroline, and Alq_3 is tris(8-quinolinolato)aluminum(III).

As discussed in the section on photophysics of organic optical materials, when the electron and hole are within the critical radius for Coulomb attraction, R_C, they form an exciton. The first step toward exciton formation is the trapping of one type of carrier in the emissive layer. Excitons may form in the matrix material and transfer their energy to the dopant, or they may form directly on the dopant. Formation directly on the dopant is preferable, to avoid energy losses due to matrix-dopant transfer[89]. Impurities in the emissive layer act as effective traps for the carriers, so material purity is critical.

Spin statistics suggest that the triplet:singlet ratio should be 3:1, although the actual ratio may be slightly less than this. Experiments by Baldo et al. and Segal et al. confirmed that singlets comprised ~20-25% of excitons[108,109]. Singlet-singlet transitions are allowed by quantum mechanics and occur very rapidly, as shown in Table 3. A transition between the S_1 excited singlet state and the S_0 ground state is termed fluorescence. Internal quantum efficiency in fluorescent is limited to a maximum of 25%, since only singlet excitons are utilized.

Intersystem crossing from triplet states to the singlet ground state are forbidden according to quantum mechanics, but does occur to a small extent in purely organic materials due to a small amount of spin-orbit coupling[110]. Transition from a singlet state to a triplet state requires a spin flip, which is a very slow process in purely organic compounds[111]. Triplet exciton radiative decay lifetimes in purely organic materials are

much longer than those of singlets due to this low probability of transition from the T_1 excited state to the S_0 ground state; therefore, non-radiative decay processes dominate. Emission due to triplet – singlet transition is termed phosphorescence. Harvesting these triplet excitons to increase emission efficiency would require drastically reducing the triplet lifetime of the emitter.

In 1998, Baldo et al. showed that using a phosphorescent material, PtOEP, where PtOEP is 2,3,7,8,12,13,17,18-octaethyl-21H,23H-porphine platinum(II), allowed the harvesting of triplet excitons via intersystem crossing (ISC), with an accompanying increase in emission efficiency[112]. The IQE under electrical excitation is given by[113]

$$\eta_{\text{int}} = [(1\text{-}X) + X\Phi_{ISC}]\frac{K_P}{K_P + K_{NP}} \qquad (16)$$

Where X is the statistical splitting of singlets, or 25%, (1- X) is ~75% triplets, Φ_{ISC} is the probability for ISC, K_P is the phosphorescence emission rate, and K_{NP} is the rate of nonemissive triplet decay.

Spin-Orbit Coupling (SOC) depends strongly on atomic number, so the addition of heavy-metal ions greatly increases the amount of SOC[114,115]. SOC results from interaction of electron spin and orbital angular momentum and allows mixing of singlet and triplet states, which increases ISC from higher excited singlet state to the triplet state[116]. Baldo et al. subsequently reported higher efficiencies in a device made with $Ir(ppy)_3$, where $Ir(ppy)_3$ is fac-tris(2-phenylpyridinato)iridium(III), which has a much shorter triplet excited state lifetime than PtOEP[117]

3.5 OLED Device Structures

Just as with inorganic light emitting diodes, organic LEDs consist of several layers with specific optoelectronic properties. Efficient charge generation, transport and recombination are achieved by utilizing materials with the appropriate properties. Because carriers are localized on the molecules in organic materials, mobilities are orders of magnitude smaller than those of inorganic compounds.

Proper material choice and device design is needed to achieve charge balance. This can be done by adding hole blocking and/or electron blocking layers (HBLs and EBLs, respectively), as well as hole- and electron-injection layers, to the structure. Layer thicknesses also affect device performance and must be optimized for best performance.

The base layer for a bottom-emitting OLED is usually the anode and commonly consists of a transparent indium-tin oxide (ITO) layer. When the anode is positively biased, electrons in the ITO are attracted to the anode and holes are repelled. The next layer is typically the hole transport layer (HTL) followed by the emissive layer (EML). In some structures, an electron blocking layer (EBL) is deposited on top of the HTL to prevent excitons from migrating toward the anode and being lost for emission. The next layer is typically the emissive layer (EML). In order to generate light, electron-hole pairs must recombine within the emissive layer. The recombination zone is expected to be closer to the electrode that injects the carriers with lower mobility, usually the cathode since electron mobility in organic materials is typically several orders of magnitude lower than hole mobility[56,118]. A hole blocking layer (HBL) is often deposited on top of the EML to prevent the more mobile holes from reaching the cathode and recombining there.

On top of the HBL is an electron transport layer (ETL) which facilitates the transport of electrons to the EML. The electrons and holes form electron-hole pairs termed excitons, and are bound to each other by Coulomb attraction. The ETL layer consists of a material with higher electron mobility relative to the other organic materials in the device. The cathode layer is deposited on top of the ETL.

One key to achieving efficient device operation is choosing materials with appropriate HOMOs and LUMOs at each interface to minimize energy barriers and facilitate charge carrier transport. Refer to the device schematic in Figure 10. Numerous studies have been done on the electronic structures at organic/organic and organic/inorganic interfaces, since a better understanding of these effects is necessary for optimizing device structures[76,119,120].

Further refinements have been made with the introduction of charge injection layers between the anode and HTL and the cathode and ETL. Materials such as MoO_3[121], LiF[122,123,124], Cs_2O_3[125], Al_2O_3[126] and others form interfacial dipoles or energy states which enhance carrier injection at the respective electrodes with an attendant increase in device efficiency.

White OLEDs (WOLEDs) for solid-state lighting applications have been fabricated using various approaches, illustrated in Figure 11.

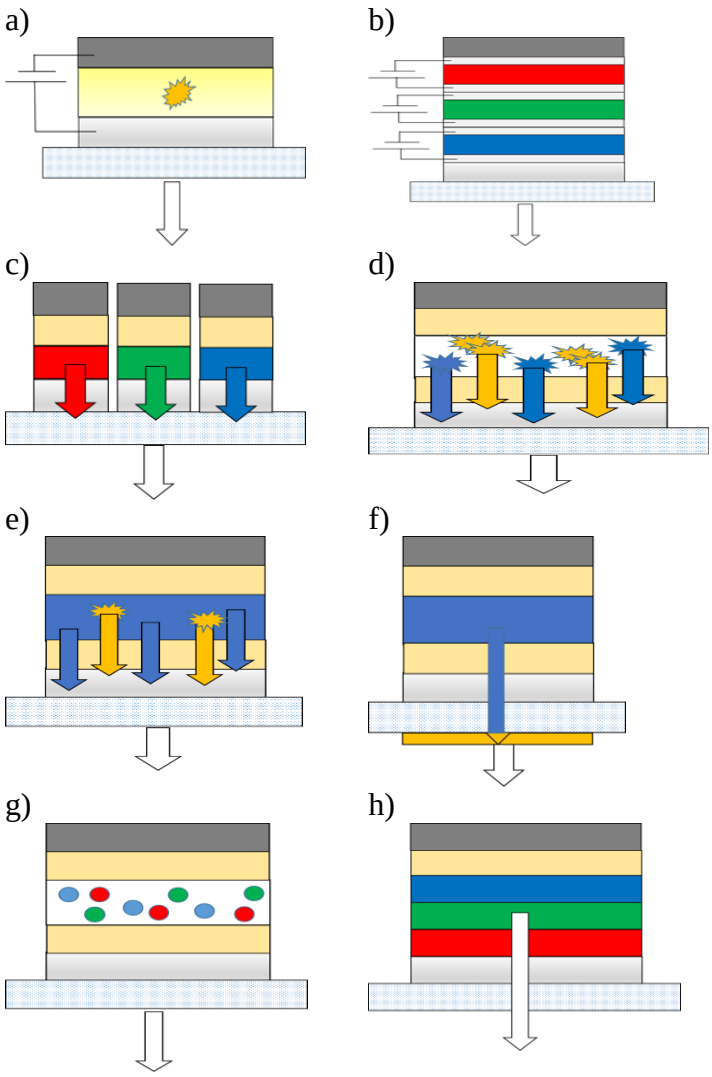

Figure 11: a) Schematic cross-section of a bottom-emitting OLED; b) stacked WOLED with separate driver circuits for each color emitter; c) pixelated monochrome OLEDs; d) exciton emitter based WOLED; e) single doped WOLED utilizing host emission and dopant emission; f) blue OLED using downconversion layer (downconversion layer may also be in between the anode and hole transport layer); g) WOLED with a multiple-doped emissive layer; and h) WOLED using red, green and blue monochrome sublayers to produce white light.

Figure 11 (a) is a schematic cross-section of a bottom-emitting OLED structure. The layers from bottom to top represent the substrate; the transparent conducting anode; the emissive layer; and the metal cathode layer. Charge injection, charge transport and charge blocking layers are not shown for simplicity.

Figure 11 (b) represents a tandem OLED structure[127,128]. A tandem OLED consists of several independent OLEDs which emit in different parts of the spectrum combined in one stack. Charge generation layers separate the individual devices. Each charge injected into a tandem OLED can produce multiple photons, so this structure has high current efficiency, although the higher driving voltage required for this structure results in little or no increase in power efficiency. Higher current efficiency makes tandem OLEDs more attractive for solid-state lighting applications rather than portable displays. The current density is equal in all devices, which minimizes the color shift with current density observed in other device architectures. Shen et al. demonstrated an alternate tandem OLED, referred to as a stacked OLED, in which each emissive layer had its own independent drive circuitry[127]. This design permits color tuning by independently varying the current density to produce a shift in the emission spectrum, but with the disadvantage that it requires a more complex fabrication process and more complicated drive circuitry. The luminance at a fixed current density in a tandem structure increases with the number of stacked and independent emissive layers, so a tandem OLED can be driven at a lower current density compared to other device structures to produce a given luminance. Lifetime is known to be a function of current density, and the lower current density in tandem devices yields a more stable device[175,244]. Further improvements in materials and device structures have reduced the driving voltages, so SOLEDs may find wider adoption in the near future[129].

Figure 11 (c) depicts a striped device. This structure is used by some display makers because the monochrome emitters eliminate the need for the color filter that is

necessary with a white backlit display. The monochrome emitters can be tuned individually to maximize performance of each color. In addition, the sub-pixels can be addressed separately, which enables color tuning of the device. However, this approach requires some method of patterning the pixels; photolithography is generally not compatible with OLED materials. Fine pixel size is required to ensure color homogeneity across the panel. Fine-metal masks (FMM) are typically used to fabricate devices on earlier generation panels, such as Gen II (370 x 470 mm), but mechanical difficulties on mask fabrication, and maintaining close contact with the substrate becomes difficult because of the sag that occurs with larger area masks. For these reasons, striped OLEDs are not a preferred approach to solid-state lighting. Striped OLEDs require higher drive current densities compared to other structures, as well as additional drive electronics to adjust the driving currents for the red, green and blue pixels independently. Higher drive currents increase the degradation rate.

Figure 11 (d) shows a single-doped WOLED using an excimer emitter. An excimer is composed of two identical molecules that exist only in the excited state; the excimer dissociates back to individual molecules in the ground state. Excimer emission is red-shifted with respect to the monomer emission of the individual molecule and can be used to produce white light, depending on the monomer and excimer emission spectra. The use of excimer emitters to generate white light avoids problems of differential aging, since one material is used to generate the entire spectrum, and has the advantage of a potentially simpler fabrication process since there are fewer layers. There are relatively few suitable excimer emitter materials available now, and efficiencies reported to date are

generally inferior to devices with multiple emissive layers. Development of new excimer emitter materials is an active research area and may yield materials with superior performance[130].

Figure 11 (e) Shows a single-doped WOLED that uses a single host with an emitter with complementary color[131,132]. This structure can use combinations of fluorescent and/or phosphorescent materials. The host is usually responsible for charge transport and blue emission. A blue host is needed so that there is sufficient energy to excite the longer wavelength dopant. The lack of stable, deep blue phosphorescent emitters means that fluorescent blue emitters are typically used. Devices which combine fluorescent emitters and phosphorescent emitters are denoted hybrid OLEDs, and will be discussed in more detail below. Fluorescent emitters have lower efficiency compared with phosphorescent emitters, since fluorescent emitters can only harvest singlet excitons, which reduces device efficiency. Proper selection of the complementary color emitter can produce efficient energy transport and yield a balanced spectrum, but these devices are also subject to spectral shift with variation in current density. Careful control of dopant concentration is critical to balance host and dopant emission. Complementary-color OLEDs often have low CRI due to insufficient emission in the green part of the spectrum.

Figure 11 (f) shows a blue OLED with a down-conversion layer. This approach is similar to that used with inorganic LEDs for lighting applications. The down-conversion layer can be either another thin-film layer within the device, or deposited on the substrate after OLED deposition has been completed. This has the advantage of a relatively simple device structure, especially if the down-conversion layer is deposited as part of the OLED

fabrication. Depositing the down-conversion layer on external substrate side adds some complexity to the process. In addition, there are no suitable blue phosphorescent emitters as of this writing; stability and color saturation have not been achieved in phosphorescent blue materials. Fluorescent blue emitters are available with excellent stability and color saturation; however, the intrinsically low quantum efficiency of fluorescent emitters is a major disadvantage to this approach.

Figure 11 (g) is an example of a double- or triple-doped WOLED[133] This device uses a single emissive layer consisting of two or three emissive materials co-doped into a host material. The single emissive layer provides a relatively simple fabrication process compared with the other structures mentioned here, but has several drawbacks. Maintaining accurate dopant concentration of multiple materials during the emissive layer deposition step requires simultaneous precise control of several deposition sources. The use of multiple emitters in a common host requires compromise in material choices, which can result in difficulty maintaining proper charge balance and recombination within the device so that the correct color balance is maintained. The blend of emitters might phase-separate over time, resulting in color shifts, localized increases in current density, and film inhomogeneities[41].

Figure 11 (h) shows a single OLED with multiple emissive layers. This structure allows optimization of each emitter layer (EML) with respect to host material, emissive layer thickness, deposition order of EMLs, and doping concentration. It also allows the use of separate hole transport and electron injection layers that reduce charge injection barriers and block charges from passing through the emissive layers and recombining

non-radiatively[41]. The individual layer thicknesses can be controlled very precisely, which can reduce run-to-run variability in device performance. The multiple EML structure adds complexity to the fabrication process due to the separate emitter deposition steps, but has been used extensively in small-molecule-based devices. As with most other OLED architectures, multiple EML WOLEDs are affected by spectral shift with drive current. This is an active research subject, and Wang et al. have demonstrated devices with stable emission spectra from luminance values from 500 to 10,000 cd/m^2 through use of a single host and optimal arrangement of emitter layers to manage excitons and charges[134].

Thermally assisted delayed fluorescence (TADF) is a relatively new and promising approach to high-efficiency OLEDs, first demonstrated by Goushi et al.[135] TADF employs materials with small singlet-triplet energy differences, on the order of thermal energies, so that triplet excitons generated within the TADF material can undergo reverse intersystem crossing (RISC) to be promoted to the singlet state of the fluorescent emitter, then undergoing emissive relaxation[136,137,138]. Thus, devices incorporating TADF materials can surpass the ~5% EQE limit of conventional fluorescent materials. TADF materials do not contain heavy metal ions such as Ir and Pt that are incorporated into phosphorescent emitters. Devices utilizing TADF materials have demonstrated EQE and power efficiencies over 20% and 47 lm/W, respectively in hybrid, single EML and multi EML structures[142,143]. However, TADF-based OLEDs exhibit high efficiency roll-off at higher luminance, and material stability is still a challenge.

A table comparing device performance for different WOLED structures is given below. More complete comparisons are difficult, since many papers include only select parameters, often under different operating conditions such as current density or luminance. The results given in Table 5 represent some of the better results reported in the literature for devices without enhanced outcoupling structures.

Table 5: CIE coordinates, CRI, current efficiency and power efficiency for representative types of white OLEDs

Type	CIE	CRI	EQE	PE, lm/W	Comments	Reference
Excimer	0.33, 0.33	80	18.2	35.2		[150]
Fl, single doped	0.332, 0.336	80	5.2	4.8	0.5% doping	[139]
Hybrid M-EML	0.40, 0.41	85	18.7	37.6	4 EMLs	[92]
Hybrid, S-EML	Not given	88	16.5	46.8		[134]
S-EML	0.32, 0.38		19.3	42.5	Blue+Orange co-doped	[140]
Tandem	0.39, 0.49		46.6	67.1	*	[141]
M-EML	0.38, 0.45	85	20.1	41.3	Red+Green co-doped/Blue EML	[140]
TADF, S-EML	0.398, 0.456		20.8	51.2		[142]
TADF, M-EML	0.438, 0.438	89	23.0	51.7		[143]
M-EML (B/R)	0.28, 0.26	65	18.0	25.0	**	This work
M-EML (R/G/B)	0.35, 0.41	77	14.9	17.3	***	This work
M-EML (R/G/B)	0.37, 0.40	80	21.0	41	****	This work

* Maximum current efficiency; power efficiency at 1000 cd/m^2
** R/B WOLED
*** PtON9-me/PtOO2/PtOO3 RGB WOLED
**** PtN3N/PtOO8/PtON1 RGB WOLED

3.6 OLED Fabrication and Characterization Methods Used in This Work

All WOLED devices in this work were fabricated by vacuum thermal evaporation and were bottom-emitting design. Most of the devices studied in this work were fabricated on glass substrates which had a previously-patterned anode layer of indium-tin oxide (ITO). Pixel area of these devices was $4mm^2$. Prior to deposition, the substrates were cleaned using a sequence of hand soap scrub then sonication in deionized water, acetone and isopropyl alcohol. Organic and cathode layers were deposited by vacuum thermal evaporation in a system from Trovato Manufacturing (Victor, NY), and all depositions were done at a pressure less than $5x10^{-7}$ Torr. Shadow masks were used to define the organic and metal layers without breaking vacuum between depositions. Film thicknesses and deposition rates were monitored using a quartz crystal microbalance. Organic materials were deposited at rates from 0.5 to 1.5 Å/s and LiF was deposited at ~0.2 Å/s. Al cathodes were deposited at 1 to 2 Å/s through a metal shadow mask, without breaking vacuum, to define device areas of $0.04cm^2$ in a crossbar structure. The devices were characterized by current-voltage-luminance measurements and electroluminescence (EL) measurements. Current-voltage-luminance data were collected using a Keithley 2400 sourcemeter, Keithley 6485 picoammeter and Newport 818-UV photodiode. Electroluminescence data of devices were taken using an Ocean Optics (Dunedin FL) HR4000 spectrometer. All electroluminescence spectra were taken at a current density of $1mA/cm^2$ unless otherwise noted. Electrical characterization was done in a dry nitrogen glovebox before doing the electroluminescence measurements in ambient environment.

The flexible full-color displays were fabricated on heat-stabilized Q65A PEN (polyethylene naphthalate) supplied by DuPont-Teijin Films. Prior to organic layer deposition, thin-film transistor (TFT) backplanes using amorphous indium gallium zinc oxide (IGZO) as the channel material for these displays were fabricated as described in previous publications[144,145]. The large-area displays were fabricated in a Sunic Sunicel 400 Plus deposition system (Sunic Systems, Korea). All layers were defined using shadow masks. The red, green and blue sub-pixels were fabricated using a fine-metal mask (FMM), while the other layers were patterned using large-area masks.

Optical characterization of the separate colors in the flexible display was performed using test diode structures with area of 0.05cm^2. The test diodes were encapsulated using a barrier film provided by 3M Company. Electroluminescence spectra were taken using an Ocean Optics HR4000CG spectrometer in ambient conditions. Luminance vs. voltage and current vs. voltage data were collected using a Newport Optics 818-UV photodiode and a Keithley 2400 source meter in ambient conditions. Threshold voltage, luminance and current efficiency were determined for each material before it was incorporated into the display.

All measurement techniques in this work were done in accordance with procedures described by Forrest et al.[146]

4: WOLED USING PLATINUM-BASED RED, GREEN AND BLUE EMITTERS

4.1 Introduction

Organic light emitting diodes using Pt-based red, green and blue dopants have been built for application to solid state lighting. All layers were deposited by thermal evaporation. Devices used a stacked design with separate red, green and blue layers. Blue devices achieved external quantum efficiencies of over 16% while devices with red / green / blue emissive layers reached quantum efficiencies of up to 15%, depending on the thickness of the red and green layers. We demonstrate an all-Pt based multiple emissive layer WOLED device.

The development of new emissive materials is essential to achieve improved device operational stability and device efficiency to compete with existing lighting technologies. Most of the research on organic materials for solid state lighting has focused on Ir-based phosphorescent emitters[92,147,148] These materials have demonstrated high efficiency, acceptable color rendering index (CRI) and color correlated temperature (CCT) which are necessary for commercial acceptance. Ir(III) compounds have distorted octahedral geometries, which generally have more-effective Spin-Orbit Coupling (SOC), with a resulting increase in radiative decay rates compared with square-planar compounds, such as those based on Pt(II)[110]**.** However, to broaden the material choices for efficient and stable emitters, it is necessary to develop new phosphorescent materials which do not use Iridium, one of the rarest elements in the earth's crust[149].

More recently, Pt-based emitter materials have been synthesized with radiative decay rates comparable to those based on Ir(III)[150,151,183]. Devices utilizing platinum-

based organic emitters have shown great promise as red, green, and blue emitters and have demonstrated high device efficiencies equivalent to or even superior to their Iridium analogs[152,153,154,155,156]. Due to their extended conjugation lengths, platinum (II) compounds have a strong tendency to form aggregates of interacting monomers, termed excimers, which can exhibit broad and red-shifted emission compared with the monomer[157, 158, 159]**.** This property has been utilized to fabricate white OLEDs using a single dopant,[160,161,162,163] but the lack of understanding of the excited state properties and the limitations on the molecular structure have hindered the development of stable and efficient excimer-based white devices. More recently, Fleetham and Li have reviewed the progress made in development of single-doped OLEDs utilizing excimer emitters; however, excimer emitter materials are still not as widely utilized as other device structures using monochrome emitters[130]. This chapter demonstrates the development of a multiple emissive layer WOLED device using all Pt-based red, green and blue emitters for efficient white lighting.

4.2 Experimental Conditions

The phosphorescent red emitter, PtON9-me was synthesized according to literature procedure[164]. The green phosphorescent emitter, PtOO3, and the blue phosphorescent emitter, PtOO2, were synthesized as in the previous literature report[156]. All chemical structures are shown in Figure 12. Furthermore, di-[4-(N,N-ditolyl-amino)-phenyl]cyclohexane (TAPC), 2,6-bis(N-carbazolyl) pyridine (26 mCPy)[151], diphenylbis(4-(pyridine-3-yl)phenyl)silane (DPPS)[165], and 1,3-bis(3,5-dipyrid-3-yl-phenyl)benzene (BmPyPB)[166] were all synthesized following previous

literature reports. Dipyrazino[2,3-f:2',3'-h]quinoxaline- 2,3,6,7,10,11-hexacarbonitrile (HAT-CN) was obtained from Lumtec, and N,N'-Bis(naphthalen-1-yl)-N,N'-bis(phenyl)-benzidine (NPB) was obtained from Chemical Alta. All materials were sublimed in a four zone thermal gradient furnace under high vacuum prior to use.

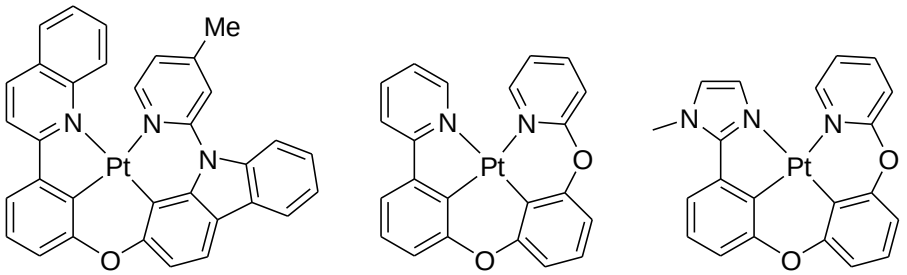

Figure 12. Molecular structure for the red, green, and blue phosphorescent emitters PtON9Me, PtOO3, and PtOO2 respectively.

Devices were fabricated by thermal evaporation in a system made by Trovato Manufacturing. All depositions were carried out at pressure below 5 x 10^{-7} Torr. Patterned indium-tin oxide (ITO) substrates were cleaned using a gentle scrub followed by successive sonication in water, acetone and isopropanol followed by a 15 minute UV-ozone treatment. Devices were fabricated in the structure: ITO/10nm HAT-CN/ 40nm NPD/10nm TAPC/6% PtON9me: 26mCPy(x nm)/6% PtOO3: 26mCPy(x nm)/ 6% PtOO2: 26mCPy(25nm)/10nm DPPS/30nm BmPyPB/LiF/Al where the thicknesses (x) of the red (PtON9Me) EML and the green (PtOO3) EML were varied from 0-3nm each. The devices were characterized by electroluminescence (EL) measurements and current-voltage-luminance measurements. Electroluminescence data were taken using

an Ocean Optics HR4000 spectrometer. Current-voltage-luminance data were taken using a Keithley 2400 sourcemeter, Keithley 6485 picoammeter and Newport 818-UV photodiode.

4.3 Results and discussion

Our approach to a WOLED used three emissive layers containing either red, green or blue emitters. It is imperative to have an efficient blue emitter with appropriate color to develop efficient white OLEDs with appropriate color and CRI. To measure the performance of each emitter, monochrome devices were made with each emitter to determine the device performance and emission characteristics from each individual dopant. Blue devices with the structure ITO/10nm HAT-CN/40nm NPD/10nm TAPC/6% PtOO2: 26mCPy(25nm)/10nm DPPS/30nm BmPyPB/1nm LiF/100nm Al were fabricated. Electroluminescence (EL) data were collected at current densities of 0.1, 0.5, 1 and 5 mA/cm^2 to see the effect on the emission spectrum.

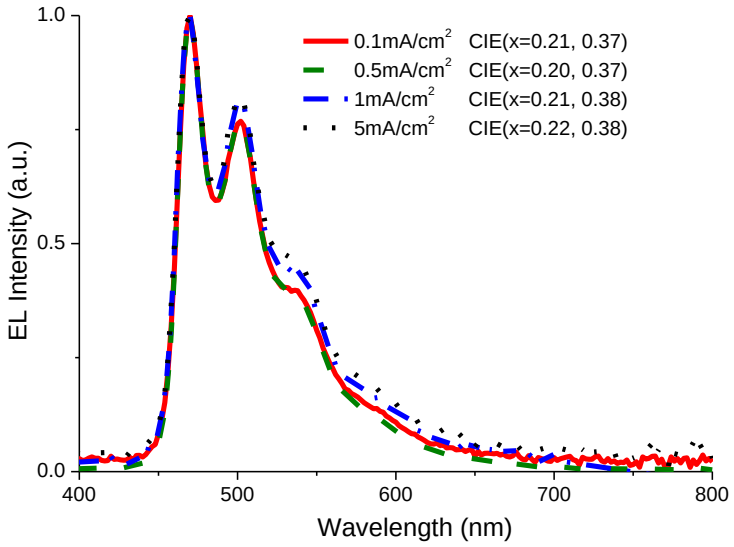

Figure 13: Normalized electroluminescence spectra for the blue device as a function of current density in the structure: ITO/10nm HAT-CN/40nm NPD/10nm TAPC/6% PtOO2: 26mCPy(25nm)/10nm DPPS/30nm BmPyPB/1nm LiF/100nm Al

The EL spectra shown in Figure 13 exhibit a primary emission peak at 470nm, with vibronic peaks at 500nm and 534nm that provide a broad emission spectrum characteristic of many platinum emitters. This provides a sky-blue color that, while not appropriate for display applications, can yield strong performance as a component in WOLEDs for solid state lighting applications. It is worth noting that at higher dopant concentrations (not shown) no excimer formation was observed. As the current density is increased, the peak intensities at 500nm and 534nm show only slight increases relative to the 470 nm peak, displaying exclusive emission and relatively good color stability across this range. Devices with 6% PtOO2 exhibited reasonable device performance of 16.4% peak EQE as shown in Figure 14 and summarized in Table 6.

Table 6: Device characteristics at 100 and 1000 cd/m^2 for devices with 0nm, 1nm, 2nm and 3nm red and green emissive layers in the structure ITO/10nm HAT-CN/ 40nm NPD/10nm TAPC/6% PtON9me:26mCPy(x nm)/6% PtOO3:26mCPy(x nm)/6% PtOO2:26mCPy(25nm)/10nm DPPS/30nm BmPyPB/1nm LiF/100nm Al

R & G EML (nm)	CIE (x,y)[a]	CRI	ηEQE (%)	ηA (cd/A) 100 cd/m2	ηP (lm/W)	ηEQE (%)	ηA (cd/A) 1000 cd/m2	ηP (lm/W)
1	(0.28, 0.42)	62	13.4	28.3	22.9	9.8	18.0	13.7
2	(0.33, 0.42)	73	13.0	26.0	20.8	10.2	25.3	13.3
3	(0.35, 0.41)	77	11.7	19.0	17.3	8.5	13.0	10.6
0	(0.21, 0.38)	44	14.1	32.8	24.5	8.7	10.2	14.2

[a] CIE and CRI were measured at j = 1 mA/cm^2

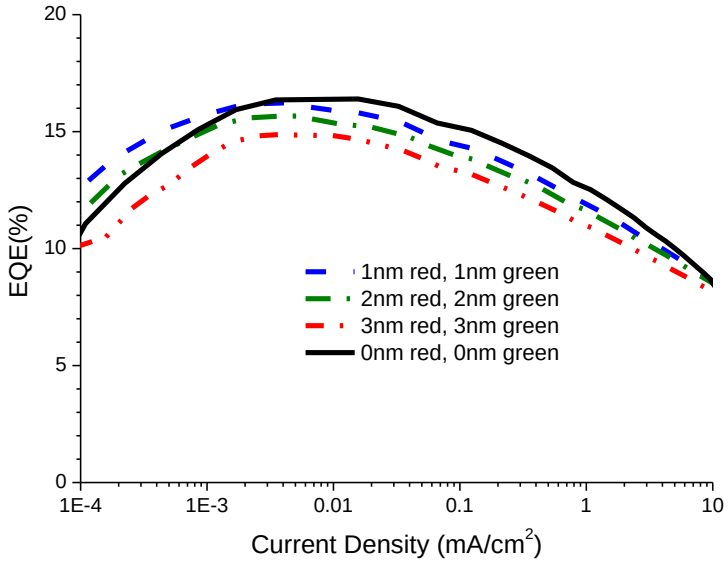

Figure 14: External quantum efficiency as a function of current density for devices with 0nm, 1nm, 2nm and 3nm red and green emissive layers in the structure ITO/10nm HAT-CN/ 40nm NPD/10nm TAPC/6% PtON9me:26mCPy(x nm)/6% PtOO3:26mCPy(x nm)/6% PtOO2:26mCPy(25nm)/10nm DPPS/30nm BmPyPB/1nm LiF/100nm Al

The stable and efficient emitter PtON9-me was chosen as the red emitter for these WOLED devices[167]. Devices for efficiency measurement were fabricated with the structure ITO/HATCN(10nm)/NPD(40nm)/TAPC(10nm)/PtON9me:CBP(2%)(25nm)/ DPPS(10nm)/BmPyPB(40nm)/LiF(1nm)/Al(100nm), and denoted structure I. NPD and

BmPyPB were chosen due to their relatively high hole and electron mobility, respectively[168].

TAPC and DPPS were used as exciton confinement layers, due to their high triplet energies of 2.7 and 2.87 eV, respectively. The deep HOMO level of DPPS (6.5 eV) confines holes to the emissive layer. This structure exhibited exclusive emission from the PtON9-me due to the exciton confinement[169]. A maximum EQE of 12.4% was achieved with this structure, denoted structure I, as shown in Figure 15.

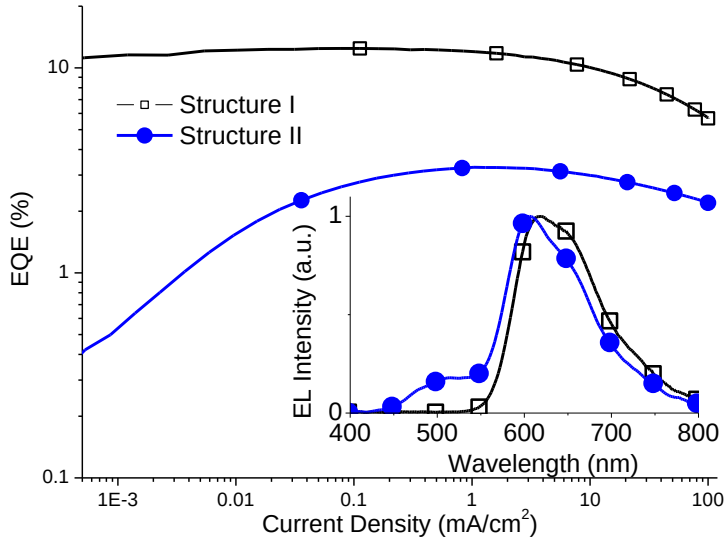

Figure 15: The normalized EL spectra (inset) and the external quantum efficiency-versus current density for PtON9-me in Structure I (open squares): ITO/HATCN(10nm) /NPD(40nm)/TAPC(10nm)/2% PtON9-me:CBP(25nm)/DPPS(10nm)/BmPyPB(40nm)/ LiF(1nm)/Al(100nm) and structure II (closed circles): ITO/HATCN(10nm)/NPD(40nm)/ 2% PtON9-me:CBP(25nm)/BAlq(10nm)/Alq(30nm)/LiF(1nm)/ Al(100nm).

Although devices using DPPS, TAPC and BmPyPB exhibited good efficiency, the operational lifetimes were low due to the electrochemical instability of these materials[170]. Therefore, a stability structure, denoted structure II, of ITO/HATCN(10nm)/NPD(40nm)/

2% PtON9-me:CBP(25nm)/BAlq(10nm)/Alq(30nm)/LiF(1nm)/Al(100nm), where BAlq is 4-biphenyloxolatoaluminum(III)bis(2-methyl-8-quinolinato)4-phenylphenolate, was fabricated due to its demonstrated high operational lifetimes[171]. The 10nm TAPC layer was omitted and the DPPS layer was replaced with BAlq, which has been shown to produce stable and efficient red phosphorescent OLEDs[171]. The 40nm BmPyPB ETL layer was replaced with a 30nm Alq layer. As shown in Figure 15, the EL spectra of devices with this structure showed non-exclusive emission from PtON9-me with an additional peak at ~525nm from Alq emission, likely due to poor exciton confinement in the emissive layer. The EQE dropped to 3.3% as a result. The non-exclusive emission was attributed to the low triplet energy of BAlq (2.2 eV)[172] This leads to a possibility of exciton migration out of the EML when the dopant concentration is low, since triplet excitons might migrate out of the EML before they are trapped on the dopant molecules[173].

Charge balance must be improved to eliminate non-exclusive emission. This can be achieved by increasing the dopant concentration[174]. Devices with EML dopant concentrations of 6, 10 and 20% in the device structure ITO/HATCN(10nm)/NPD(40nm)/x% PtON9-me:CBP(25nm)/BAlq(10nm)/Alq(30nm)/ LiF(1nm)/Al(100nm) were fabricated to test the influence of dopant concentration. The electroluminescence and EQE data for these devices are shown in Figure 16.

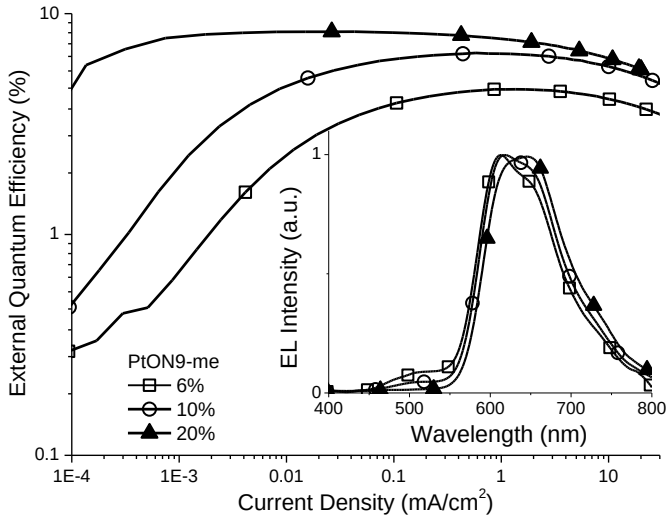

Figure 16: The normalized EL spectra (inset) and the external quantum efficiency-versus current density for PtON9-me in device Structure II: ITO/HATCN(10nm)/NPD(40nm)/x% PtON9-me:CBP(25nm)/BAlq(10nm)/Alq(30nm)/ LiF(1nm)/Al(100nm) for 6% (open squares), 10% (open circles), and 20% (solid triangles) PtON9-me concentration in CBP.

Increasing the concentration to 10% reduced the intensity of the 525nm emission. Increasing the dopant concentration further to 20% eliminated the non-exclusive emission and resulted in higher EQE compared with the devices with lower dopant concentrations. Maximum forward viewing EQE values of 4.5%, 6.1% and 8.3% were observed for the devices with 6%, 10% and 20% dopant concentration, respectively.

The device operational lifetime of PtON9-me was examined using the optimized structure II with PtON9-me concentration of 20%. Luminance vs time data were acquired under accelerated conditions using a constant driving current density of 20 mA/cm^2. The devices were operated under steady-state conditions until a final luminance equal to 97%, or $T_{0.97}$, of the initial luminance value was reached. The initial luminance value L_0 at 20 mA/cm^2 for the structure II device was 1104 cd/m^2 with a $T_{0.97}$ value of 26.3 h. The

lifetime $T_{0.97}$ for the device at an initial luminance L_1 of 100 cd/m^2 was determined using the relationship from Féry et al.[175]:

$$T_{0.97}(L_1) = T_{0.97}(L_0)\ (L_0/L_1)^{1.7} \qquad (17)$$

and yielded $T_{0.97}$ = 1560 h for this device. For comparison, devices were also made using the well-known emitter iridium(III) bis(2-phenyl quinolyl-N,C$^{2'}$)acetylacentonate (PQIr) in structure II[171]. These devices exhibited L_0 = 2400 cd/m^2 and $T_{0.97}$ = 8.2 h. Dopant concentration was 20% for the PQIr device as well. The $T_{0.97}$ lifetime for the PQIr device at initial luminance L_1 of 100 cd/m^2 was 1776 h. The PtON9-me device exhibited a luminance decay of $0.9L_0$ at 246 h at a drive current density of 20 mA/cm^2. The lifetime results are shown in Figure 17.

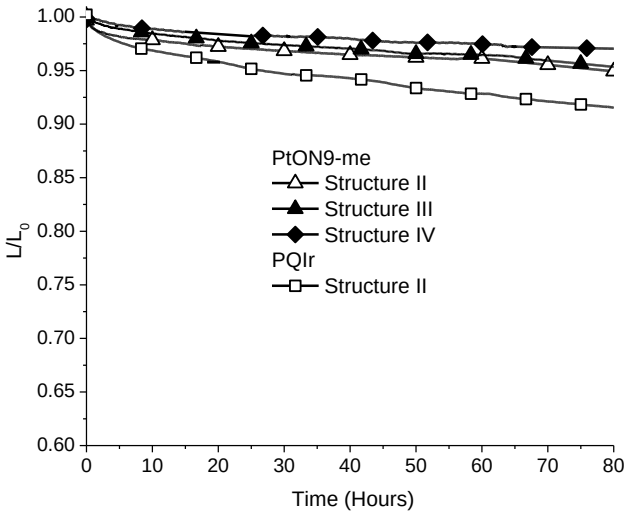

Figure 17: Normalized luminance vs. time under constant direct current of 20 mA/cm^2 for devices of PtON9-me in Structure II, (open triangles), Structure III (solid triangles), and Structure IV (solid diamonds). The Normalized Luminance vs. time for devices of PQIr in structure II (open squares) is shown for comparison.

Use of a cohost structure combining a hole transporting material and an electron transporting material in the emissive layer has been shown to improve the operational lifetime in some cases due to improved charge balance and emission zone broadening[176,177]**.** Therefore, devices using a cohost structure, denoted structure III, of ITO/HAT-CN(10nm)/NPD(40nm)/20%PtON9me:CBP:BAlq(25nm)/ BAlq(10nm)/Alq(30nm)/LiF(1nm)/Al(100nm) with a 1:1 CBP:BAlq ratio. This structure yielded a device with $T_{0.97}$ = 42 h at L_0 = 1200 cd/m^2, corresponding to $T_{0.97}$ = 2870 h at 100 cd/m^2. Further lifetime improvement was achieved using structure IV consisting of ITO/HATCN(10nm)/NPD(40nm)/6%PtON9me:mCBP:BAlq[1:1](25nm)/BAlq(10nm)/ Alq(30nm)/LiF(1nm)/Al(100nm). Use of mCBP in the cohost produced an estimated lifetime $T_{0.97}$ = 3112 h at 100 cd/m^2. These results are summarized in .

Table 7.

Table 7: A summary of device characteristics of PtON9-me in the 4 different red device structures. Device characteristics for a device made with the emitter PQIr are shown for comparison.

Type	Emitter	CIE	EQE Peak (%)	EQE at 100 cd/m^2	L_0[b] (cd/m^2)	EQE[b] (%)	$T_{0.97}$[b]	$T_{0.97}$[c] at 100 cd/m^2
I	PtON9-me 2%	0.63,0.36	12.5	12.1	1942	9.0	a	a
II	PtON9-me 2%	0.54,0.40	3.3	3.3	904	2.8	a	a
II	PtON9-me 6%	0.59,0.38	4.5	4.5	980	3.7	a	a
II	PtON9-me 10%	0.61,0.37	6.3	6.2	1150	5	a	a
II	PtON9-me 20%	0.61,0.36	8.3	7.5	1104	5.6	26.2	1560
III	PtON9-me 20%	0.61,0.36	8	7.4	1200	5.6	42	2870
IV	PtON9-me 6%	0.6,0.36	4.7	4.6	902	3.9	74	3112
II	PQIr 20%	0.66.0.34	7.7	7.4	2400	7.4	8.2	1776

a: Operational lifetime was only determined for electrochemically stable device architectures and for devices which exhibited exclusive dopant emission
b: Device characteristics at j = 20 mA/cm^2
c: Device operational lifetime estimated using the relationship $T_{0.97}(L_1) = T_{0.97}(L_0)(L_0/L_1)^{1.7}$ [175]

Detailed synthesis methods, photophysical properties and device results for PtOO3 were reported by Turner et al. in a previous publication[154]. Quantum efficiency vs current density and EL date for monochrome devices made with PtOO3 with the structure ITO/PEDOT:PSS/TAPC/26mCPy:emitter(8%)/PO15/BmPyPB/LiF/Al are shown in Figure 18. Results for a device made using the stable green emitter $Ir(ppy)_3$ using the same structure are included for comparison.

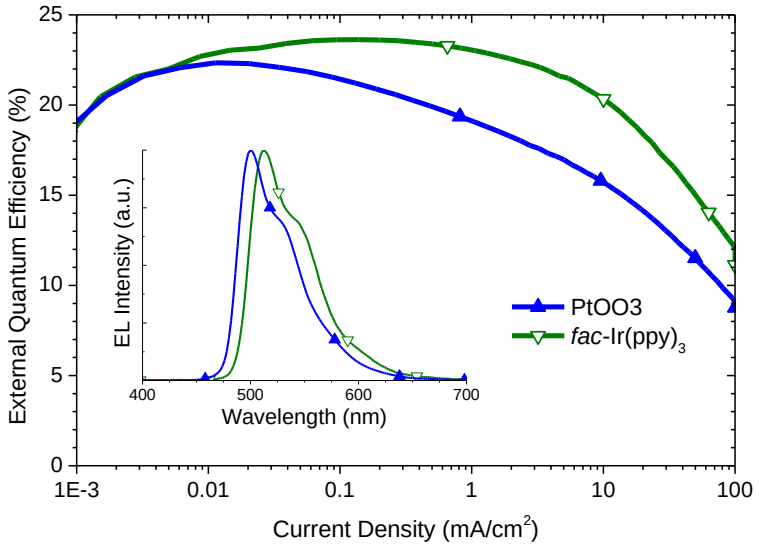

Figure 18: Quantum efficiency-current density characteristics of PtOO3 and *fac*-Ir(ppy)$_3$ devices with the structure of ITO/PEDOT:PSS/TAPC/26mCPy:emitters(8%)/PO15/BmPyPB/LiF/Al. Inset shows the EL spectra of the PtOO3 and *fac*-Ir(ppy)$_3$ devices

Devices made with PtOO3 exhibited a maximum external quantum efficiency of 22.3%, although the EQE drops off rapidly as current density is increased. This droop in efficiency has been attributed to charge imbalance at higher current densities[94,178,179]. After determining the characteristics of the individual emitters, WOLED devices with different thicknesses of the red and green emissive layers were fabricated to determine the effect of red and green emissive layer thickness on the CIE color coordinates of the complete device. The thickness of the blue emissive layer was fixed at 25nm for all devices. Electroluminescence data were collected for each device at a fixed current density of 1 mA/cm^2 to see the effect of changing the red and green emissive layer thicknesses. The normalized spectra are shown in Figure 19. The devices with a green emissive layer show a more intense peak at 500nm compared with the blue device, due

to the contribution from the green emissive layer. However, the intensity of the 500nm peak stays constant even as the thickness of the green emissive layer increases. The intensity of the red emissive layer contribution at ~610nm, however, continues to increase as the red emissive layer thickness increases. A warm white color was achieved with CIE (0.35, 0.41) with CRI 77 for devices with 3nm each of the red and green emissive layers. The primary reason attributed to the large increase in red emission while only minimal increase in emission from the green emissive layer is that exciton formation in the host material primarily occurs at the host blocker interface where there is a buildup of injected charges[92]. Thus, PtON9-me emission increases as the layer thickness is increased but the green layer emission is nearly constant. To further illustrate this point, the electroluminescence spectra were collected for the device with 3nm thick red and green EMLs at different current densities. In Figure 20, it is apparent that once the current density exceeds 5mA/cm^2 the charge balance shifts, leading to an increased green emission with a concurrent decrease in red emission. The EL spectra showed little change in relative intensities as the current density increased, and the CRI ranged from 72 to 77.

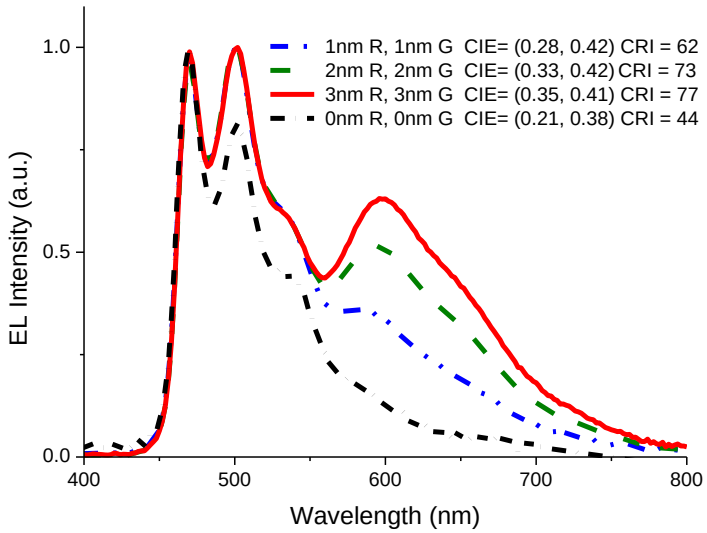

Figure 19: Normalized electroluminescence spectra for devices with 0nm, 1nm, 2nm and 3nm red and green emissive layers at 1mA/cm^2 for devices with the structure: ITO/10nm HAT-CN/40nm NPD/10nm TAPC/6% PtON9me: 26mCPy(x nm)/6% PtOO3: 26mCPy(x nm)/6% PtOO2: 26mCPy(25nm)/10nm DPPS/30nm BmPyPB/LiF/Al

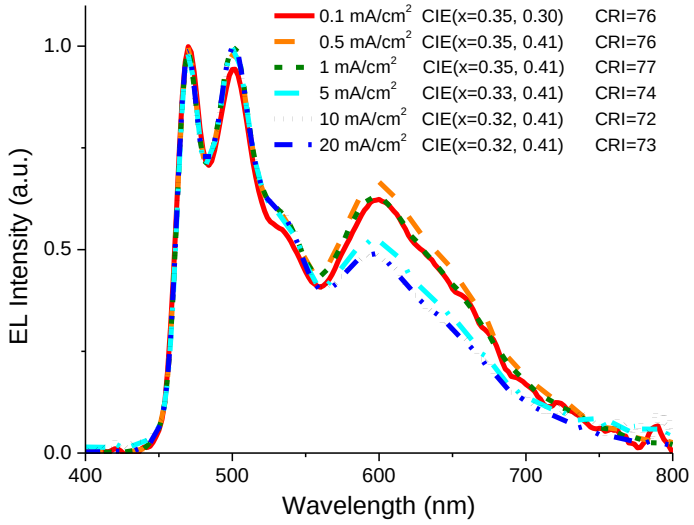

Figure 20: Normalized electroluminescence spectra as a function of current density for devices with the structure: ITO/10nm HAT-CN/40mn NPD/10nm TAPC/6% PtON9me: 26mCPy(3nm)/6% PtOO3: 26mCPy(3nm)/6% PtOO2: 26mCPy(25nm)/10nm DPPS/30nm BmPyPB/LiF/Al

The performance of the various devices at 100 cd/m^2 and 1000 cd/m^2 was shown previously in Table 6 and the external quantum efficiency was given in Figure 14. The blue device had the highest peak quantum efficiency of 16.4%. The peak quantum efficiency decreased as the thickness of the red and green layers increased. This slight decrease in peak EQE can be attributed to slightly lower quantum efficiency of the PtON9-me emitter relative to the PtOO2 emitter. The device with 3nm thick red and green layers had the best white color and had a peak quantum efficiency of 14.9% with a slight roll off to 11.7% at 100cd/m^2. The power conversion efficiency was 17.3 lm/W at 100 cd/m^2. Thus, while the EQE is comparable to many Iridium based white OLEDs, the power efficiency is much lower because of a high turn on voltage of the selected device structure[147,148].

4.4 Conclusion

White OLEDs using Pt-based red, green and blue emitters were fabricated. A monochrome blue device using the emitter PtOO2 had an EQE as high as 16.4%. The red and green emissive layer thicknesses in a white OLED structure were varied to see the effect on the electroluminescence spectra. The red and green EML thicknesses were equal in each different structure. The intensity in the red portion of the spectrum increased with increasing red EML thickness, but the intensity in the green part of the spectrum remained unchanged. The device with 3nm thick red and green EMLs had the best white color, with a CRI of 77 at a current density of 1mA/cm^2. This device showed peak efficiency near 15% with low efficiency roll-off. These results show that

tetradentate Pt-based emitters can be used to make white OLEDs for lighting applications. Improvements in emitter efficiency, emission spectrum and device structure should lead to continued progress in quantum efficiency, power efficiency and CRI.

5: WOLED USING RED AND BLUE PLATINUM EMITTERS

5.1 Introduction

Platinum-based blue and red emitters were used to make stacked organic light emitting devices for potential use in solid state lighting. The electroluminescence spectra were strongly dependent on the red layer thickness and relative position of the red and blue emissive layers. Although all devices had very little electroluminescence in the green region, a color rendering index as high as 65 was achieved. Addition of a suitable phosphorescent green emissive layer should produce higher color rendering index values. All devices tested exhibited external quantum efficiencies greater than 20%, indicating that the Pt-based emitters reported here are potentially useful for solid state lighting applications.

Rising worldwide energy demand and limited supply of traditional energy sources have spurred research in alternative energy generation methods and improving energy efficiency for existing applications. Lighting, which by some estimates accounts for 20% of electrical energy consumption, is one major field targeted for improved energy efficiency[42]. In fact, one United States Department of Energy (USDOE) estimate predicts that increased use of solid-state lighting could halve the domestic lighting energy demand by 2030, saving up to 395 terawatt-hours (TW-h) of energy and saving up to $40B[46]. Current lighting sources primarily employ either short lasting, inefficient incandescent bulbs or fluorescent lighting which contain hazardous materials such as mercury that complicates their disposal. Solid-state approaches using inorganic or organic materials are becoming increasingly studied due to their potential to produce light much more

efficiently, with longer operational lifetime, while using environmentally benign materials[180]. Inorganic lighting sources have reached laboratory power efficiencies greater that 250 lm/W and have been commercially available since 2008[181]. However, the cost of these sources remains high and fabrication limitations may prohibit production on a large enough scale to replace all the current incandescent and fluorescent bulbs. Organic lighting sources have been proposed as an alternative solid state lighting source due to potentially low cost fabrication processes, the ability to be deposited on a wide array of inexpensive substrates in numerous unique form factors, and their ability to be easily color tuned [48,192]. Furthermore, white organic light emitting diodes (WOLEDs) have demonstrated efficiencies exceeding fluorescent light[54]. However, more work is needed to meet commercial needs and be competitive with the efficiency and stability of inorganic solid state lighting or the cost effectiveness of fluorescent lighting.

Stable and efficient emitters are vital to develop in order to achieve mass production of WOLEDs for solid state lighting. A large number of efficient red, green, and blue OLEDs have been reported based on phosphorescent complexes due to their ability to harvest up to 100% of electrogenerated excitons[112]. However, the development of stable and efficient white devices remains a challenge[182]. Most of the phosphorescent emitters for WOLEDs have focused on Ir-based compounds due to their high efficiencies, well studied photo- physical properties, and demonstrated stability across a wide range of the visible spectrum[80,147,]. Recently, platinum-based emitters have demonstrated efficiencies that are similar or superior to their iridium analogs and are receiving increased interest[154,183]. This chapter describes the development of novel Pt compounds as red-

orange and blue emitters for application to solid-state lighting, along with the performance of WOLEDs incorporating these materials.

5.2 Experimental Conditions

Dipyrazino[2,3-f:2',3'-h]quinoxaline- 2,3,6,7,10,11-hexacarbonitrile (HATCN) was obtained from Lumtec and N,N'-Bis(naphthalen-1-yl)-N,N'-bis(phenyl)-benzidine (NPD) was obtained from Chemical Alta. Di-[4-(N,N-ditolyl-amino)-phenyl]cyclohexane (TAPC)[177], 2,6-bis(N-carbazolyl) pyridine (26mCPy)[151], diphenylbis(4-(pyridine-3-yl)phenyl)silane (DPPS)[165], 1,3-bis(3,5-dipyrid-3-yl-phenyl)benzene (BmPyPB)[166], and PtON1 (shown in Figure 1)[155] were prepared following previous literature procedures. All organic materials were sublimed in a thermal gradient furnace prior to use. PtON1 and PtN3N-ptb synthesis was conducted as described in previous literature reports[155,184]. The room temperature photoluminescence spectra and structures of PtON1 and PtN3N-ptb are given in Figure 21.

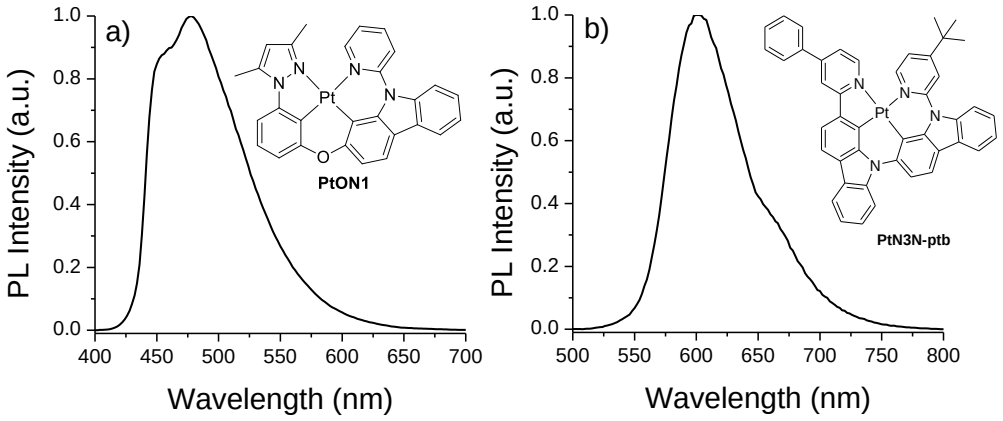

Figure 21: Room temperature photoluminescence emission spectra of a) PtON1 and b) PtN3N-ptb in a dilute solution of CH_2Cl_2 with molecular structures shown in inset.

Devices were fabricated on glass substrates with previously patterned indium tin oxide (ITO) which formed the anode. Prior to deposition, the substrates were cleaned using a sequence of hand soap scrub then sonication in deionized water, acetone and isopropyl alcohol. Organic and cathode layers were deposited by vacuum thermal evaporation in a system from Trovato Manufacturing (Victor, NY), and all depositions were done at a pressure less than $5x10^{-7}$ Torr. Film thicknesses and deposition rates were monitored using a quartz crystal microbalance. Organic materials were deposited at rates from 0.5 to 1.5 Å/s and LiF was deposited at ~0.2 Å/s. Al cathodes were deposited at 1 to 2 Å/s through a metal shadow mask, without breaking vacuum, to define device areas of $4mm^2$ in a crossbar structure. The devices were characterized by current-voltage-luminance measurements and electroluminescence (EL) measurements. Current-voltage-luminance data were collected using a Keithley 2400 sourcemeter, Keithley 6485 picoammeter and Newport 818-UV photodiode. Electroluminescence data were taken using an Ocean Optics (Dunedin FL) HR4000 spectrometer. All electroluminescence spectra were taken at a current density of $1mA/cm^2$ unless otherwise noted. Electrical characterization was done in a dry nitrogen glovebox before doing the electroluminescence measurements in ambient environment.

5.3 Results and Discussion

Two tetradentate Pt emitters were selected for use in WOLED devices: PtN3N-ptb (red), and PtON1 (blue) due to their complementary emission spectra shown in Figure 22. Monochrome devices of these emitters were fabricated to determine the current-voltage-luminance and external quantum efficiency (EQE) of each emissive layer. The

device structure was as follows: ITO/HAT-CN (10 nm)/NPD (40 nm)/TAPC (10 nm)/EML (x% emitter:26mCPy (25 nm)/DPPS (10 nm)/BmPyPB (40 nm)/LiF (1 nm)/Al (100 nm). The blue dopant was PtON1 and the red dopant was PtN3N-ptb. Dopant concentration was 6% PtON1 for the blue in order to optimize the EQE following the previous literature report[155] [1]. Red devices, however, were fabricated with dopant concentrations of both 2% PtN3N-ptb and 6% PtN3N-ptb in order to see the effect of dopant concentration on both the EL spectrum and the EQE. Electroluminescent emission (EL) spectra were collected at a current density of 1 mA/cm^2. The results are summarized in Figure 22.

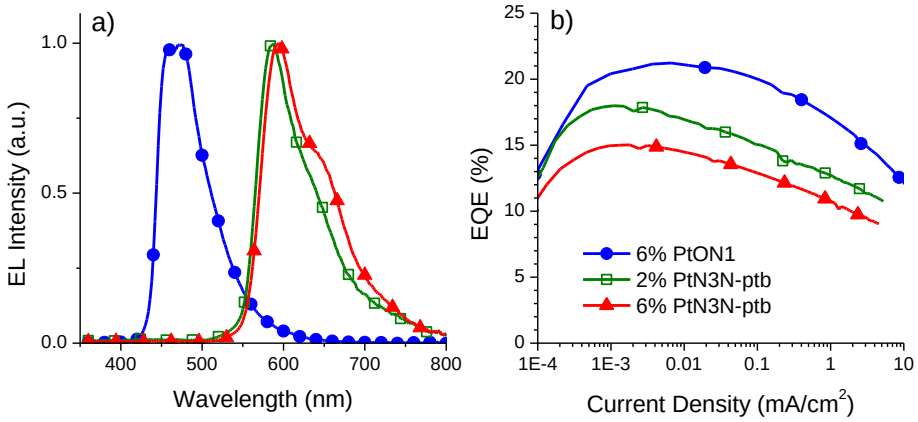

Figure 22. a) Electroluminescence spectra at 1mA/cm^2 and b) external quantum efficiency vs. current density for devices in the structure: ITO/HATCN/NPD/TAPC/EML/DPPS/BmPyPB/LiF/Al where EML is 6% PtON1:26mCPy(25nm) (circles), 2% PtN3N-ptb:26mCPy(25nm) (squares), or 6% PtN3N-ptb:26mCPy(25nm) (triangles)

The blue device demonstrated strong deep blue emission between 450nm and 500nm, like previously reported values, and should yield appropriate breadth of emission to achieve high Color Rendering Index (CRI)[155]. Furthermore, the blue device was very

efficient with a maximum EQE of 21.2 %. The 2% PtN3N-ptb doped device had λ_{max} at 588 nm but with a sharp drop off in emission intensity beyond 600nm, yielding Commission Internationale de l'Eclairage (CIE) coordinates of (0.57, 0.42). The 6% PtN3N-ptb doped device was slightly red-shifted with λ_{max} at 594 nm and an elevated shoulder around 650nm yielding slightly improved CIE coordinates of (0.59, 0.40). However, this improved color is accompanied by a significant drop in device performance with peak EQE of 15.0% compared to 18.0% for devices with 2% PtN3N-ptb. The reasons for this drop off in efficiency may be related to charge imbalance and triplet-triplet annihilation processes at the higher dopant concentration, but will require more study to determine which factors affect the efficiencies in these red emitting devices[185].The high efficiencies of both the blue and red emitters and the complementary nature of their emission spectra make them good candidates for the fabrication of simple two layer white OLEDs employing platinum emitters. Furthermore, such a simple structure will elucidate the energy transfer and emission processes within the device to give a clear understanding of the optimal device design.

WOLEDs employing two emissive layers (EML) were made using the blue and red emitters in the structure: ITO/HAT-CN (10 nm)/NPD (40 nm)/TAPC (10 nm)/EML1 (6% emitter: 26mCPy (x nm)/ EML2 (6% emitter:26mCPy (y nm)/DPPS (10 nm)/BmPyPB (40 nm)/LiF (1 nm)/Al (100 nm). A doping concentration of 6% was chosen for the red EML, despite the slightly lower EQE than the 2% red device, since the slight red shift and the more pronounced shoulder were expected to produce WOLEDs with higher CRI. Two structures for the white devices were tested to explore the nature of

exciton formation and energy transfer within the devices: one with an EML composed of a red emissive layer followed by a blue emissive layer, denoted R/B, and another structure with blue emissive layer followed by a red emissive layer which is denoted as B/R. Schematic diagrams of the devices with EMLs in the order R/B and B/R are shown in Figure 23.

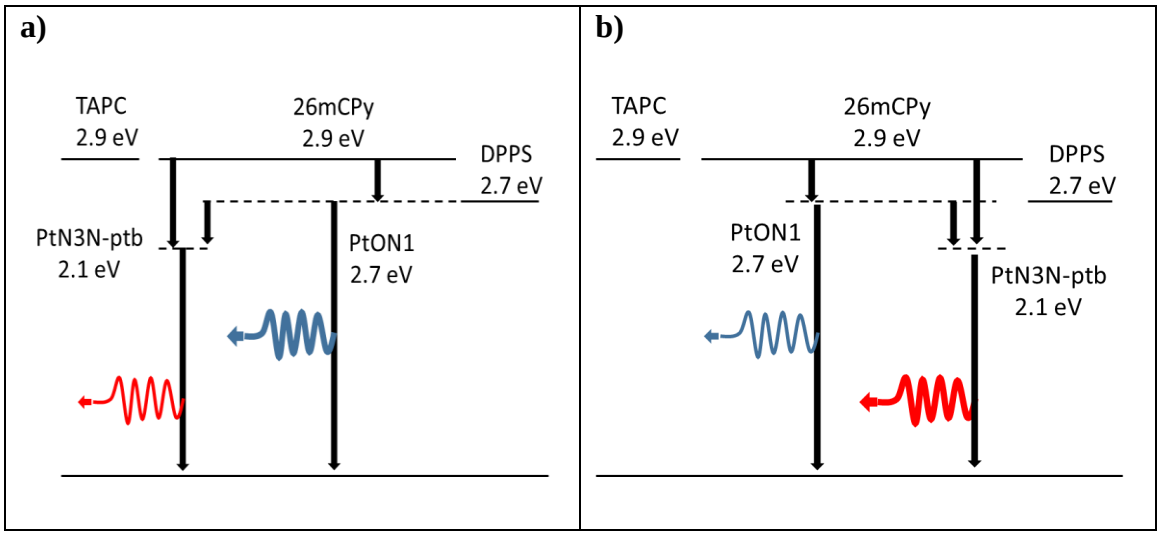

Figure 23: Schematic of the various energy transitions for devices with the structure a) R/B EML and b) B/R EML

The blue emissive layer thickness was fixed at 20 nm for all devices, while the red EML thickness was set at either 2 nm or 3 nm. The red layer is kept very thin to balance the emission by accounting for favorable energy transfer to the red dopant molecules from other regions of the device as has been documented in various literature reports[133] The results are shown in Figure 24 and a summary of CIE and CRI values and efficiency data is presented in Table 8.

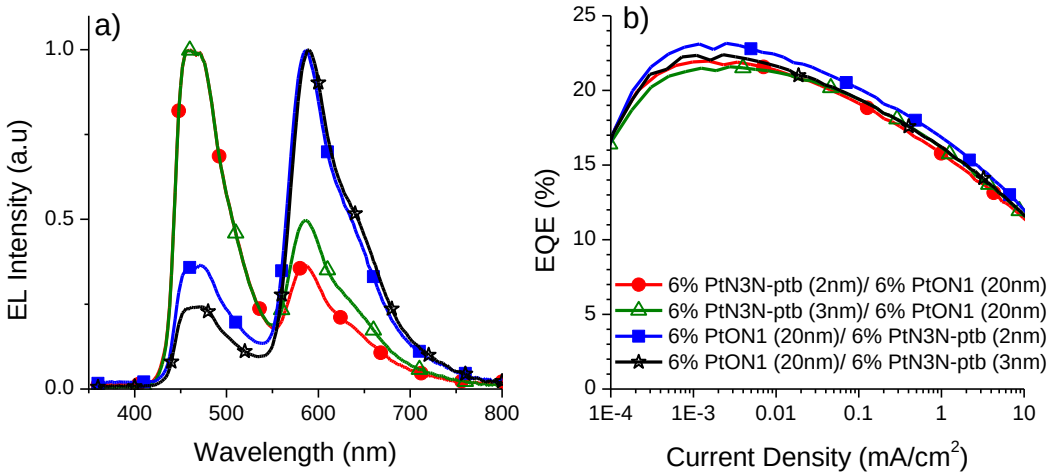

Figure 24. a) Electroluminescent spectra at 1mA/cm^2 and b) external quantum efficiency vs. current density for the devices in the structure: ITO/HATCN/NPD/TAPC/EML/DPPS/BmPyPB/LiF/AL where EML is 6% PtN3N-ptb(2nm)/6% PtON1(20nm) (circles), 6% PtN3N-ptb(3nm)/6% PtON1(20nm)(triangles), 6% PtON1(20nm)/6% PtN3N-ptb(2nm)(squares), or 6% PtON1(20nm)/6% PtN3N-ptb (3nm)(stars)

Table 8. CIE and CRI Values by Device Structure for Red/Blue and Blue/Red WOLEDs

Structure	CIE‡	CRI ‡	100 cd/m^2			1000 cd/m^2		
			η_{EQE} (%)	η_A (cd/A)	η_P (lm/W)	η_{EQE} (%)	η_A (cd/A)	η_P (lm/W)
2nm R / 20nm B	(0.25, 0.25)	--	16.5	29.4	18.5	12.2	22.0	11.0
3nm R / 20nm B	(0.28, 0.26)	65	18.0	31.6	19.5	13.6	24.0	11.8
20nm B / 2nm R	(0.45, 0.36)	56	18.8	39.8	25.0	14.5	30.8	15.4
20nm B / 3nm R	(0.49, 0.37)	50	18.1	36.0	21.7	13.8	27.6	13.0

‡ Electroluminescence spectra data collected at 1mA/cm^2

One major drawback the multiple emissive layer structure is the relatively poor color stability with changing driving conditions as a result of shifting or spreading the primary recombination zone. As an example, the dependence of the EL spectrum on current density for the device ITO/HATCN (10 nm)/NPD (40 nm)/TAPC (10 nm)/(6% PtON1: 26mCPy (20 nm)/ (6% PtN3N-ptb:26mCPy (3 nm)/DPPS (10 nm)/BmPyPB (40 nm)/LiF (1 nm)/Al (100 nm) is given in Figure 25. As the current density increases, the ratio of blue to red emission increases by nearly 500%. Consequently, the devices exhibit significant color shift within the current density range of 0.1mA/cm^2 to 10mA/cm^2 with CIE coordinates ranging from (0.54,0.39) to (0.45,0.35), respectively. More work is needed to develop better charge transport materials and to optimize device architectures to reduce this strong driving condition dependence.

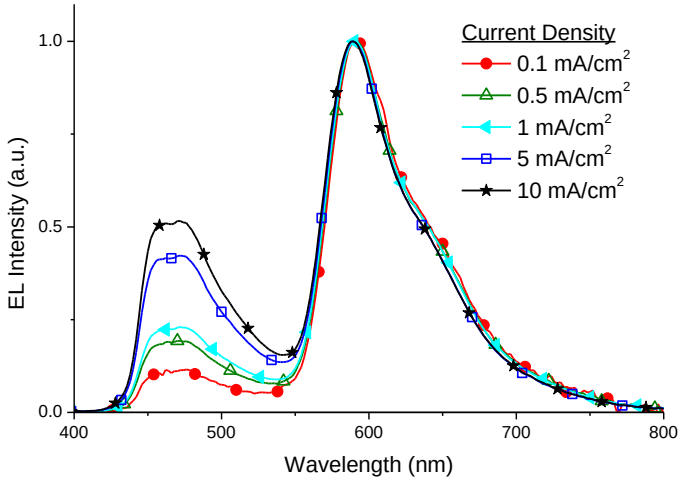

Figure 25. Electroluminescent spectra vs. current density for the device: ITO/HATCN/NPD/TAPC/6% PtON1(20nm)/6% PtN3N-ptb(3nm)/DPPS/ BmPyPB/LiF/Al.

5.4 Conclusion

This work demonstrated for the first time that a WOLED with EQE over 20% can be fabricated using exclusively Pt-based emitters. Blue and red emitters were used to fabricate devices with emitters in the order of blue/red or red/blue to compare the effect of emitter order on the electroluminescence spectra. Devices with the structure [hole transport layer/electron blocking layer/red emissive layer/blue emissive layer/hole blocking layer] had dominant emission in the blue part of the spectrum, while devices with the layer order reversed had dominant emission in the red portion of the spectrum. These results confirmed that most excitons are generated at in the interface of the layer closest to the hole blocker and the hole blocker layer. A CRI as high as 65 was obtained with the emitter of [3nm red/20nm blue]. The CRI was limited by insufficient emission in the green part of the spectrum, and should improve with the addition of a green emissive layer. This work is discussed in the next chapter.

6: PLATINUM-BASED WOLED USING IMPROVED RED, GREEN AND BLUE EMITTERS FOR HIGHER EFFICIENCY AND HIGHER CRI

6.1 Introduction

Solid-state lighting technologies which are efficient, long-lasting, and made from environmentally benign materials are being developed to reduce energy consumption. White Organic light-emitting devices (WOLEDs) are promising because they can be fabricated on a variety of substrate materials to produce large-area panels, curved panels, and lightweight, rugged flexible displays. Organic-based devices can be made using vapor deposition, inkjet printing and solution-processing techniques which can enable high-throughput production, and thus have the potential for mass production and low cost[186,187]. Widespread research in the design of new emissive materials, device architectures, and outcoupling techniques has produced WOLEDs exceeding 100 lm/W with a high color quality of light[188].

Two parameters describe the color quality of a white light source: Commission Internationale de l'Éclairage coordinates (CIE) and the Color Rendering Index (CRI) value, where CIE coordinates of (0.33, 0.33) is considered “pure white” and a CRI value as close to 100 as possible is desired[189,190]. As discussed in Chapter 3, there are numerous approaches to achieve high color quality white organic light emitting diodes. Some of these are i) double- or triple-doped multiple emissive layers; ii) separate layers of monochrome emitters, e.g. red, green and blue; iii) striped regions of red, green, and blue emission, iv) use of a blue emitter with down-conversion phosphor; and v) the combination of monomer and excimer emission from square planar metal

complexes[191,192,193,194,195]. Of these options, the combination of three emissive dopants has typically been favored due to the relative ease of obtaining a broad spectrum of high-quality white light by controlling the relative contribution. The use of multiple emissive layers (EMLs) to separate the red, green and blue emissive dopants has seen success in minimizing interaction between emitters to achieve balanced color quality and high efficiencies[134,54]. However, the efficiency, color quality, and stability of these devices are still far from commercial application[54,195,196,197,198,199]. Improved device architectures as well as improved emitter materials must be achieved to produce commercially viable WOLEDs for lighting.

The earliest report of triplet harvesting to enable phosphorescent emission was reported with the platinum compound PtOEP[112]. This group was able to achieve external quantum efficiencies of up to 4%. They were able to increase the EQE to 5.6% through use of a more suitable host and a hole blocking layer[200] However, subsequent research produced much higher quantum efficiency using the iridium compound $Ir(ppy)_3$, and much of the research into emissive materials since then has focused on iridium-based complexes, for which external quantum efficiencies of 25% and higher have been reported for emission ranging across the whole visible spectrum[201,110]. Iridium complexes also tend to have a shorter radiative decay time, which makes it easier to achieve higher efficiency with low roll-off. However, numerous researchers have reported Pt complexes with radiative decay rates comparable to Ir complexes[202,203,204]. The square planar ligand coordination of Pt complexes also allows the design of rigid tetradentate metal complexes, which shortens radiative decay process and increases the photoluminescence

quantum efficiency. As a result, platinum complexes are being vigorously pursued as alternative emissive materials for lighting applications. This chapter describes the development of WOLEDs utilizing red, green, and blue Pt-based phosphorescent emitters. In addition, the charge transport and energy transfer processes for a WOLED employing multiple platinum-based emitters are studied. WOLED devices with a CRI value of 80, CIE coordinates of (0.35, 0.35), maximum external quantum efficiency (EQE) of 21.0%, and maximum power efficiency (PE) of 41 lm/W were obtained. Such performance is comparable to the state-of-the-art of WOLEDs employing multiple Ir-based phosphorescent emitters[205,206,207]. To the best of our knowledge, this is the first report of multiple Pt-based emitting layer WOLED that demonstrates a peak EQE as high as 21.0%.

6.2 Experimental Conditions

Three tetradentate Pt complexes of PtN3N-ptb (red), PtOO8 (green), and PtON1 (blue) are selected to cover a broad range of visible spectrum[155]. Synthetic methods for the three Pt complexes are described elsewhere[208]. The general structure used for all OLEDs fabricated is: ITO/ HATCN (10nm)/ NPD (40nm)/ TAPC (10nm)/ EML/ DPPS (10nm)/ BmPyPB (40nm)/ LiF (1nm)/ Al (100nm). Here, HATCN is 1,4,5,8,9,11-hexaazatriphenylene-hexacarbonitrile[209]. NPD is N,N'-diphyenyl-N,N'-bis(1-naphthyl)-1,1'-biphenyl-4,4''-diamine. TAPC is di-[4-(N,N-di-toylyl-amino)-phenyl] cyclohexane[210]. The EML is an emissive layer consisting of emissive materials doped in 26mCPy, 2,6-bis(N-carbazolyl) pyridine.[12b] DPPS is diphenyl-bis[4-(pyridin-3-

yl)phenyl]silane[166]. BmPyPB is 1,3-bis[3, 5-di(pyridin-3-yl)phenyl]benzene[168]. Details of materials synthesis are given in Norby et al.[208]

Device Fabrication and Testing

Organic light-emitting devices were fabricated by thermal evaporation onto pre-patterned indium-tin oxide (ITO) substrates. Substrates were cleaned by hand washing in soapy water, then sonication in DI water, followed by sonication in acetone, then sonication in isopropyl alcohol. All layers were deposited by thermal evaporation in a system made by Trovato Manufacturing (Victor, NY). Chamber pressure during deposition was less than 10^{-7} Torr, with deposition rates up to 1Å/s. Device area was 0.04cm^2. Current density, voltage and luminance measurements were made using a Keithley (Cleveland, OH) 2400 SourceMeter and a Newport (Irvine, CA) 818-UV calibrated photodiode. Electroluminescence spectra were obtained using an Ocean Optics (Dunedin, FL) HR4000 spectrometer with 1000μm fiber optic cable and calibrated using an LS-1-CAL tungsten halogen lamp.

6.3 Results and Discussion

Monochromatic devices using each individual emitter were fabricated in a general structure of ITO/ HATCN/ NPD/ TAPC/ 26mCPy: x% emitter (25nm)/ DPPS/ BmPyPB/ LiF/ Al. The electroluminescence (EL) spectra, EQE, and the corresponding molecular structures of each emitter are shown in Figure 26. The current density-voltage (J-V) curve for each device is shown in Figure 27. Peak external quantum efficiency (EQE) values of 17%, 23%, and 21% were achieved for 2% PtN3N-ptb, 6% PtOO8, and 6% PtON1 doped devices, respectively. The device with 6% PtON1 exhibited a deep blue emission

spectrum, which covers much of the blue region necessary to achieve high CRI value. The device employing 6 % PtOO8 showed an emission peak at 498 nm and a secondary emission peak at 530 nm to provide an appropriate green color. The emission spectrum of the 2% PtN3N-ptb device peaks at 588 nm but drops off sharply, missing a significant portion of the red spectrum beyond 650nm. Upon increasing the dopant concentration of PtN3N-ptb from 2% to 6%, the spectrum was broadened and red-shifted to a peak wavelength of 593 nm, due to a rise in the vibronic emission sideband. This sideband is desirable to include more of the red spectrum for a high quality white light. A linear combination of the emission intensities of the three emitters suggests that the use of 2% PtN3N-ptb emissive layer would lead to a maximum possible CRI value of 79, while the use of 6% PtN3N-ptb emissive layer would lead to a maximum possible CRI value of 82, neglecting interactions between the emitters or optical interference effects[189,211,212]. However, the increase in the dopant concentration of PtN3N-ptb based red OLED decreased the peak EQE to 15%. Thus, the PtN3N-ptb concentration poses a trade-off between optimizing the device efficiency and the color quality.

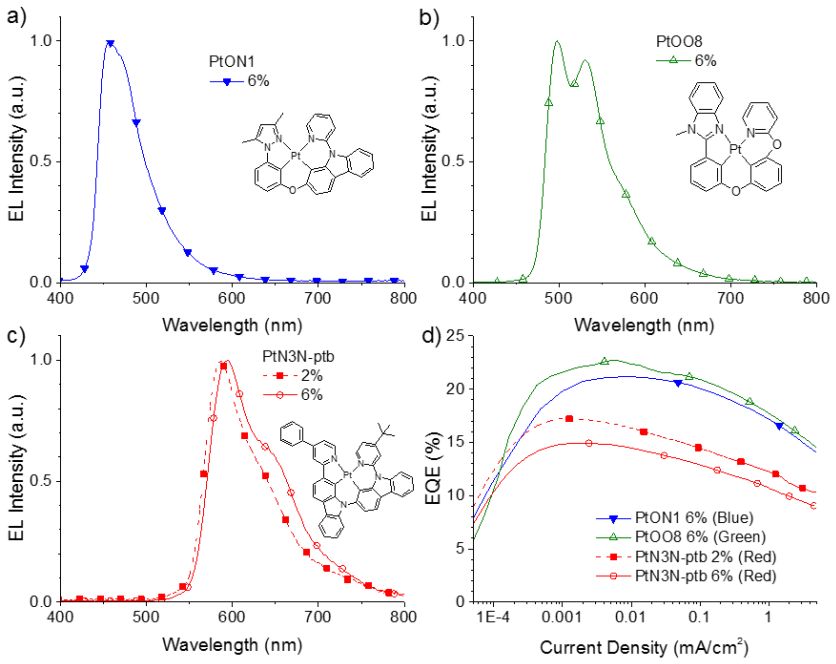

Figure 26. a)-c) EL Spectra and d) EQE vs. Luminance for the emitters a) PtON1 (Blue), b) PtOO8 (Green), and c) PtN3N-ptb (Red). Molecular structures are shown in the inset. Device structure used was ITO/ HATCN/ NPD/ TAPC/ Emitter: 26mCPy(25nm)/ DPPS/ BmPyPB/ LiF/ Al.

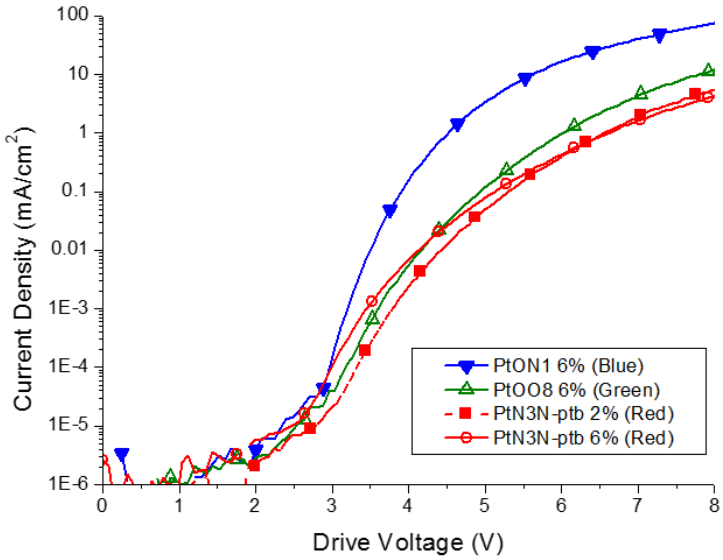

Figure 27. J-V curves from the single-emitter device data for devices with the structure ITO/ HATCN/ NPD/ TAPC/ Emitter: 26mCPy(25nm)/ DPPS/ BmPyPB/ LiF/ Al

White OLEDs with separate layers of red and blue emitters were fabricated and discussed in a previous chapter. Two emissive layer (EML) structures were compared to see what effect the deposition order would have on device performance: one EML was deposited in the order [red/blue] and the other was deposited as [blue/red]. As shown in the EL spectra in Figure 28, the device with TAPC/PtN3N-ptb:26mCPy/PtON1:26mCPy/DPPS structure exhibits a strong blue emission from the PtON1 complex. However, when the PtN3N-ptb layer is adjacent to the hole blocking layer DPPS, the PtN3N-ptb becomes a major contributor to the EL spectrum even though the thickness of the PtN3N-ptb layer (3nm) is much thinner than that of the PtON1 layer (20nm). This result suggests that for a WOLED with three emissive layers, the emitter deposited next to DPPS will likely exhibit the strongest emission. However, the lower EQE (16%) of PtN3N-ptb based red OLED appears not to translate to the multiple emissive layer WOLEDs. As illustrated in Figure 28, both devices show similar peak EQE values above 22%, albeit with sharp roll-off at a higher current density. Current density vs voltage curves for the R/B and B/R devices are shown in Figure 29.

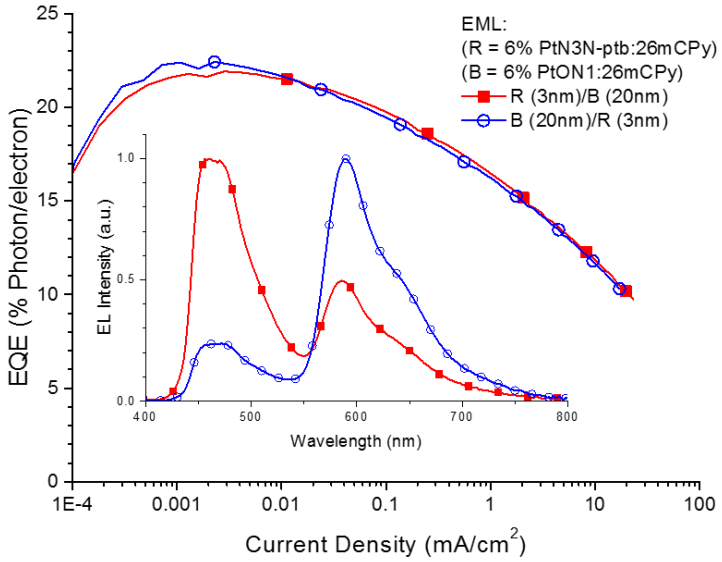

Figure 28. EQE vs. current density & EL spectra (inset) of WOLEDs made with structure ITO/ HAT-CN/ NPD/ TAPC/ EML/ DPPS/ BmPyPB/ LiF/ Al.

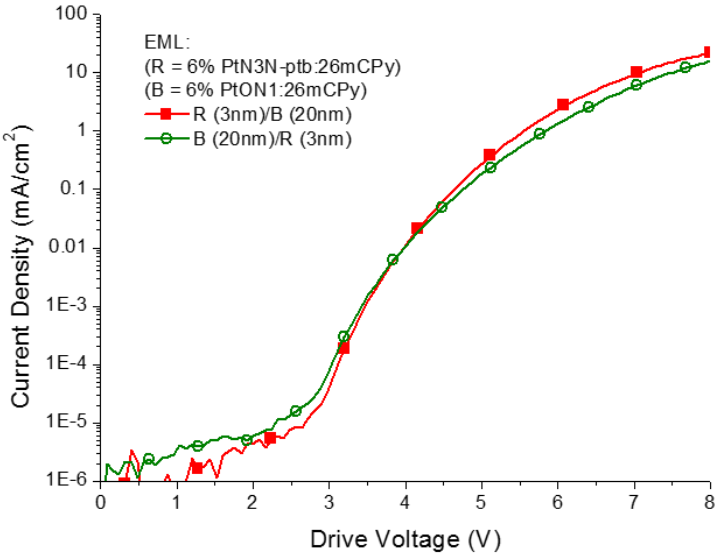

Figure 29. Current density vs drive voltage curves of WOLED devices with the structure ITO/ HAT-CN/ NPD/ TAPC/ EML/ DPPS/ BmPyPB/ LiF/ Al

WOLEDs with three emissive layers were prepared by replacing the emissive layer in the aforementioned general structure with multiple layers of single-doped red,

green, or blue emitters. In multilayer WOLEDs, it is necessary to tune the contribution of emitters to produce a balanced emission spectrum. Two major order-dependent factors affect the relative output between emitters: variation of recombination zone within the emissive layers, and energy transfer between dopants. Without a perfect charge carrier balance, the recombination zone is likely to be localized adjacent to one of the charge blocking layers[244]. Thus, whichever dopant is present in the recombination region is predicted to have the most contribution to the EL spectrum of devices. Schematic diagrams of the devices with EMLs in the order B/G/R and R/B/G are shown in Figure 30.

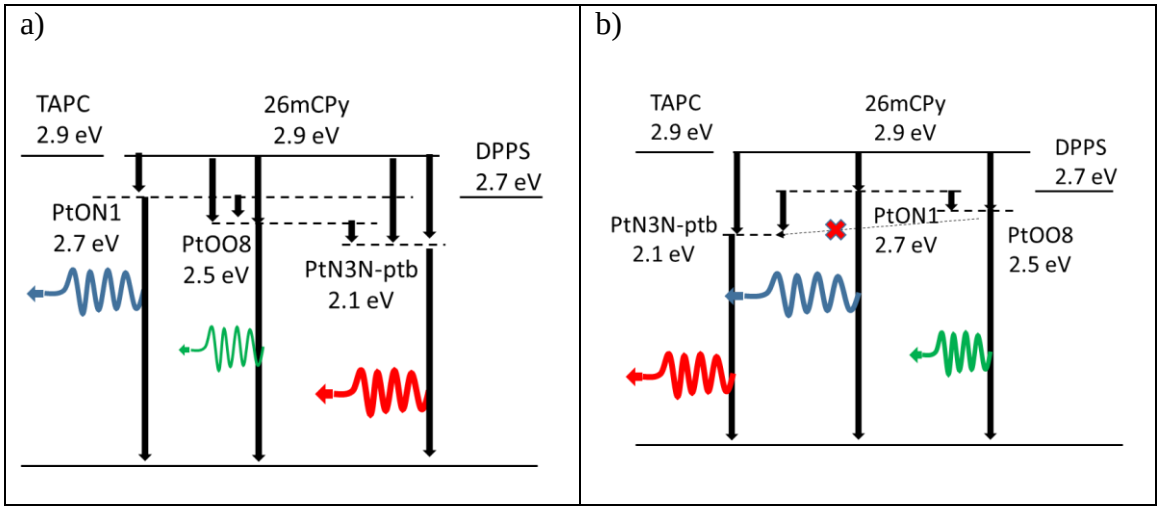

Figure 30: Schematic diagrams for WOLED devices with a) the emissive layer structure I: blue/green/red, and b) the emissive structure II: red/blue/green. Triplet energies for each material are given in eV. Arrows indicate energy transfer pathways.

WOLEDs were fabricated with three emissive layers in the order of 6% PtON1:26mCPy/6% PtOO8:26mCPy/2% PtN3N-ptb:26mCPy, denoted Structure I: ITO/ HATCN/ NPD/ TAPC/ 6% PtON1: 26mCPy (20nm)/ 6% PtOO8: 26mCPy (**x**)/ 2% PtN3N-ptb: 26mCPy (3nm)/ DPPS/ BmPyPB/ LiF/ Al, where x is 2, 3, 4 nm. In Structure

I, a thin (3nm), lightly doped (2%) PtN3N-ptb layer is deposited nearest to the DPPS interface, while a 6% PtOO8 doped layer is inserted between PtON1 and PtN3N-ptb doped layers to add the green portion of the visible spectrum. In order to examine the effect of the PtOO8 layer on the device performance, the thickness of 6% PtOO8 layer is varied from 2nm to 4nm, while the thicknesses of PtON1 and PtN3N-ptb doped layers are fixed to 20nm and 3nm, respectively. The resulting EL spectra and EQE vs. current density curves are given in Figure 31 and the current density-voltage data are shown in Figure 32. The EQE and PE of the devices show minimal variation with increasing the thickness of the PtOO8 doped layer with peak EQE ranging from 20.8% to 21.2%, and peak PE of 43 to 45 lm/W. Despite the high overall efficiencies, there is a minimal PtOO8 contribution to the emission spectrum, resulting an unsatisfactory CRI value of 70. The low contribution of PtOO8 layer is likely due to a high rate of energy transfer from PtOO8 complex, with a triplet energy E_T = 2.5 eV, to nearby PtN3N-ptb complex with E_T = 2.1 eV[92]. Moreover, as the thickness of the PtOO8 layer increases from 2nm to 4 nm, the blue emission of PtON1 complex decreases, and then results in the change of the CIE coordinates from (0.38, 0.35) to (0.42, 0.39) and a decrease of CRI value from 70 to 67, respectively. The decrease in the PtON1 emission can be explained regarding the depth of a recombination zone. When a recombination zone is formed at an interface between an emissive layer and a charge blocking layer, typically, the depth of a recombination zone is known to be less than 10 nm. Thus, as the thickness of the PtOO8 layer increases, the PtON1 layer is pushed away from the recombination zone, which results in the decreased emission of PtON1 complex, as illustrated in Figure 31.

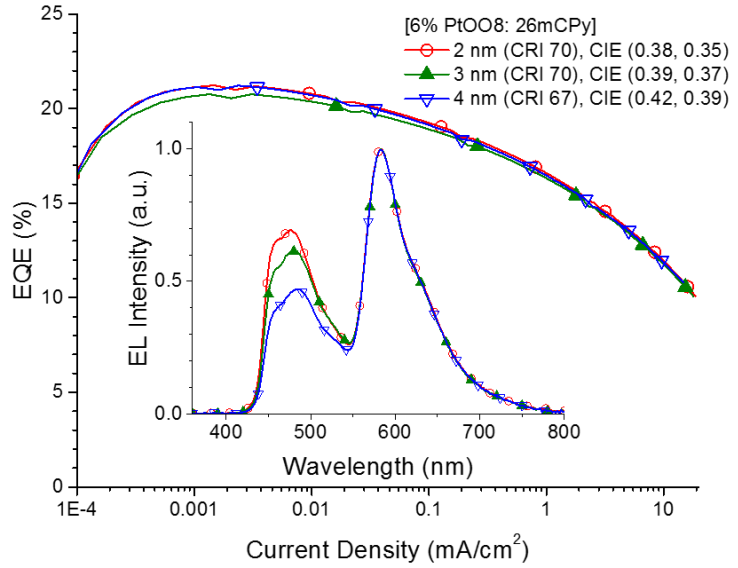

Figure 31. EL Spectra and EQE vs. current density of WOLEDs made with EML Structure I: 6% PtON1: 26mCPy (20nm)/ 6% PtOO8: 26mCPy (x)/ 2% PtN3N-ptb: 26mCPy (3nm). The thickness of 6% PtOO8: 26mCPy was varied as x. The EL spectra are normalized to the PtN3N-ptb peak.

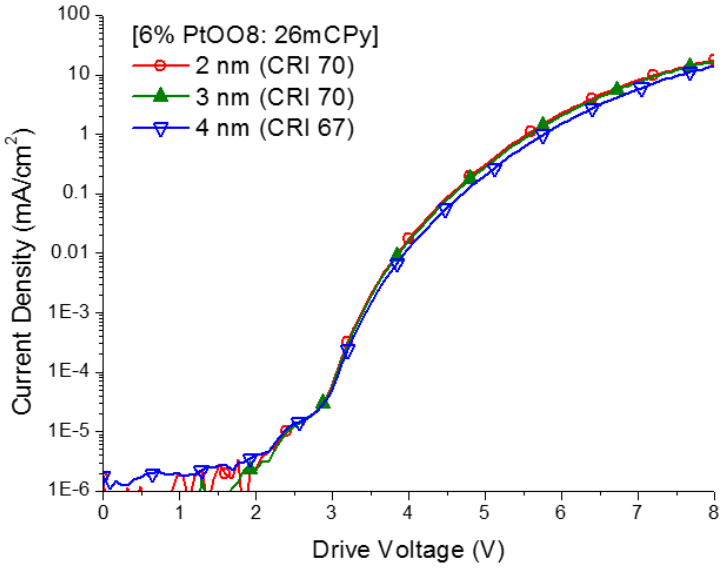

Figure 32. JV curves from the device data for devices with the EML structure I: 6% PtON1: 26mCPy (20nm)/ 6% PtOO8: 26mCPy (x)/ 2% PtN3N-ptb: 26mCPy (3nm). The thickness of 6% PtOO8: 26mCPy was varied as x. The EL spectra are normalized to the PtN3N-ptb peak.

To account for the strong energy transfer from PtOO8 to PtN3N-ptb, their respective emitting layers were separated to opposite sides of the thick PtON1-doped emissive layer with a device Structure II: ITO/ HATCN/ NPD/ TAPC/ **x**% PtN3N-ptb: 26mCPy(3 nm)/ 6% PtON1: 26mCPy(20 nm)/ 6% PtOO8: 26mCPy(2.5nm)/ DPPS/ BmPyPB/ LiF/ Al. In this configuration, the thick (20 nm), high-bandgap PtON1 doped layer inhibits the energy transfer from PtOO8 to PtN3N-ptb complex, allowing more contribution of PtOO8 complex to the EL spectrum. The EL spectra and EQE data for the devices employing Structure II are shown in Figure 33. Typical spectral results and efficiencies at operational conditions for all the devices studied are also summarized in Table 9. The EL spectra show that, by separating the PtOO8 and PtN3N-ptb doped layers with the thick (20nm) PtON1 layer, the energy transfer from PtOO8 to PtN3N-ptb is substantially reduced, resulting in increased contribution of PtOO8 to the EL spectrum compared to that of the devices with Structure I. Moreover, as the dopant concentration of PtN3N-ptb increased from 2% to 6%, both PtON1 and PtN3N-ptb emission increased relative to the PtOO8 emission. The increased PtN3N-ptb emission can be explained by the increased dopant concentration of PtN3N-ptb complex which allows trapping more charges to form red-emitting excitons and subsequently results in the stronger red emission[155,166]. The increase in PtON1 emission is also attributed to the increase in the dopant concentration of PtN3N-ptb that causes a shift of recombination zone to the interface between PtN3N-ptb and PtON1 layer. The CIE coordinates of (0.32, 0.40) and CRI value of 76 for the device with Structure II device containing a 2% PtN3N-ptb doped layer are much improved from the devices with Structure I. The devices employing

Structure II maintain a high maximum EQE of 21.0% and a maximum power efficiency of 41 lm/W. Upon increasing the PtN3N-ptb dopant concentration to 6%, the CIE coordinates shifted to (0.35, 0.35), and the CRI value increased to 80, respectively. Maximum EQE for the device with 6% PtN3N-ptb doped layer remained at 21.0%, but a high EQE roll-off is observed with increasing current density, dropping to 11.5% at 1000 cd/m^2 compared to 13.5% for the device employing 2% PtN3N-ptb doped layer. Also, the device containing a 6% PtN3N-ptb doped layer showed more significant roll-off with increasing current density. This higher roll-off is related to the increased level of trapped charges and excitons with increased dopant concentration[213].

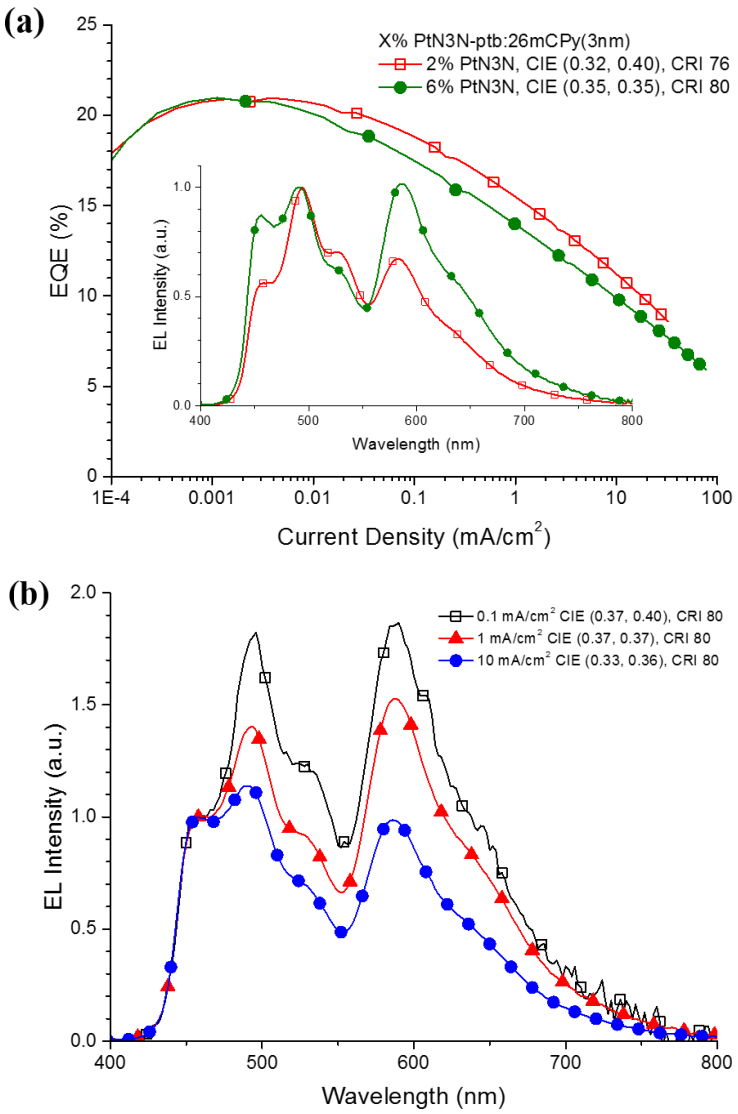

Figure 33. a) EQE and EL Spectra (inset) and b) variable current density EL Spectra of a WOLED with Structure II and EML consisting of 6% PtN3N-ptb: 26mCPy(3 nm)/ 6% PtON1: 26mCPy(20 nm)/ 6% PtOO8: 26mCPy(2.5 nm). The EL spectra are normalized to the PtON1 peak.

Table 9. Device Results for color quality (CIE), color balance (CRI), EQE, current efficiency (cd/A), and luminous efficacy (lm/W). Here "B" denotes PtON1, "G" denotes PtOO8, and "R" denotes PtN3N-ptb. CIE and CRI were measured at J = 1 mA/cm^2.

Structure	R Conc. (wt %)	Width (nm)		CIE (x,y)	CRI	100 cd/m^2			1000 cd/m^2		
		R	G			η_{EQE} (%)	η_A (cd/A)	η_P (lm/W)	η_{EQE} (%)	η_A (cd/A)	η_P (lm/W)
I (BGR)	2	3	2	(0.38,0.35)	70	18.4	40	25	14.6	31	15.8
	2	3	3	(0.39,0.37)	70	18.0	40	25	14.4	32	15.9
	2	3	4	(0.42,0.39)	67	18.3	42	26	14.5	33	16.0
II (RBG)	2	3	2.5	(0.32,0.40)	76	17.6	41	28	13.5	31	16.9
	6	3	2.5	(0.35,0.35)	80	15.8	32	24	11.5	24	14.0

To better understand the efficiency roll-off and the color stability of the device with Structure II, EL spectra were recorded at various driving current densities in the range of 0.1 - 10 mA/cm^2 for a device with a 6% PtN3N-ptb doped layer. The resulting spectra, shown in Figure 33(b), demonstrate a significant increase in PtON1's contribution with increasing current density, relative to PtOO8 and PtN3N-ptb emission. At low current densities, charges are trapped in the PtN3N-ptb and PtOO8 doped layers, and primary recombination occurs near the two blocking layers. As the current density increases, charge accumulation in the PtN3N-ptb-doped layer, as well as saturation of PtOO8 sites, shifts the recombination zone deeper into the PtON1-doped emissive layer. Furthermore, the charge and exciton saturation in the PtN3N-ptb-doped layer lead to high rates of non-radiative decay via triplet-triplet annihilation and a significant loss in quantum efficiency. As a result, the emission from PtN3N-ptb and PtOO8 are reduced

relative to PtON1 emission. This relationship between current density and the quantum efficiency is reflected by a large efficiency roll-off in the EQE curves.

Despite the enhancement made in the device efficiencies, further improvement of the color quality of the devices is limited by this materials system due to the significant gap in the spectrum between the PtON1 (blue) and PtN3N-ptb (red) emission spectra. The replacement of PtOO8 with a yellow emitter and further development of efficient and broad red emitters would yield an even better color quality, and CRI values of 85 to 90 should be within reach. Similarly, further improvement in efficiency is limited by the current structure's use of thin EMLs for PtOO8 and PtN3N-ptb. These layers trap large quantities of charge carriers and excitons, leading to increased triplet-triplet annihilation losses. Further optimization of the device architecture to reduce charge and exciton build-up, the selection of more efficient transport materials, and the use of advanced outcoupling techniques should yield improved efficiency, reduced roll-off, and enhanced color stability in future OLEDs.

6.4 Conclusion

The effects of local recombination rate, energetic dopant-to-dopant transfers, and charge trapping on color balance in triple platinum emitter WOLEDs have been investigated. Thickness, dopant concentrations, and emitting layer stacking order were the variables used to investigate the charge balance and energetic processes occurring within the device. Spectral and electrical data indicate that significant energy transfers occur from PtOO8 to PtN3N-ptb for the devices employing PtON1(blue)/PtOO8(green)/PtN3N-ptb(red) structure. The PtN3N-ptb spectrum also

exhibits interdependence of emissive layer thickness and dopant concentration: a thin layer with high dopant concentration will produce a spectrum similar to that of a thicker layer with lower dopant concentration. Peak color balance and external quantum efficiency (EQE) were achieved with the emissive layer structure of PtN3N-ptb (red)/PtON1 (blue)/PtOO8 (green) which inhibited undesirable energy transfer. The device with 6% doping concentration in red, blue and green emissive layers exhibited a peak EQE of 21.7%, CRI value of 81 and CIE coordinates of (0.34,0.37). We believe this is the first report of a WOLED using all Pt-based emitters that achieved an EQE as high as 21.7%. The CRI was limited by the emitter system used here due to the gap between the red and green regions. Adding an emitter with a EL spectrum in the yellow region should produce a higher CRI. More research into emitter materials and device architecture are needed to produce all Pt-based emitter WOLEDs with higher CRI. Incorporating outcoupling structure(s) should increase the EQE.

6.5 Outlook for WOLEDs in SSL

Inorganic LEDs dominate the solid-state lighting market as of this writing, but white OLEDs are being increasingly adopted for some applications. Although inorganic LEDs are much more efficient than other common lighting sources, recent studies have shown that the high color temperatures of >4000K that are typically produced by inorganic LEDs have negative impact on humans and other living species[214]. They are also point sources, and require additional fixturing to produce the diffuse light that is desired for indoor lighting applications. Inorganic LEDs produce significant amounts of heat, and require heat sinks, which further adds to their cost.

White OLEDs with warmer color temperatures can easily be fabricated using an appropriate choice of emissive materials. They are also better able to produce a broad, nearly continuous spectrum that better replicates the solar spectrum to which we are accustomed. Luminaires for reading and indoor lighting benefit from inherent advantages of WOLEDs such as the ability to fabricate large-area light sources that produce diffuse light without requiring any additional hardware. Their operating temperature is much lower than inorganic LEDs, so WOLEDs do not require heat sinks. Manufacturers are moving to larger substrates to reduce costs; one manufacturer estimates cost reductions of up to 95% by moving production from a Gen II substrate size to Gen 5[215]. Further cost reductions can be expected as more manufacturers begin production. WOLEDs have been fabricated by roll-to-roll process on flexible substrates, demonstrating the feasibility of high-volume manufacturing which should further reduce costs[216].

Monochrome OLEDs are now being incorporated by automobile manufacturers as novel and efficient exterior lighting[217]. The OLED advantages of efficiency, color tunability, and flexible substrates allow designers to create styles which differentiate their products from those of competitors. Initial adoption of OLED-based lighting is occurring in luxury automobiles, but will almost certainly become available on lower-priced models as the technology and supply chain mature lead to lower product costs.

7: FULL COLOR LARGE AREA ACTIVE MATRIX FLEXIBLE OLED DISPLAY

7.1 Introduction

Displays based on organic light emitting diodes (OLED) are lighter and thinner than comparable liquid crystal displays. OLEDs have been adopted for use in applications such as cell phones, and major display companies have demonstrated OLED televisions with 55" diagonal with commercial sales starting in 2013[218]. Displays built on glass substrates have demonstrated excellent stability, but the demand for lighter and more rugged displays requires more resilient substrates. Metal foils have been used for displays, but generally have higher surface roughness compared with plastic[219,220]. In addition, metal is electrically conductive and thus requires deposition of an insulating layer prior to TFT backplane fabrication. Since one of the electrodes in an OLED must be transparent, metal substrates require a top-emitting structure which requires a transparent cathode. Plastic substrates with lower surface roughness are commercially available and are electrically insulating as well. They are also transparent and may be used for top- or bottom-emitting architectures. This chapter will discuss the fabrication of the backplanes, which control the display, utilizing thin film transistors (TFTs) made using an amorphous metal oxide material for the channel, as well as the device engineering process to develop the red, green and blue OLED devices which comprise the sub-pixels in the display.

Amorphous silicon (a-Si:H) TFTs have been used extensively for liquid-crystal display (LCD) applications[221]. These displays are fabricated on glass substrates and can thus withstand the typical process temperatures of ~300-350ºC. Low-temperature deposition of a-Si has been demonstrated at temperatures less than ~150ºC[222,223].

Mobilities were lower than films deposited at higher temperature and were attributed to scattering caused by surface roughness. matrix OLEDs (AMOLED) with amorphous silicon (a-Si:H) TFT backplanes have been demonstrated by previous researchers on plastic substrates with maximum process temperature as low as 150°C[231,223]. Higher deposition temperatures are known to improve the threshold voltage stability of a-Si:H TFTs but are not compatible with plastic substrates, as mentioned above.

Polycrystalline Si has much higher mobility than amorphous Si. Polycrystalline silicon films are created from amorphous Si films that have had a subsequent anneal to form the polycrystalline structure. However, an anneal temperature of >400ºC is required to crystallize the amorphous film, which precludes the use of plastic substrates[234]. Metal foils can withstand the anneal temperature but have the disadvantages noted above, and are prone to creasing if bent sharply.

Researchers at Arizona State University's Flexible Display Center have previously demonstrated AMOLED displays on heat stabilized polyethylene naphthalate (PEN) substrates supplied by DuPont-Teijin Films, tradename Teonex, using a-Si:H TFTs deposited at <185°C[232]. The PEN substrates were temporarily bonded to rigid carriers and processed in standard 150mm semiconductor processing equipment, then debonded before being built into a display. Backplane performance was adequate for demonstration purposes on the 4.1" displays, but the low mobility of a-Si makes it unsuitable for use in larger displays.

Experiments by Nomura et al. and Hosono et al. using mixtures of various metal oxides showed their potential for use as channel materials in TFTs[224,225]. One of these

materials, indium zinc oxide (IZO), has been used to fabricate TFTs at a maximum temperature of 200°C with mobilities over ten times higher than a-Si:H as well as much better forward bias stability[226]. However, IZO tends to crystallize easily, which reduces the mobility of the TFT due to grain boundary scattering as well as the roughening of the gate dielectric/channel interface. Indium gallium zinc oxide (IGZO) has been shown to have better stability with respect to re-crystallization and is better suited for TFT applications. Since OLEDs are current driven as opposed to voltage driven liquid-crystal displays (LCDs), drive current and forward bias stability are critical for a useful OLED display. Several commercial display manufacturers are developing IGZO-based backplanes for their products, and commercially available displays are already on the market[227,228].

ASU has developed a low temperature (200°C) IGZO process in its Gen II (370 x 470 mm) line with performance comparable to that obtained in its 150mm development line[229]. This process enabled the fabrication of OLED displays on flexible substrates up to 14.7". Typical properties of TFTs made at ASU from a-Si:H and IGZO are shown in Table 10.[230]

Table 10: Comparison of typical characteristics of thin film transistors fabricated at the Arizona State University Flexible Display Center made with a-Si:H channel compared with those made with indium gallium zinc oxide channel

Parameter	a-Si Channel	IGZO Channel
Saturation Mobility	0.70 cm^2/V-s	13.5 cm^2/V-s
Threshold Voltage	1.6 V	3.52 V
Subthreshold Slope	0.49 V/dec	0.29 V/dec
Hysteresis	0.31 V	0.75 V

7.2 Experimental Procedure

OLED pixel design, TFT fabrication, electrical testing and OLED deposition procedures are discussed in more detail in the following sections.

7.2.1 OLED Pixel design

A current driven two transistor, one capacitor bottom emitting structure was used to drive the subpixels. Subpixel pitch was 312x104μm, which translates to a full-color RGD display of 81 pixels per inch (ppi). Aperture ratio, which is the open area in each pixel through which light can pass, was approximately 38%. A more detailed description of the circuitry is given by O'Brien et al.[230]. A schematic circuit is shown in Figure 34, and a detailed view of one subpixel is shown in Figure 35.

Table 11 lists the display specifications.

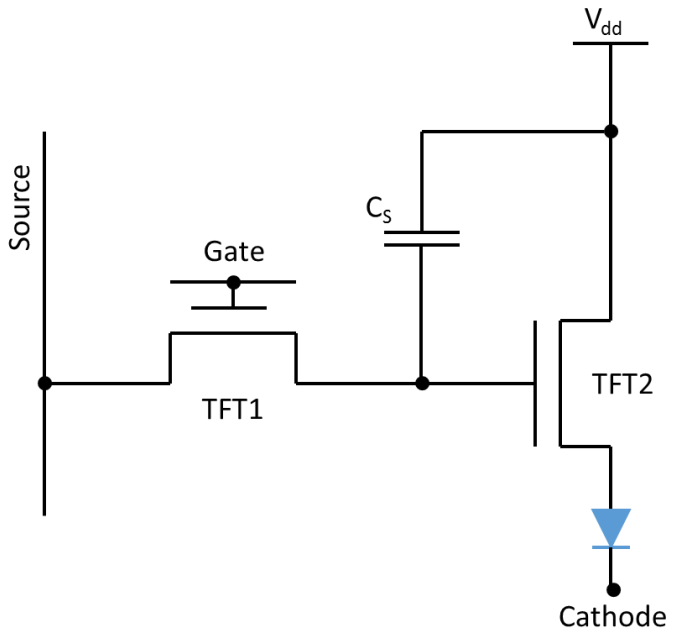

Figure 34: Schematic of 2T1C OLED Sub-Pixel Driving Circuit

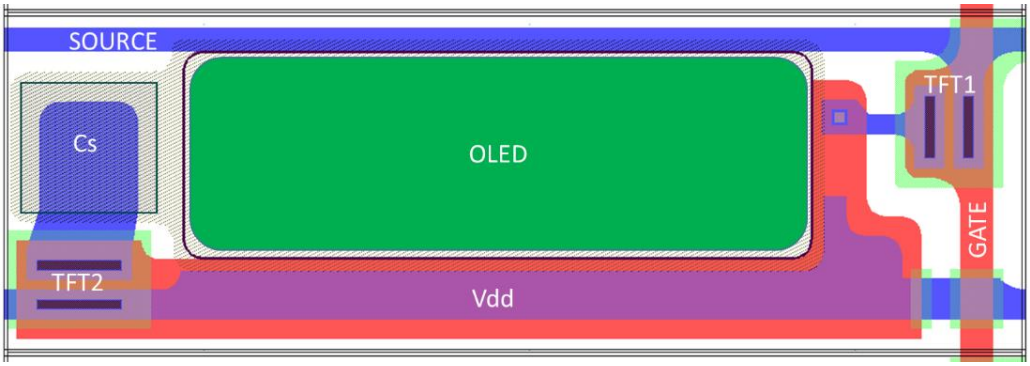

Figure 35: Detailed view of one subpixel for a bottom-emitting OLED display (cathode not shown)

Table 11: Specifications for 14.7” flexible OLED display

Display Size	14.7” diagonal
Display Resolution	960 x 720 RGB (rotated)
RGB Sub-Pixel Size	312µm x 104µm
Pixels per Inch	81ppi
Active Area	300mm x 225mm
Architecture	Bottom Emitting Pixel
Operation	2T1C
Aperture Ratio	38%
Signal Voltage	7.5V
Sub-Pixel Current	~1µA
V_{dd} - V_{cath}	18V

7.2.2 TFT Fabrication

Thin film transistor backplanes were fabricated on heat stabilized polyethylene naphthalate (PEN) substrates (tradename Teonex) provided by DuPont-Teijin Films. The PEN was temporarily bonded to a rigid carrier using a proprietary adhesive provided by Henkel. A key component of successfully processing on plastic substrates is minimizing distortion which occurs because of elevated process temperatures and thermal expansion coefficient mismatch between the plastic substrate and the carrier[231]. Permanent distortion makes accurate photolithography impossible in subsequent steps and results in poorly- or non-functional devices. A substrate-adhesive-carrier system was developed at ASU’s Flexible Display Center (FDC) which virtually eliminated distortion and allowed processing on metal as well as plastic substrates[232,233].

After bonding, a 300nm thick SiN film was deposited by plasma enhanced chemical vapor deposition (PECVD). This served as a barrier coating which minimized moisture ingress through the substrate during processing and after debonding. The backplanes used an inverted staggered gate with etch stopper structure[234]. The fabrication sequence is described briefly below.

A molybdenum gate metal layer was deposited by DC magnetron sputtering in a KDF 744 sputter system. This layer was patterned by a photolithography step followed by a dry etch process. Next, the TFT active layer consisting of SiO/IGZO/SiO was deposited sequentially: SiO gate dielectric by PECVD in an AKT 1600 hybrid deposition and etch system; IGZO channel layers by DC magnetron sputtering in a Sunic Sunicel 400 Plus process system; and SiO intermetal dielectric (IMD) by PECVD in the AKT. The SiO and IGZO layers were deposited in separate deposition systems, with the substrates exposed to atmosphere in between the PECVD and sputter deposition steps. The IGZO channel layer was deposited in two steps without breaking vacuum. The first layer was deposited with no additional oxygen gas in the argon working gas, while the second layer was deposited with about 2% oxygen in argon as the working gas. The dual-layer channel allows better process control of threshold voltage and mobility of the TFTs[229]. After the SiO/IGZO/SiO active stack was patterned and etched, an SiO mesa passivation was deposited by PECVD to protect the edges of the channel layer exposed by the mesa etch process.

After the active stack deposition/pattern/etch/mesa passivation deposition steps were completed, vias were etched through the SiO mesa passivation, IMD and IGZO

channel layers to form contacts to the gate metal lines. Next, the source-drain (S-D) metal was deposited by DC magnetron sputtering, patterned and etched to form the signal lines. An interlayer dielectric (ILD) layer was solution-coated and baked at 200ºC to cure, then capped with a PECVD SiN layer to protect the ILD from oxygen plasma exposure during a subsequent resist strip step. Vias were patterned and etched in the SiN and ILD layers to create contact openings to the S-D metal where the ITO anode layer would later make contact.

A DC magnetron sputtered molybdenum layer was deposited and etched to contact the S-D metal as a barrier to the subsequent indium-tin oxide (ITO) anode layer deposition. The barrier layer prevented reaction between the top Ta layer in the S-D lines and the ITO. The conductivity of ITO is dependent on the concentration of oxygen vacancies, so any changes in stoichiometry will affect the conductivity. Next, an ITO layer was deposited by DC magnetron sputtering. The Mo etch prior to ITO deposition formed windows in the pixel area so that light from the OLEDs can pass through the transparent ITO anode and PEN substrate. The final step in backplane fabrication was to deposit a SiN layer by PECVD to passivate the devices. Vias were etched in the SiN layer to form contacts to the ITO for the OLED devices. Figure 36 summarizes the fabrication steps, described below.

a) Deposit SiN barrier layer by PECVD onto the flexible substrate. Flexible substrate was previously bonded to a rigid carrier (not shown here)
b) Deposit gate metal by magnetron sputtering; pattern with photoresist
c) Etch gate metal and strip photoresist

d) Deposit SiO gate dielectric stack by PECVD

e) Deposit the IGZO channel layer by magnetron sputtering

f) Deposit SiO intermetal dielectric layer; [SiO/IGZO/SiO] active stack pattern/etch/resist strip

g) Deposit mesa passivation to protect sides of IGZO channel layer during subsequent processing

h) Etch vias for source/drain metal contacts to IGZO layer; deposit S/D metal by magnetron sputtering; pattern/etch/strip

i) Coat interlayer dielectric by solution process

j) Etch vias in ILD; deposit ITO anode layer by magnetron sputtering; pattern/etch/strip

k) Deposit SiN overglass layer by PECVD; pattern contact vias/etch/strip

l) Deposit OLED layers on ITO anode layer using shadow masks to define pattern. The arrow represents the light emitted through the substrate by the bottom-emitting OLED.

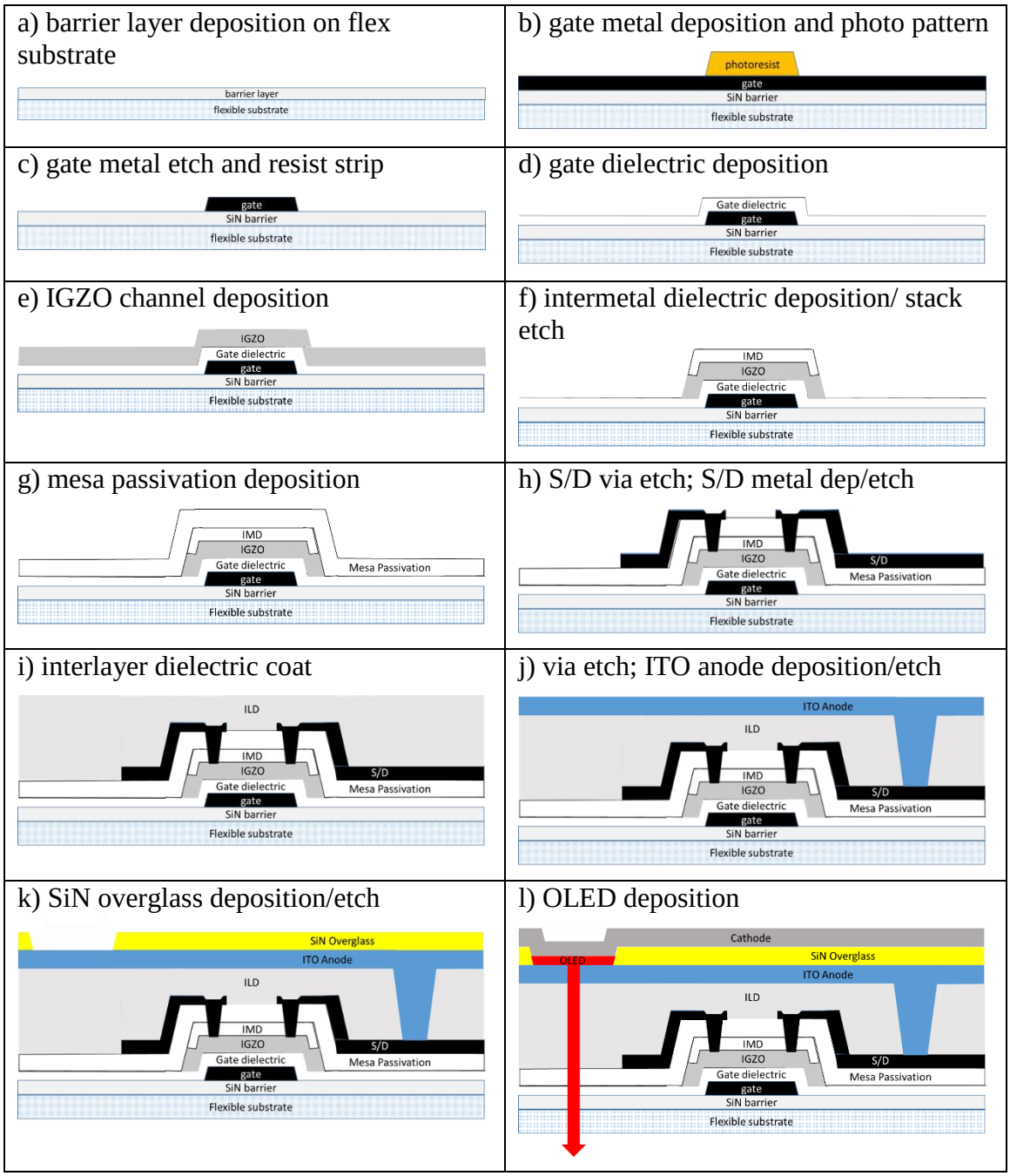

Figure 36: Fabrication sequence for thin film transistor backplane and bottom-emitting OLED for display application

7.2.3 OLED Deposition and device architecture design

Prior to OLED deposition, electrical tests were performed on process control monitor (PCM) devices that were formed as part of the backplane process. Thin film transistor test structures with the same 9µm/9µm width/length ratio as the array transistors were used to monitor process stability as well as to characterize device performance. Typical performance results for the IGZO TFTs are shown in Table 12.

Table 12: Median Values for IGZO TFT Properties on PEN Substrates

Saturation Mobility	13.5 cm^2/V-s
Threshold Voltage	3.52 V
Subthreshold Slope	0.29 V/dec
Hysteresis	0.75 V

7.3 Results and Discussion

OLED materials for commercial applications in displays and lighting must meet several requirements. They must be able to reproduce the desired color spectrum; they must have a long operational lifetime; and they should be efficient, particularly for portable display and lighting applications. Displays must be able to produce saturated red, green and blue colors so that they can render images as accurately as possible, while devices for lighting applications should be able to cover the entire visible spectrum with a color rendering index (CRI) over 80 to replicate the solar spectrum as closely as possible. The key parameters for evaluating suitability for display and lighting applications include CIE coordinates, CRI, electroluminescence spectrum, current efficient and power efficiency.

Initial OLED development used non-proprietary $Ir(btp)_2(acac)$ red, $Ir(ppy)_2(acac)$ green and FIrpic blue phosphorescent materials that were purchased from Lumtec (Taiwan). Here, $Ir(btp)_2(acac)$ is bis[2-(2'-benzothienyl)pyridinato-,C3'(acetylacetonato)iridium(III), $Ir(ppy)_2(acac)$ is bis(2-phenylpyridine)(acetylacetonate)iridium(III), and FIrpic is iridium(III) bis(4,6-(difluorophenyl)pyridinato-N,C20)picolinate. Although not as efficient or stable as the proprietary materials used by commercial display manufacturers, these emitters were easily obtainable and less expensive. Other materials listed in Table 13 are HAT-CN, or Dipyrazino[2,3-f:2',3'-h]quinoxaline- 2,3,6,7,10,11-hexacarbonitrile); NPD, or N,N'-Bis(naphthalen-1-yl)-N,N'-bis(phenyl)-benzidine; CBP, or N,N'-dicarbazolyl-4–4'-biphenyl; mCP, or 1,3-bis(N-carbazolyl)benzene; BCP, or 2,9-dimethyl-4,7-diphenyl-1,10-phenanthroline; and Alq, or tris(8-quinolinolato)aluminum(III).

OLED structures were optimized using a simple diode test device structure with area of $0.05cm^2$ before integration into the display itself. The structures that were optimized using the non-proprietary materials provided a baseline structure used when we could purchase more efficient, more stable proprietary materials. A basic OLED structure is shown in Figure 37. Table 13 lists the HOMO, LUMO and triplet (E_T) energy levels for the materials used in these runs. Schematic diagrams of the initial red, green and blue device structures including the HOMO/LUMO levels of each layer are shown in Figure 38, Figure 39 and Figure 40. Electroluminescence spectra for the $Ir(btp)_2(acac)$ red, $Ir(ppy)_2(acac)$ green and FIrpic blue are shown in Figure 41.

Table 13: HOMO, LUMO and triplet energy levels of materials used for initial OLED development for full-color display on flexible substrate.

Material	HOMO, eV	LUMO, eV	E_T, eV	ref
HAT-CN	9.5	5.7	n/a	[103]
NPD	5.5	2.4	2.3	[104]
CBP	6.1	2.8	2.6	[104]
mCP	5.9	2.4	2.9	[235]
FIrpic	6.2	3.5	2.7	[235]
$Ir(ppy)_2(acac)$	5.6	3.2	2.4	[58]
$Ir(btp)_2(acac)$	5.1	3.2	2.0	*
BCP	6.5	3.0	2.6	[104]
Alq	5.8	3.0	2.2	[236]

*triplet energy level for Ir(btp)2(acac) was estimated from its peak emission wavelength at 617nm

Figure 37: A basic OLED structure showing the organic layers and cathode layer. The anode is located under the HIL and is not shown here. HIL is hole injection layer; HTL is hole transport layer; EML is the emissive layer which typically consists of a host matrix doped with an emissive material; HBL is hole blocking layer; ETL is electron transport layer; EIL is electron injection layer; cathode is typically a metal such as aluminum or a magnesium:silver alloy.

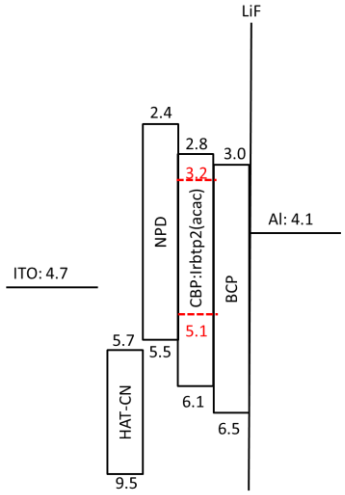

Figure 38: Schematic structure of initial red OLED device showing HOMO and LUMO levels of constituent layers. ITO is the anode layer; HAT-CN is a hole injection layer; NPD is a hole transport layer; CBP is the host for the emissive layer; $Ir(btp)_2(acac)$ is the red dopant; BCP is the hole blocking layer; LiF is an electron injection layer; the cathode layer is Al.

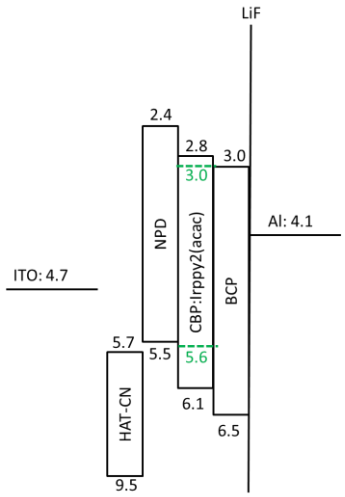

Figure 39: Schematic structure of initial green OLED device showing HOMO and LUMO levels of constituent layers. ITO is the anode layer; HAT-CN is a hole injection layer; NPD is a hole transport layer; CBP is the host for the emissive layer; $Ir(ppy)_2(acac)$ is the green dopant; BCP is the hole blocking layer; LiF is an electron injection layer; the cathode layer is Al.

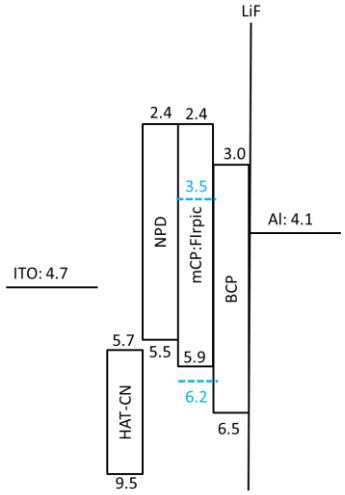

Figure 40: Schematic structure of initial blue OLED device showing HOMO and LUMO levels of constituent layers. ITO is the anode layer; HAT-CN is a hole injection layer; NPD is a hole transport layer; mCP is the host for the emissive layer; FIrpic is the blue dopant; BCP is the hole blocking layer; LiF is an electron injection layer; the cathode layer is Al.

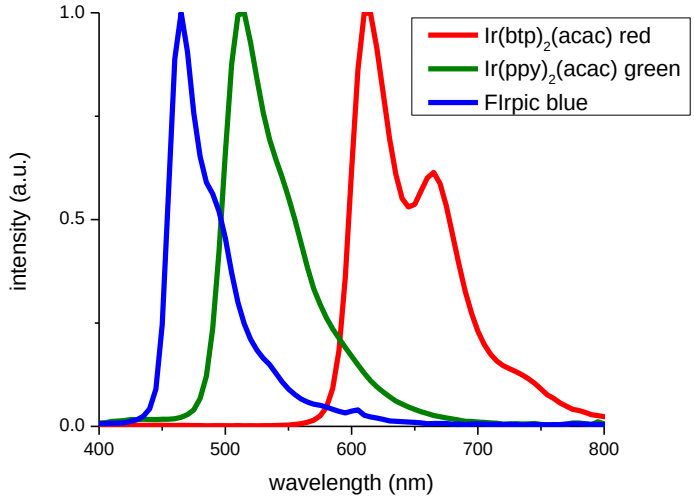

Figure 41: Electroluminescence spectra for $Ir(btp)_2(acac)$ red, $Ir(ppy)_2(acac)$ green and FIrpic blue emitters used in the initial development of full color OLED displays. Red device structure was 10nm HAT-CN/40nm NPD/CBP:14%$Ir(btp)_2(acac)$(30nm)/20nm BCP/20nm Alq_3/1nm LiF/100nm Al. Green device structure was 10nm HAT-CN/40nm NPD/CBP:6%$Ir(ppy)_2(acac)$(30nm)/20nm BCP/20nm Alq_3/1nm LiF/100nm Al. Blue device structure was 10nm HAT-CN/40nm NPD/mCP:8%FIrpic(30nm)/20nm BCP/20nm Alq_3/1nm LiF/100nm Al.

Peak blue emission from FIrpic occurs at ~ 465nm, with a shoulder at ~490nm. This does not produce a saturated blue and thus is not an optimal choice for display applications. Emission from $Ir(ppy)_2(acac)$ green produces a relatively narrow peak at 515nm. $Ir(btp)_2(acac)$ red emitter produced a saturated red color. Its spectrum showed peak emission at 617nm, with a significant shoulder at 670nm as well as a smaller shoulder at ~735nm. Plots of current density vs voltage and luminance vs voltage are shown in Figure 42.

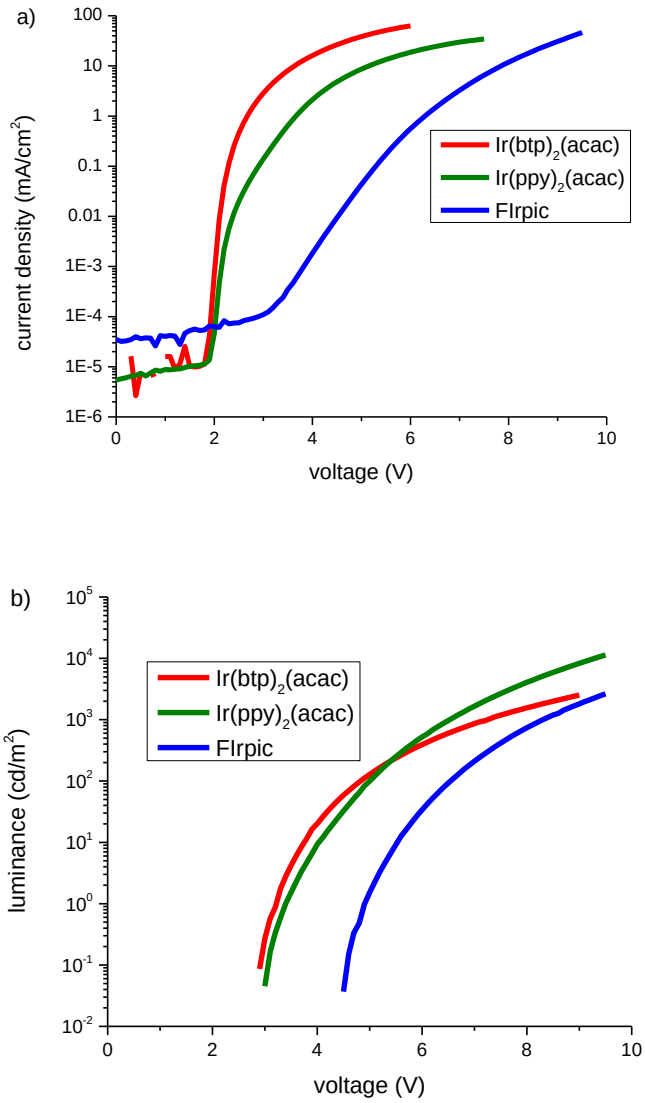

Figure 42: Plots of a) current density vs voltage and b) luminance vs voltage for devices with Ir(btp)$_2$(acac) red, Ir(ppy)$_2$(acac) green and FIrpic blue emitters

Turn-on voltage is normally stated as the voltage at which the device emission is 1 cd/m^2. The red and green emitters exhibit similar turn on voltages. Figure 38 shows the favorable energy transfer in the red device due to the differences in HOMO and LUMO levels between the Ir(btp)2(acac) emitter and CBP host. Although the CBP HOMO level

is lower than that of the dopant, the HOMO level of the dopant is higher than that of the NPD hole transport layer. This facilitates the energy transfer from NPD directly to the dopant. In addition, the LUMO of BCP is higher than that of the dopant, which also facilitates energy transfer. In the case of the green device shown in Figure 39, the HOMO and LUMO levels of the dopant are very close to the HOMO and LUMO levels of the hole transport and hole blocking layers, respectively. Energy transfer between these materials is resonant. In contrast, there is a significant energy level offset between the HOMO levels of the NPD HTL and the FIrpic dopant, shown schematically in Figure 40, which creates a barrier to hole injection into the dopant. The result is a higher turn-on voltage as seen in Figure 42.

The EQE, current efficiency and power efficiency at luminance of 100 cd/m^2 and 1000 cd/m^2 are given in Table 14. A computer screen has a luminance of ~200-300 cd/m^2, while 1000 cd/m^2 has been the level proposed in the literature as the basis for lighting application comparison. The current efficiency is the most relevant parameter for display applications, since only the light emitted perpendicular to the device is important and the angular dependence of the light emission is not considered[243]. For solid-state lighting applications, however, all light that is emitted into the hemisphere normal to the substrate should be considered, so the most meaningful metric for that application is the power efficiency in lm/W[243].

Table 14: CIE Values, External Quantum Efficiency, Current Efficiency and Power Efficiency at 100 cd/m^2 and 1000 cd/m^2 for Ir(btp)$_2$(acac) red, Ir(ppy)$_2$(acac) green, and FIrpic blue emitters

Emitter	CIE	100 cd/m^2			1000 cd/m^2		
		EQE, %	CE, cd/A.	PE, lm/W	EQE, %	CE, cd/A.	PE, lm/W
Ir(btp)$_2$(acac) red	(0.633, 0.299)	6.74	6.68	4.19	5.25	5.20	2.18
Ir(ppy)$_2$(acac) green	(0.270, 0.620)	9.90	33.6	21.1	7.7	25.9	12.3
FIrpic blue	(0.187, 0.297)	4.36	6.50	3.09	4.18	6.23	2.3

External quantum efficiency as a function of current density for all three emitters is shown in Figure 43. The EQEs for the red and green devices are consistent with other literature reports[237]. The efficiency of our blue device is lower than that reported by other groups. However, the known instability of FIrpic makes it unsuitable for commercial applications[238, 239]**.** All emitters used here exhibit a decrease in efficiency with increasing current density due to the increase in exciton density, which increases the probability of annihilation and quenching processes as discussed in Chapter 3.

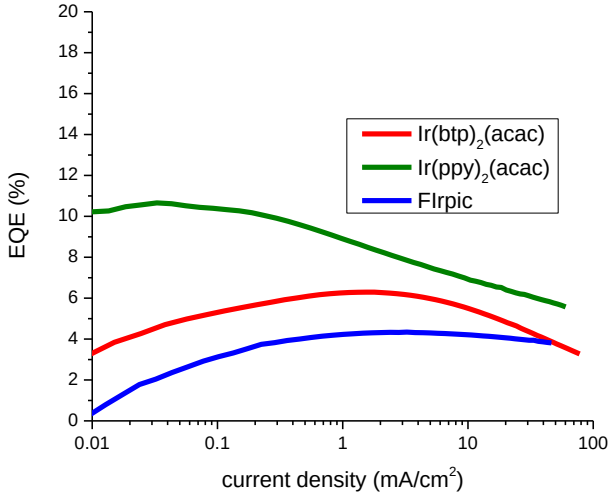

Figure 43: External quantum efficiency vs current density for initial $Ir(btp)_2(acac)$ red, $Ir(ppy)_2(acac)$ green and FIrpic blue emitters

Stability is another critical metric, and these materials do not exhibit satisfactory lifetime. Lifetime tests were conducted by driving the devices at a constant current density such that the initial luminance value was 1000 cd/m^2 and monitoring the luminance vs time. Figure 44 shows the results obtained with these emitters.

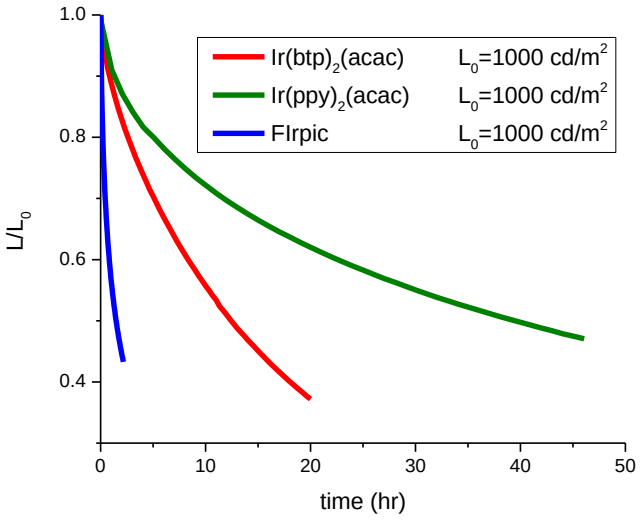

Figure 44: Normalized luminance vs time for diodes using $Ir(btp)_2(acac)$ red, $Ir(ppy)_2(acac)$ green and FIrpic blue emitters. Red device structure was 10nm HAT-CN/40nm NPD/CBP:14%$Ir(btp)_2(acac)$(20nm)/20nm BCP/20nm Alq_3/1nm LiF/100nm Al. Green device structure was 10nm HAT-CN/40nm NPD/CBP:6%$Ir(ppy)_2(acac)$(20nm)/20nm BCP/20nm Alq_3/1nm LiF/100nm Al. Blue device structure was 10nm HAT-CN/40nm NPD/mCP:6%FIrpic(20nm)/20nm BCP/20nm Alq_3/1nm LiF/100nm Al.

The lifetime on an OLED depends on several factors such as: chemical stability, structural stability of the molecule, doping concentration, charge balance, and thermal stability of the material. Chemical degradation of the organic materials is a widely accepted explanation for the intrinsic (i.e., not due to material impurities or poor encapsulation) loss mechanism in OLEDs[240,241]. Radical fragments produced by bond cleavage react with other fragments and form more degradation products which act as luminescence quenchers, deep charge traps and non-radiative recombination centers, depending on their energy levels. Triplet-polaron [guest triplet exciton - host polaron] annihilation was the dominant mechanism responsible for reduced lifetime[242]. The effects due to this mechanism could be reduced by increasing the recombination zone width[243,244]

Instabilities in the other organic layers can also contribute to degradation. As one example, Meerheim et al. made a series of devices based on the red-orange emitter $Ir(MDQ)_2(acac)$ comparing Alq_3, TPBI, BPhen and BAlq hole blockers[244] They found that devices made with BAlq exhibited much longer lifetimes than those made using TPBI or BPhen, which they attributed to formation of BPhen dimers under excitation as reported by Scholz et al.[245]. The dimers act as electron trap states and exciton quenchers. The electron deficiency causes the emission zone to move closer to the hole blocker and become narrower. The result is a higher exciton density, which increases the probability of exciton-exciton quenching which further reduces the device efficiency. BAlq, in contrast, does not dimerize due to its fivefold coordination sphere and remains stable even under heavy excitation[245].

Another factor affecting stability is charge balance. Charge balance can be achieved by selection of materials with suitable HOMO and LUMO levels to minimize injection barriers[168]. Hole transport and electron transport materials with high hole mobility and high electron mobility, respectively, are also required to balance the hole and electron concentrations in the emissive layer.

The next step in the display development was to acquire materials with higher efficiencies and better stabilities. Currently available blue phosphorescent emitters are unstable, require higher driving voltages compared with red and green, and emit sky-blue hues rather than the deeper blues needed for wide-color gamut displays. For these reasons, fluorescent emitters are commonly used for display applications, even though their efficiencies are low compared with phosphorescent emitters.

We could purchase commercial-grade materials under the condition that we not try to analyze them in any way, so we were not able to determine the HOMO, LUMO and triplet energy levels[246]. The basic device structures were like that shown in Figure 37. The new red and green emissive layers used a co-host structure which consisted of a material with high electron mobility and one with high hole mobility to enhance charge transport. The co-host structure improves charge balance by incorporating a material with high hole transport with a material with high electron transport properties[236]. Although there are some ambipolar host materials, their properties are often a compromise between hole and electron transport. The development of better ambipolar host materials is an active area of research[86,56,247]. In the meantime, co-host structures provide an effective means of improving charge balance. The fluorescent blue emissive layer used a single host material. Electroluminescence spectra for the new red, green and blue emitters are shown in Figure 45

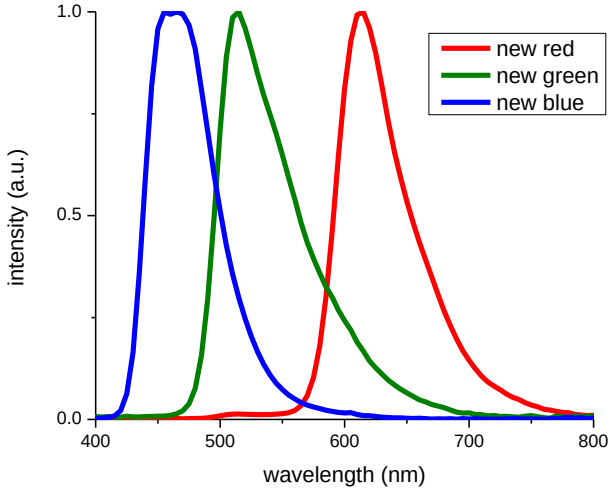

Figure 45: Electroluminescence spectra for new red, green and blue emitters used in the fabrication of full color OLED displays. Red device structure was 10nm HAT-CN/40nm NPD/NS:RH:RD(30nm)/10nm NS/30nm Liq:ETL/2nm Liq/100nm Al. Green device structure was 10nm HAT-CN/40nm NPD/NS:GH:GD(30nm)/10nm NS/30nm Liq:ETL/2nm Liq/100nm Al. Blue device structure was 10nm HAT-CN/40nm NPD/BH:BD(30nm)/10nm NS/30nm Liq:ETL/2nm Liq/100nm Al.

The EQE, current efficiency and power efficiency at luminance of 100 cd/m^2 and 1000 cd/m^2 are given in Table 15.

Color standards were established in the 1950s by the National Television System Committee (NTSC) to define the color space used in analog television broadcasting and make color reproduction more uniform.[248] The analog broadcasting system with which the NTSC standards were developed has since been replaced by digital television along with the CIE coordinates of the NTSC color points for comparison. Figure 46 is a CIE diagram showing CIE coordinates for the NTSC standard, the HDTV standard, the old Ir(btp)$_2$(acac) red, Ir(ppy)$_2$(acac) green, and FIrpic blue emitters, along with those of the new red, green, and blue emitters. The new red and green emitters do not produce colors

as saturated as the old emitters, but are much more stable and efficient. The new emitters cover a greater portion of the NTSC space compared with the old emitters, but more saturated blue and green emitters are needed to cover more of the NTSC space.

Table 15: CIE Values, External Quantum Efficiency, Current Efficiency and Power Efficiency at 100 cd/m^2 and 1000 cd/m^2 for new red, new green and new blue emitters

		100 cd/m^2			1000 cd/m^2		
Emitter	CIE	EQE	cd/A	lm/W	EQE	cd/A	lm/W
New red	(0.635, 0.355)	13.1	18.4	22.2	13.3	18.5	16.6
New green	(0.293, 0.650)	10.3	34.7	34.0	12.0	40.3	30.9
New blue	(0.150, 0.200)	3.54	3.74	2.14	3.10	3.28	1.32

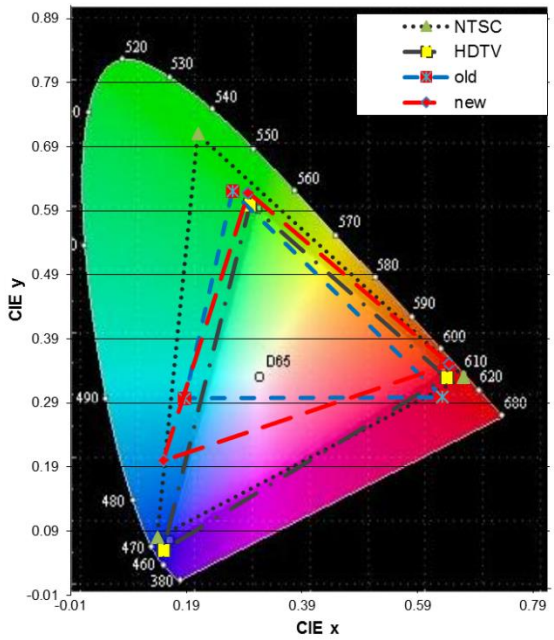

Figure 46: CIE diagram showing approximate coordinates for NTSC standard, HDTV standard, old Ir(btp)$_2$(acac) red, Ir(ppy)$_2$(acac) green and FIrpic blue emitters, and new red, green and blue emitters. The point labeled D65 indicates the standard illuminant. Compared with the old emitters, the new emitters cover a larger portion of the color space, but still show room for improvement.

Figure 47 shows plots of current density vs voltage and luminance vs voltage for the new red, green and blue emitters. A cursory examination shows that devices made with the new emitters have lower turn-on voltages compared with those made with the old emitters.

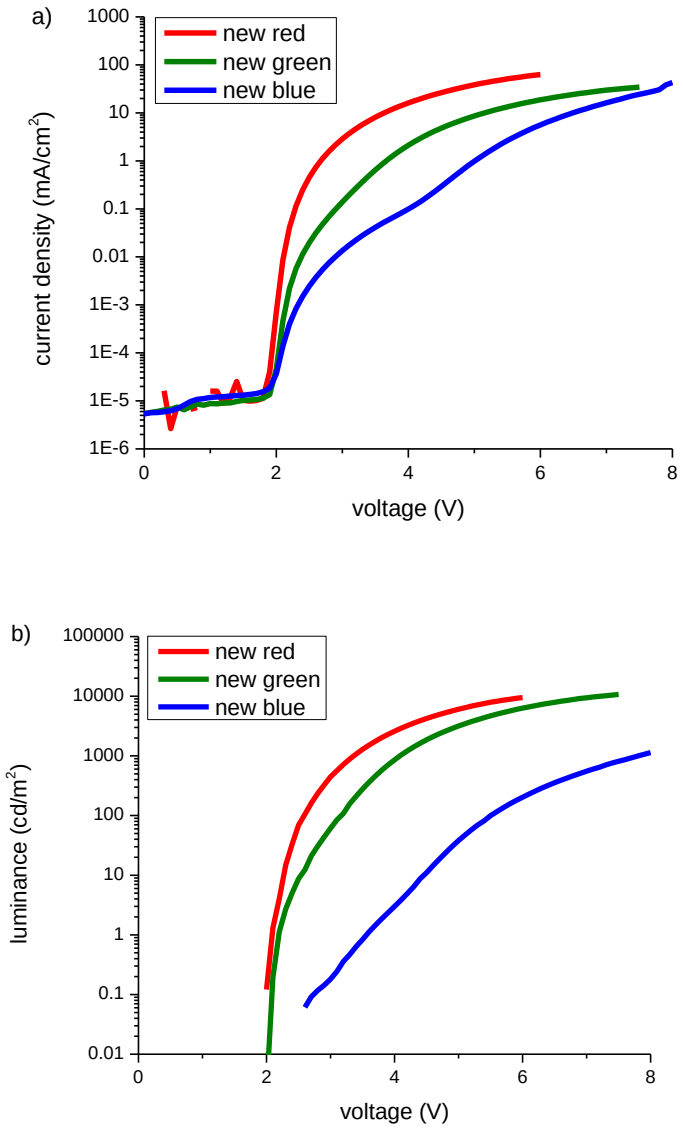

Figure 47: Plots of a) current density vs voltage and b) luminance vs voltage for devices employing new red, green and blue emitters.

Table 16 summarizes the turn-on voltages for devices made with the old and new emitter materials. The new materials show significant reduction in turn-on voltage compared with the old ones. The improvement in performance observed when using the new materials could be attributed to one or more of the following factors: i) red and green dopant materials with higher internal quantum efficiencies; ii) better charge balance in the red and green devices due to the use of a co-host structure; iii) higher charge carrier mobilities in the new materials; and iv) better alignment of the HOMO and LUMO energy levels between the layers. Although we were not permitted to determine HOMO/LUMO levels for the new materials, they most likely have been designed for smaller energy offsets to enhance charge injection. Although the new blue emitter was fluorescent and therefore less inherently efficient than the phosphorescent blue used previously, it also had lower turn-on voltage compared with the old device. This can also be attributed to one or more of the above-mentioned factors. External quantum efficiency vs current density for the new emitters is plotted in Figure 48.

Table 16: Turn-on voltage values for devices made with old $Ir(btp)_2(acac)$ red, $Ir(ppy)_2(acac)$ green and FIrpic blue vs. new red, green and blue emitters

Color	V_f, old (V)	V_f, new (V)	Δ, %
Red	3.2	2.1	-34.4
Green	3.4	2.2	-35.3
Blue	4.9	3.6	-26.5

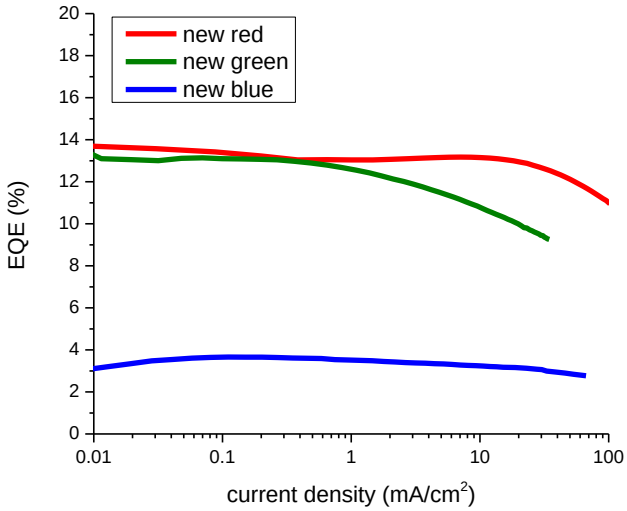

Figure 48: External quantum efficiency vs current density for devices employing new red, green and blue emitters.

The maximum EQEs for the new red and new green materials are 12.4% and 13.1%, respectively. This represents an increase in efficiency of 85% for red and 23.5% for green. The new fluorescent blue emitter showed a decrease of 18.9% compared with the old phosphorescent emitter, which was expected due to the phosphorescent emitter's ability to harvest triplet excitons as well as singlet excitons, while the fluorescent emitter can only harvest singlet excitons. However, the greatly increased emission lifetime of the fluorescent material more than compensated for its decreased efficiency, as discussed below.

Samples for stability testing the new materials were fabricated and tested using constant drive currents of 10 mA/cm^2 and 20 mA/cm^2, using separate devices for each condition. Since the new materials were much more stable than to old materials, accelerated test conditions were used to obtain some basis for comparison with the old

materials. Even under accelerated conditions, the devices did not drop to LT_{50} after several days' time, so we used LT_{98} instead. A summary of results for the 20 mA/cm^2 test condition is shown in Table 17 and plots of normalized luminance vs time are shown in Figure 49.

Table 17: Initial luminance, L_0, and $0.98L_0$ values for new red, green and blue emitters. LT_{98} is the time required for the initial luminance to decay to 98% of its initial value.

Emitter	L_0, cd/m^2	$0.98L_0$, cd/m^2	LT_{98}, hr
New red	2934	2876	1.35
New green	9480	9292	4.35
New blue	988	987*	>>98.8*

*The new blue emitter decayed by only ~0.1% after almost 100 hr, so the test was terminated before reaching LT_{98}

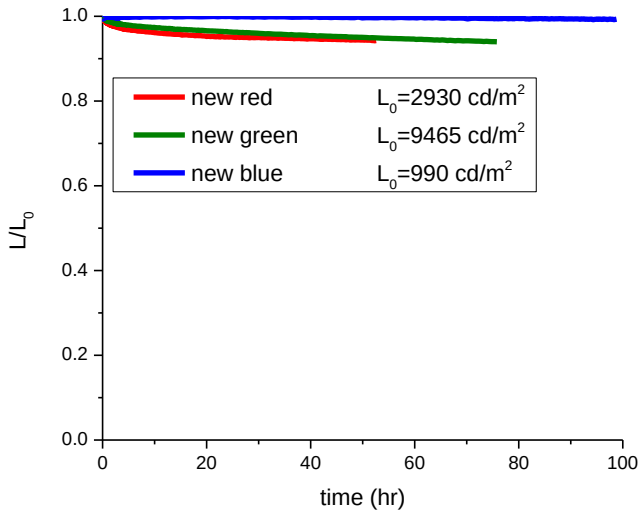

Figure 49: Normalized luminance vs time for devices made with new red, green and blue emitters. All devices were driven at constant 20mA/cm^2 current density. Structures were: 10nm HAT-CN/40nm NPD/30nm EML/10nm HBL/30nm ETL:Liq/2nm Liq/100nm Al. Red EML was [NS:RH:RD (1:0.3):3% RD]. Green EML was [NS:GH:GD (0.3:1):15% GD]. Blue EML was [BH:BD, 8%]

Finally, these red, green and blue OLED materials were incorporated to fabricate a full-color display on flexible substrates. All layers except for the emitter layers (EMLs) were deposited using an open area shadow mask to pattern the display area. The EMLs were deposited sequentially and delineated using a fine metal mask to ensure that the red, green, and blue EMLs were deposited in the appropriate pixels. After deposition, the displays were encapsulated in an inert-atmosphere glovebox using a barrier film provided by 3M Company.

After encapsulation, the displays were debonded from the carriers and tape automated bonded (TAB) to four Solomon SSD1205 gate driver chips and six NEC μPD160038 source driver chip-on-flex integrated circuits, and subsequently TAB bonded to a separate signal distribution flex using anisotropic conducting film (ACF). This architecture enables good flexibility and single-axis rollability, as seen in Figure 50.

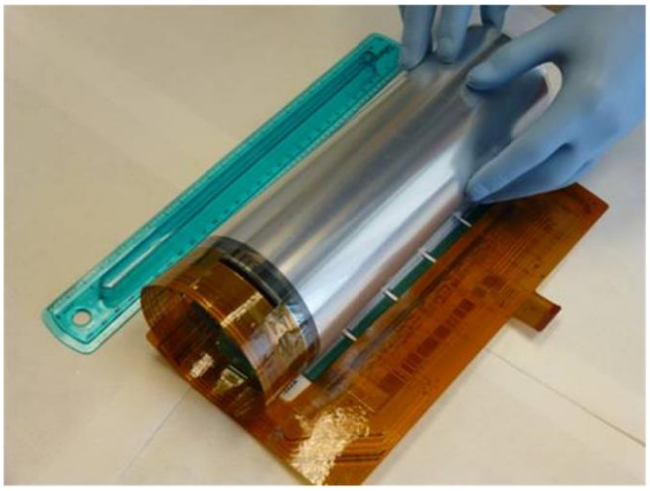

Figure 50: Example of rollability of completed 14.7" full color flexible OLED display after final ACF TAB bonding process.

Light-up images from a completed 14.7” flexible hybrid display are shown in Figure 51. The driver chips and signal distribution flex can be seen in the uppermost part of the figure. The bright rows and columns are the result of shorts in the backplane array. The large dark areas in the lower part of the display are due to defects arising from the backplane fabrication process. Some of the defects may be attributed to manual handling at some of the process steps; most of the process tools used in fabrication have automated substrate handling systems to eliminate manual handling.

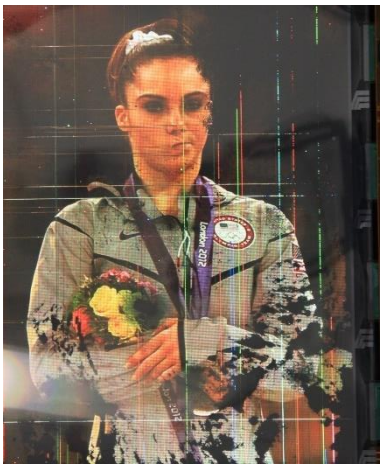

Figure 51: Light-up images on 14.7" flexible full color OLED display

7.4 Summary

A full color OLED display on flexible substrate was fabricated using a low temperature thin-film transistor process with Indium Gallium Zinc Oxide (IGZO) active layer as the backplane. The evaluation and selection of different red, green and blue emitter layers was described. Red and green pixels were fabricated with phosphorescent emitter materials due to the higher efficiency of phosphorescent emitters compared with fluorescent emitters. A blue phosphorescent emitter, FIrpic, was used initially, but its poor stability and sky-blue color led us to incorporate a fluorescent blue emitter instead. The fluorescent blue emitter had a deeper blue than the FIrpic, and enabled the displays to better reproduce the NTSC color space. A deeper blue emitter would enable the display to reproduce an even larger portion of NTSC space.

7.5 Outlook for flexible OLED displays

OLED displays have proven superior to LCDs, and although LCDs still dominate the market, some sources predict that OLEDs will be the display of choice for smartphones and could become a US $20B market by 2020 [249,250,251]. Smaller OLED displays such as those in mobile applications are currently fabricated using fine metal masks (FMM), but other patterning methods such as inkjet printing and laser-transfer are better suited for processing on large-area substrates. The television and monitor market is growing as well, as prices decrease due to increased fabrication capacity and the number of suppliers. These large-area devices are currently made on rigid substrates, but development efforts to produce these on flexible substrates are underway. The advantages of lighter weight and flexibility are not as significant for large-area displays, since these

are typically used for stationary applications. However, the rugged nature of flexible displays is a distinct advantage in harsh environments where they may be subjected to shock and impact.

8: SUMMARY AND PROPOSED FUTURE RESEARCH

8.1 Summary of this work

This dissertation discussed materials and applications of organic light-emitting devices for solid-state lighting and display applications. Chapters 4, 5, and 6 described devices made with new platinum-based emissive materials for solid-state lighting applications. Chapter 7 described the fabrication of a 14.7" diagonal full-color OLED display on a flexible substrate.

Chapter 4 described devices made with a new sky-blue phosphorescent emitter, PtOO2, which attained peak external quantum efficiency (EQE) of 16.4%. White OLED devices made using PtOO2, along with Pt-based red and green emitters (PtON9-me and PtOO3, respectively) in a sublayer architecture achieved EQE of almost 15%, with low efficiency rolloff and a CRI of 77. This showed that Pt-based emissive materials can achieve performance comparable to Ir-based emissive materials.

Chapter 5 documented white OLED devices made with more-efficient Pt-based red (PtN3N-ptb) and blue (PtON1) emitters. The two sublayer architecture provides a simpler fabrication sequence compared with three sublayers. To the author's knowledge, this is the first time that a white OLED with EQE greater than 20% has been demonstrated using exclusively Pt-based emitters. The electroluminescence (EL) spectra depended strongly on the deposition order of the emissive layers, with the layer closest to the hole blocking material showing the dominant emission wavelengths in the spectra. The devices also showed a strong dependence of EL with respect to current density due to the change in red/blue emission ratio. A maximum CRI of 65 was achieved with

devices made using these two emitters. The CRI was limited by the low emission intensity in the green portion of the spectrum.

Pt-based green emitter PtOO8 to achieve a higher CRI. Devices made with the emitter structure B/G/R showed the highest EQE and power efficiency of 18.4% and 25 lm/W, respectively, but only achieved a CRI of 70. This was due to energy transfer from the green to red emissive layers, resulting in a reduction in the green part of the EL spectrum. Devices made with the emitter structure R/B/G showed an EQE as high as 18.3%, but were able to achieve CRI as high as 80. Placing the blue emissive layer between the red and green emitters greatly reduced energy loss from the green to the red layer, and placing the green layer next to the hole blocking layer increased the green emission because of the high exciton concentration at that interface.

Chapter 7 described the fabrication of a full-color flexible OLED-based display, including the fabrication sequence of the thin-film transistor (TFT) backplane. The displays were fabricated on a substrate of heat-stabilized polyethylene naphthalate (PEN). The PEN substrate limited process temperatures to < 200°C, so a suitable material had to be developed for the backplane. TFTs based on amorphous Si active layers were not suitable because of a low mobility of ~0.7 cm^2/V-s. We used an indium-gallium-zinc oxide (IGZO) active layer because of its higher mobility, typically 13 cm^2/V-s for our process. Initial efforts used commonly available phosphorescent red, green, and blue emitters, but poor stability required a change in emissive materials to make a display with acceptable stability. Incorporation of a less-efficient but more stable fluorescent blue and proprietary red and green phosphorescent materials resulted in displays with much longer

lifetimes. Lifetimes were then limited by the availability of a robust encapsulation method.

8.2 Proposed Research Plans

Displays based on organic light-emitting diodes are becoming increasingly common in mobile applications and are expected to become the preferred technology as prices drop due to increased production. Large-area displays for monitors and televisions are also available, with prices becoming competitive with liquid-crystal displays. Research and development continue to design materials with higher efficiency, longer lifetimes, and better color saturation. A stable, efficient, deep blue phosphorescent emitter is critical to achieve the highest performance in OLEDs.

White OLEDs are available commercially, although the high cost compared with existing lighting sources has limited their adoption to specialty applications for the time being. Prices for OLED-based solid-state lighting should continue to drop as material and production methods continue to improve, and programs by the US Department of Energy and other countries have put a priority on developing white OLEDs as a source of inexpensive, high-efficiency, high-quality lighting.

Challenges remain. Research on emissive materials with better stability, higher efficiency and better color saturation continues, particularly for stable and efficient blue emitters. Phosphorescent materials have the potential to achieve 100% internal quantum efficiency, but new approaches such as thermally assisted delayed fluorescence (TADF) have demonstrated efficiencies approaching phosphorescent emitters using purely organic

materials, eliminating the added cost of expensive of metals such as iridium, platinum, osmium, and rhenium.

Other factors which will lead to more-efficient devices are: improved charge injection, charge transport, host, and charge blocking layers; structures with improved outcoupling; reduced EQE roll-off; and reduced resistive losses. Tyan calculated a theoretical maximum efficacy of 249 lm/W for an all-phosphorescent, single stack white OLED, assuming 100% outcoupling efficiency and an operating voltage of 2.9 V[43]. Some of these assumptions, such as 100% outcoupling efficiency, are not realistic. WOLED luminaires with efficacies as high as 90 lm/W are commercially available as of this writing[252]. In its 2016 Solid-State Lighting R&D Plan, the US Department of Energy set a panel efficacy goal of 100 lm/W by 2020, with a goal of 160 lm/W by 2025 and a goal of 190 lm/W[46]. The price reduction goal is < $50/klm by 2020, to make WOLEDs cost-competitive for widespread adoption.

OLED televisions on glass substrates are commercially available at prices competitive with liquid-crystal displays that are the dominant technology. OLED displays are most commonly used where ruggedness is not a factor, so they can utilize rigid glass encapsulation materials. However, fabrication of OLEDs for display and solid-state lighting on more-rugged flexible substrates requires encapsulation methods that are also flexible. Common approaches are deposition of multiple dyads of inorganic and organic materials, or deposition processes that produce a single inorganic-organic hybrid layer. Recent advances in inkjet printing equipment and materials for thin-film encapsulation

have demonstrated excellent results and should further reduce production costs, enabling wider adoption of flexible OLED devices in the near future.

REFERENCES

1 Someya, T., Pal, B., Huang, J., & Katz, H. E. (2008, July). Organic Semiconductor Devices with Enhanced Field and Environmental Responses for Novel Applications. MRS Bulletin, 33, p. 609

2 Shinar, J., & Shinar, R., "Organic light-emitting devices (OLEDs) and OLED-based chemical and biological sensors: an overview," J Phys D: Appl Phys, 41, (2008) 13301. doi:10.1088/0022-3727/41/13/133001

3 Bernards, D. A., Owens, R. M., & Malliaras, G. G. (2008). Organic Semiconductors in Sensor Applications (Vol. 107). Heidelberg: Springer Series in Materials Science

4 Joseph Shinar, Zhaoqun Zhou, Yuankun Cai, and Ruth Shinar, "Recent Developments in OLED-Based Chemical and Biological Sensors," Organic-based Chemical and Biological Sensors, Proc. of SPIE 6659 (2007) 665906-1, doi:10.1117/12.731775

5 http://blog.sony.com/press/technicolor-stays-ahead-of-hdr-curve-with-sony-x300/

6 http://olednet.com/wp-content/uploads/2015/01/141110_LGDPOLED3.jpg

7 Forrest, S. R. (2004, April 29). The path to ubiquitous and low-cost organic electronic devices on plastic. Nature, 428, 911-918

8 V. Y. Merritt and H. J. Hovel, "Organic solar cells of hydroxyl squarylium," Applied Physics Letters 29 (1976); doi: 10.1063/1.89101

9 C. W. Tang, "Two layer organic photovoltaic device," Appl. Phys. Lett. 48 (1986) 183; doi: 10.1063/1.96937

10 Yang (Michael) Yang, Wei Chen, Letian Dou, Wei-Hsuan Chang, Hsin-Sheng Duan, Brion Bob, Gang Li and Yang Yang, "High-performance multiple-donor bulk heterojunction solar cells," Nature Photonics, 9 February 2015, doi:10.1038/NPHOTON.2015.9

11 Peter Peumans, Aharon Yakimov, and Stephen R. Forrest, "Small molecular weight organic thin-film photodetectors and solar cells," Journal of Applied Physics 93(7) (2003) 3693-3723; doi: 10.1063/1.1534621

12 Kim, Inho. Efficient organic solar cells based on phthalocyanines. Ph.D. dissertation, Arizona State University (2011)

13 Fleetham, Tyler Blain. Organic Optoelectronic Devices Employing Small Molecules. Ph.D. dissertation, Arizona State University (2014)

14 Chang-Zhi Li, Hin-Lap Yip and Alex K.-Y. Jen, "Functional fullerenes for organic photovoltaics," J Mater Chem 22 (2012) 4161-4177; doi: 10.1039/C2JM15126J

15 Claudia N. Hoth, Pavel Schilinsky, Stelios A. Choulis, and Christoph Brabec, "Printing Highly Efficient Organic Solar Cells," Nano Letters 8(9) (2008) 2806-2813 doi: 10.1021/nl801365k

16 Navpreet Kaur, Mandeep Singh, Dinesh Pathak, Tomas Wagner, J. M. Nunzi, "Organic materials for photovoltaic applications: Review and mechanism," Synthetic Metals 190 (2014) 20-26, doi: 10.1016/j.synthmet.2014.01.022

17 Martin A. Green, Keith Emery, Yoshihiro Hishikawa, Wilhelm Warta and Ewan Dunlop, "Solar Cell Efficiency Tables (Version 45)," Prog. Photovolt. Res. Appl. 2015; 23:1-9, doi:10.1002/pip.2573

18 M. Eritt, C. May, K. Leo, M. Toerker, C. Radehaus, "OLED manufacturing for larger area lighting applications," Thin Solid Films 518 (2010) 3042-3045

19 http://www.lgdisplay.com/eng/prcenter/newsView?articleMgtNo=5003

20 Richard R. Lunt and Vladimir Bulovic, "Transparent, near-infrared organic photovoltaic solar cells for window and energy-scavenging applications," Applied Physics Letters 98 (2011) 113305, doi: 10.1063/1.3567516

21 Jens A. Hauch, Pavel Schilinsky, Stelios A. Choulis, Richard Childers, Markus Biele, Christoph Brabec, "Flexible organic P3HT:PCBM bulk-heterojunction modules with more than 1 year outdoor lifetime," Solar Energy Materials and Solar Cells 92 (2008) 727-731

22 Kang-Jun Baeg, Maddalena Binda, Dario Natali, Mario Caironi, and Yong-Young Noh," Organic Light Detectors: Photodiodes and Phototransistors," Advanced Materials 25 (2013) 4267-4295, doi: 10.1002/adma.201204979

23 Takao Someya, Ananth Dodabalapur, Jia Huang, Kevin C. See, and Howard Katz, "Chemical and Physical Sensing by Organic Field-Effect Transistors and Related Devices," Adv. Mater. 22 (2010) 3799-3811, doi: 10.1002/adma.200902760

24 Ross D. Jansen-van Vuuren, Almantas Pivrikas, Ajay K. Pandey and Paul L. Burn, "Colour selective organic photodetectors utilizing ketocyanine-cored dendrimers," J. Mater. Chem. C, 2013, 1, 3532, doi: 10.1039/c3tc30472h

25 Yu, Gang. Image sensors made from organic semiconductors. US Patent 6,300,612

26 http://www.isorg.fr/

27 E. Kraker, B. Lamprecht, A. Haase, G. Jakopic, T. Abel, C. Konrad, S. Köstler, M. Tscherner, B. Stadlober, T. Mayr, "Optochemical sensor, based on screenprinted fluorescent sensorspots surrounded by organic photodiodes for multianalyte detection," Proc. Of SPIE vol. 7779, Organic Semiconductors in Sensors and Bioelectronics III, Ruth Shinar, Ioannis Kymissis, (2010) 777904-1, doi: 10.1117/12.859857

28 Timothy M. Woudenberg; J. Stevens," Quantitative PCR by real-time detection," Proc. SPIE 2680, Ultrasensitive Biochemical Diagnostics, 306 (April 1, 1996); doi: 10.1117/12.237619

29 Andrea Pais, Ansuman Banerjee, David Klotzin and Ian Papautsky, "High-sensitivity, disposable lab-on-a-chip with thin-film organic electronics for fluorescence detection," Lab Chip 8 (2008) 794-800, doi: 10.1039/b715143h

30 Ansuman Banerjee, Yun Shuai, Rahul Dixit, Ian Papautsky, and David Klotzkin, "Concentration dependence of fluorescence signal in a microfluidic fluorescence detector," Journal of Luminescence 130 (2010) 1095-1100, doi: 10.1016/j.jlumin.2010.02.002

31 Joseph T. Smith, Benjamin A. Katchman, Dixie E. Kullman, Uwadiae Obahiagbon, Yong-Kyun Lee, Barry P. O'Brien, Gregory B. Raupp, Karen S. Anderson, Jennifer Blain Christen, "Application of Flexible OLED Display Technology to Point-of-Care Medical Diagnostic Testing," IEEE Journal of Display Technology 12(3) (2016) 273 10.1002/adma.201002636

32 Yindar Chuo, Clint Landrock, Badr Omrane, Jeydmer Aristizabal, Jasbir N. Patel, Marcin Marzencki, Bozena Kaminska, "Towards Self-Powering Touch/Flex-Sensitive OLED Systems," IEEE Sensors Journal 11(11) (2011) 2771-2779; doi 10.1109/JSEN.2011.2160337

33 http://www.scientificamerican.com/article/optogenetics-controlling/

34 Lief Fenno, Ofer Yizhar, and Karl Deisseroth, "The development and application of optogenetics," Annu Rev Neurosci 34 (2011) 389-412, doi: 10.1146/annurev-neuro-061010-113817

35 Chenchen Song and Thomas Knöpfel, "Optogenetics enlightens neuroscience drug discovery," Nature Reviews 15 (2016) 97, doi: 10.1038/nrd.2015.15

36 Jing Wang, Fabien Wagner, David A Borton, Jiayi Zhang, Ilker Ozden, Rebecca D Burwell, Arto V Nurmikko, Rick van Wagenen, Ilka Diester and Karl Deisseroth, "Integrated device for combined optical neuromodulation and electrical recording for chronic in vivo applications," J. Neural Eng. 9 (2012) 016601, doi: 10.1088/1741-2560/9/1/016001

37 Joseph T. Smith, Barry O'Brien, Yong-Kyun Lee, Edward Bawolek, and Jennifer Blain Christen, "Application of Flexible OLED Display Technology for Electro-Optical Stimulation and/or Silencing of Neural Activity," Journal of Display Technology 10(6) (2014) 514; doi: 10.1109/JDT.2014.2308436

38 D. Feili, M. Schuettler, and T. Siteglitz, "Flexible microelectrode arrays with integrated organic semiconductors," in 9th Annu. Conf. Int. FES Soc., 2004

39 International Energy Agency, Key World Statistics: https://www.iea.org/publications/freepublications/publication/key-world-energy-statistics-2015.html

40 Enerdata, Global Statistics Energy Yearbook 2015, https://yearbook.enerdata.net/world-electricity-production-map-graph-and-data.htm

41 Malte C. Gather, Anne Köhnen and Klaus Meerholz, "White Organic Light-Emitting Diodes," Advanced Materials 23 (2011) 233-248, doi

42 Humphreys, C. J. (2008). Solid State Lighting. MRS Bulletin, 33(4), 459-470. doi:10.1557/mrs2008.91

43 Yuan-Sheng Tyan, "Organic light-emitting-diode lighting overview," Journal of Photonics for Energy 1 (2011) 011009-1, doi: 10.1117/1.3529412

44 Buy Light Fixtures. (n.d.). http://www.buylightfixtures.com/led-light-fixtures-1.aspx. Retrieved 2015

45 Home Depot. (n.d.). Retrieved from http://www.homedepot.com/c/SPC_LF_LEDLightFixtures.

46 DOE SSL Program, "R&D Plan," edited by James Brodrick, Ph.D. (2016); http://energy.gov/eere/energybasics;

47 Pacific Northwest National Lab (2014, February) CALiPER Retail Lamps Study. Retrieved March 18, 2016 from US Department of Energy, Energy Efficiency and Renewable Energy: http://apps1.eere.energy.gov/buildings/publications/pdfs/ssl/caliper_retail-lamps-study3.pdf

48 P. A. Levermore, A. B. Dyatkin, Z. Elshenawy, H. Pang, J. Silvernail, E. Krall, S. R. Forrest, “Phosphorescent organic light-emitting diodes for high-efficiency long-lifetime solid-state lighting,” Journal of Photonics for Energy 2 (2012) 021-205; doi:10.1117/1.JPE.2.021205

49 G. Parthasarathy, C. Adachi, P. E. Burrows, and S. R. Forrest, “High-efficiency transparent organic light-emitting devices,” Applied Physics Letters 76 (2000) 2128; doi:10.1063/1.126275

50 K. Werner, “Ten Intriguing Display Discoveries from CES 2016,” Information Display 32(2) (2016) 30-32

51 Y. K. Lee, B. O’Brien, J. Kaminski, and N. Colaneri, “Highly Transparency Cathode Prepared by Sputtering and Its Application to Transparent OLED Achieved Consistent Behavior from Bottom and Top Emission,” IMID 2012 Digest, p152-153

52 B. Tian, S.-W. Kim, K.-S. Lee, and H. Aziz,” Transparent organic light-emitting devices using a MoO3/Ag/MoO3 cathode,” Journal of Applied Physics 110 (2011) 104507; doi:10.10631.3662194

53 J. Kido, M. Kimura, and K. Nagai,”Multilayer White Light-Emitting Electroluminescent Device,“ Science 267 (1995) 1332

54 Reineke, S., Lindner, F., Schwartz, G., Seidler, N., Walzer, K., Lüssem, B., & Leo, K. (2009). White organic light-emitting diodes with fluorescent tube efficiency. Nature, 459, 234. doi:10.1038/nature08003

55 Kazuyuki Yamae, Hiroya Tsuji, Varuut Kittichungchit, Nobuhiro Ide, Takuya Komoda, “Highly efficient white organic light-emitting diodes with over 100 lm/W for next-generation solid-state lighting,” Journal of the SID (2014), doi: 10.1002/jsid.2-3

56 Y. Shirota and H. Kageyama, “Charge Carrier Transporting Molecular Materials and Their Applications in Devices,” Chem. Rev. 107 (2007) 953-1010; doi:10.1021/cr050143

57 H. Jeong, H. Shin, J. Lee, B. Kim, Y.-I. Park, K. S. Yook, J. Park, ”Recent progress in the use of fluorescent and phosphorescent organic compounds for organic light-emitting diode lighting,” Journal of Photonics for Energy 5 (2015) 057608-1; doi:10.1117/1.JPE.5.057608

58 Grayson L. Ingram and Zheng-Hong Lu, “Design Principles for highly efficient organic light-emitting diodes,” Journal of Photonics for Energy 4 (2014) 040993; doi:10.1117/1.JPE.4.040993

59 Kamtekar, K. T., Monkman, A. P., & Bryce, M. R. (2010). Recent Advances in White Organic Light-Emitting Materials and Devices (WOLEDs). Advanced Materials, 22, 572-582. doi:10.1002/adma.200902148

60 Sebastian Reineke, Michael Thomschke, Björn Lüssem and Karl Leo, "White organic light-emitting diodes: Status and perspective," Reviews of Modern Physics 85 (2013) 1-53. doi:10.1103/RevModPhys.85.1245

61 http://hyperphysics.phy-astr.gsu.edu/hbase/vision/colcon.html#c1, accessed May 2016

62 http://hyperphysics.phy-astr.gsu.edu/hbase/vision/colcon.html#c1, accessed May 2016

63 http://physics.nist.gov/cuu/Units/candela.html, accessed May 2016

64 http://hyperphysics.phy-astr.gsu.edu/hbase/vision/lumpow.html#c2, accessed May 2016

65 M. H. Lu and J. C. Sturm, "Optimization of external coupling and light emission in organic light-emitting devices: modeling and experiment," Journal of Applied Physics 91 (2002) 595; doi:10.1063/1.1425448

66 Zhongbin Wu, Dongge Ma, "Recent advances in white organic light-emitting diodes," Materials Science and Engineering R 107 (2016) 1-42; doi: 10.1016/j.mser.2016.06.001

67 C. Adachi, M. A. Baldo, M. E. Thompson, and S. R. Forrest, "Nearly 100% internal phosphorescence efficiency in an organic light-emitting device," Journal of Applied Physics 90 (2001) 5048; doi: 10.1063/1.1409582

68 U. S. Department of Energy, Building Technologies Office. (2013). Solid State Lighting: Brilliant Solutions for America's Energy Future.

69 http://www.lrc.rpi.edu/programs/NLPIP/glossary.asp

70 Nouredine Zettili, "Quantum Mechanics: Concepts and Applications, 2ed" Wiley, West Sussex, United Kingdom (2009)

71 T. Azuma, H. Einhorn, M. Halstead, C. Jerome, J. de Kerf, J. Kritl, W. Münch, E. Barth, J. Ouweitjes, M. Richter, and G. Siljeholm, CIE Publications 13.3, 1 (1995)

72 Shirakawa, H., Louis, E. J., MacDiarmid, A. G., Chiang , C. K., & Heeger , A. J. (1977). Synthesis of Electrically Conductive Organic Polymers: Halogen Derivatives of Polyacetylene, (CH)x. J. C. S. Chem. Comm., 578.

73 M. Pfeiffer, K. Leo, X. Zhou, J. S. Huang, M. Hoffmann, A. Werner, J. Blochwitz-Nimoth, "Doped organic semiconductors: Physics and application in light emitting diodes," Org. Elect. 4 (2003) 89-103

74 Atkins, P., & De Paula, J. (2010). Physical Chemistry (9th ed.)

75 Yersin, H., & Finkenzeller , W. J. (2008). Triplet Emitters for Organic Light-Emitting Diodes: Basic Properties. In H. Yersin (Ed.), Highly Efficient OLEDs with Phosphorescent Materials (pp. 1-97). WILEY-VCH Verlag.

76 I. G. Hill, A. Kahn, Z. G. Soos, and R. A. Pascal, "Charge-separation energy in films of pi-conjugated organic molecules," Chemical Physics Letters 327 (2000) 181

77 Pierret, R. F. (1996). Semiconductor Device Fundamentals. New York: Addison-Wesley.

78 Michael Kasha, "Characterization of electronic transitions in complex molecules," Discuss. Faraday Soc 9 (1950) 14-19; doi: 10.1039/DF9500900014

79 M. A. Baldo, "The Electronic and Optical Properties of Amorphous Organic Semiconductors," Ph.D. dissertation, Princeton University, 2001

80 Sergey Lamansky, Peter Djurovich, Drew Murphy, Feras Abdel-Razzaq, Raymond Kwong, Irina Tsyba, Manfred Bortz, Becky Mui, Robert Bau, and Mark E. Thompson, "Synthesis and Characterization of Phosphorescent Cyclometalated Iridium Complexes," Inorganic Chemistry, 40(7), 1704-1711. doi:10.1021/ic0008969

81 Nicholas J. Turro, "Modern Molecular Photochemistry," University Science Books, Sausalito CA, 1991

82 M. Born and R. J. Oppenheimer, "Zur Quanttheorie der Moleculen," Annals of Physics 87 (1927) 457; doi: andp.19273892002

83 J. Franck, "Elementary processes of photochemical reactions," Trans. Faraday Soc. 21 (1926) 536-542; doi: 10.1039/TF9262100536; Edward Condon, "A Theory of Intensity Distribution in Band Systems," Phys. Rev. 28 (1926) 1182-1201; doi: 10.1103/PhysRev.28.1182

84 M. Pope and C. E. Swenberg, Electronic Processes in Organic Crystals and Polymers, Oxford University Press, New York (1999)

85 T. Förster, "Transfer mechanisms of electronic excitation," Discussions of the Faraday Society 27 (1959) 7-17

86 Youtian Tao, Chuluo Yang and Jingui Qin, "Organic host materials for phosphorescent organic light-emitting diodes," Chem. Soc. Rev. 40 (2011) 2943–2970; doi: 10.1039/C0CS00160K

87 Dexter, D. L., "A Theory of Sensitized Luminescence in Solids," Journal of Chemical Physics, 21 (1953) 836. doi:10.1063/1.1699044

88 Kawamura, Y., Brooks , J., Brown , J. J., Sasabe , H., & Adachi , C. (2006). Intermolecular Interaction and a Concentration-Quenching Mechanism of Phosphorescent Ir(III) Complexes in a Solid Film. Physical Review Letters, 96, 017404. doi:10.1103/PhysRevLett.96.017404

89 Baldo, M. A., & Forrest , S. R. (2000). Transient analysis of organic electrophosphorescence: I. Transient analysis of triplet energy transfer. Physical Review B, 62, 10958.

90 Baldo, M. A., Adachi , C., & Forrest , S. R. (2000). Transient analysis of organic electrophosphorescence. II. Transient analysis of triplet-triplet annihilation. Physical Review B, 62, 10967.

91 Zakya H. Kafafi, (2005) Organic Electroluminescence, CRC Press, Boca Raton, FL

92 Y. Sun, N. C. Giebink, H. Kanno, B. Ma, M. E. Thompson, and S. R. Forrest, "Management of singlet and triplet excitons for efficient white organic light-emitting devices," Nature 440 (2006) 908-912

93 Y. Divayana and X. Sun, "Observation of Excitonic Quenching by Long-Range Dipole-Dipole Interaction in Sequentially Doped Organic Phosphorescent Host-Guest System," Phys. Rev. Lett. 99(14) (2007) 143003

94 N. C. Giebink, B. W. D'Andrade, M. S. Weaver, P. B. Mackenzie, J. J. Brown, M. E. Thompson, and S. R. Forrest,"Intrinsic luminance loss in phosphorescent small-molecule organic light emitting devices due to bimolecular annihilation reactions," Journal of Applied Physics 103 (2008) 044509; doi: 10.1063/1.2884530

95 Dandan Song, Suling Zhao, Yichun Luo, and Hany Aziz, "Causes of efficiency roll-off in phosphorescent organic light emitting devices: Triplet-triplet annihilation versus triplet-polaron quenching," Appl. Phys. Lett. 97 (2010) 243304; doi: 10.1063/1.3527085

96 Bernanose, A., "Electroluminescence of Organic Compounds," British Journal of Applied Physics 6 (1955) S54

97 Helfrich, W., & Schneider, W. G., "Recombination Radiation in Anthracene Crystals," Physical Review Letters 14 (1965) 229; doi: 10.1103/PhysRevLett.14.229

98 Vincett, P. S., Barlow, W. A., Hann, R. A., & Roberts, G. G. (1982). Electrical conduction and low voltage blue electroluminescence in vacuum-deposited organic films. Thin Solid Films, 94, 171-183

99 Tang, C. W., & VanSlyke, S. A. (1987). Organic Electroluminescent Devices. Applied Physics Letters, 51(12), 65

100 Tang, C. W., VanSlyke , S. A., & Chen , C. H. (1989). Electroluminescence of doped organic thin films. Journal of Applied Physics, 65, 3610. doi:10.1063/1.343409

101 Friend, R. H; Brown, A. R; Burns, P. L; Mackay, K; Burroughes, J. H; Marks, R. N; Holmes, A. B; Bradley, D. D. C., "Light-emitting diodes based on conjugated polymers," Nature, 347, 539-541; doi: 10.1038/347539a0

102 Brian W. D'Andrade, Russell J. Holmes, and Stephen R. Forrest, "Efficient Organic Electrophosphorescent White-Light-Emitting Device with a Triple Doped Emissive Layer," Adv. Mater. 16(7) (2004), 624; doi: 10.1002/adma.200306670

103 Kyoung Soo Yook, Byung Doo Chin, Jun Yeob Lee, Brian E. Lassiter, and Stephen R. Forrest, "Vertical orientation of copper phthalocyanine in organic solar cells using a small molecular weight organic templating layer," Applied Physics Letters 99 (2011) 043308; doi: 10.1063/1.3621837

104 Lixin Xiao, Zhijian Chen, Bo Qu, Jiaxiu Luo, Sheng Kong, Qihuang Gong, and Junji Kido, "Recent Progresses on Materials for Electrophosphorescent Organic Light-Emitting Devices," Adv. Mater. 23 (2011) 926-952; doi: 10.1002/adma.20103128

105 Guijiang Zhou, Wai-Yeung Wong, Si Suo, "Recent progress and current challenges in phosphorescent white organic light-emitting diodes (WOLEDs)," Journal of Photochemistry and Photobiology C: Photochemistry Reviews 11 (2010) 133-156; doi: 10.1016/j.jphotochemrev.2011.01.001

106 Gerwin H. Gelinck, Abhishek Kumar, Date Moet, Jan-Laurens P. J. van der Steen, Albert J. J. M. van Breemen, Santosh Shanmugam, Arjan Langen, Jan Gilot, Pim Groen, Ronn Andreesen, Matthias Simon, Walter Ruetten, Alexander U, Douglas, Rob Raaijmakers, Pawel E. Malinowski, and Kris Myny, "X-Ray Detector-on-Plastic With High Sensitivity Using Low Cost, Solution-Processed Organic Photodiodes," IEEE Transactions on Electron Devices 63(1) (2016) 197-204; doi: 10.1109/TED.2015.2432572

107 M. A. Baldo and S. R. Forrest, “Interface-limited injection in amorphous organic semiconductors,” Physical Review B 64 (2001) 085201; doi: 10.1103/PhysRevB.64.085201

108 Baldo, M. A., O'Brien, D. F., You, Y., Shoustikov, A., Sibley, S., Thompson, M. E., & Forrest, S. A. (1999, Nov 15). Highly Efficient Phosphorescent Emission form Organic Electroluminescent Devices. Physical Review B, 60(20), 14442.

109 Segal, M., Baldo, M. A., Holmes, R. J., Forrest, S. R., & Soos, Z. G. (2003). Excitonic Singlet-Triplet Ratios in Molecular and Polymeric Organic Materials. Physical Review B, 68(7), p. 075211

110 Yersin, H., Rausch , A. F., Czerwieniec, R., Hofbeck, T., & Fischer, T. (2011). The triplet state of organo-transition metal compounds. Triplet harvesting and singlet harvesting for efficient OLEDs. Coordination Chemistry Reviews, 255, 2622-2652. doi:10.1016/j.ccr.2011. 01.042

111 Pope, M., & Swenberg , C. E. (1999). Electronic Processes in Organic Crystals and Polymers. Oxford University Press.

112 M. A. Baldo, D. F. O’Brien, Y. You, A. Shoustikov, S. Sibley, M. E. Thompson & S. R. Forrest, “Highly efficient phosphorescent emission from organic electroluminescent devices,” Nature 395 (1998) 151-154

113 Chihaya Adachi, Marc A. Baldo, and Stephen R. Forrest, “High-efficiency organic electrophosphorescent devices with tris(2-phenylpyridine)iridium doped into electron-transporting materials,” Applied Physics Letters 77 (2000) 904; doi: 10.1063/1.1306639

114 Colombo, M. G., Hauser , A., & Güdel , H. U. (1993). Evidence for Strong Mixing between the LC and MLCT Excited States in Bis(2-phenylpyridinato-C2,N’)(2,2’-bipyridine)iridium(III). Inorganic Chemistry, 32, 3088-3092

115 Beljonne, D., Shuai , Z., Pourtois , G., & Bredas , J. L. (2001). Spin-Orbit Coupling and Intersystem Crossing in Conjugated Polymers: A Configuration Interaction Description. J. Phys. Chem. A, 105, 3899-3907

116 Rausch, A. F., Homeier , H. H., Djurovich , P. I., Thompson , M. E., & Yersin , H. (2007). Spin-orbit coupling routes and OLED performance - Studies of blue-light emitting Ir(III) and Pt(II) complexes. Proceedings of SPIE , 6655, 66550F-1. doi:10.1117/12.731225

117 M. A. Baldo, S. Lamansky, P. E. Burrows, M. E. Thompson, and S. R. Forrest, "Very high-efficiency green organic light-emitting devices based on electrophosphorescence," Applied Physics Letters 75 (1999); doi: 10.1063/1.124258

118 Jan Kalinowski, Organic Light-Emitting Diodes: Principles, Characteristics, and Processes, Marcel Dekker, New York (2005)

119 Ishii, H., Sugiyama, K., Ito, E., & Seki, K. (1999). Energy Level Alignment and Interfacial Electronic Structures at Organic/Metal and Organic/Organic Interfaces. Advanced Materials, 11(8), 605-625.

120 Koch, N. (2012). Electronic structure of interfaces with conjugated organic materials. Phys. Status Solidi RRL, 6(7), 277-293. doi:10.1002/pssr.201206208

121 Xiao-Ming Yu, Hoi-Sing Kwok, Wai-Yeung Wong, and Gui-Jiang Zhou, "High-Efficiency White Organic Light-Emitting Devices Based on a Highly Amorphous Iridium(III) Orange Phosphor," Chem. Mater. 18(21) (2006) 5097-5103; doi: 10.1021/cm061030p

122 Hung, L. S., Tang , C. W., & Mason , M. (1997). Enhanced electron injection in organic electroluminescence devices using an Al/LiF electrode. Applied Physics Letters, 70, 152. doi:10.1063/1.118344

123 Ma, J. W., Xu , W., Jiang , X. Y., & Zhang , Z. L. (2008). Organic light-emitting diodes based on new n-doped electron transport layer. Synthetic Metals, 158, 810-814. doi:10.1016/j.synthmet.2008.05.009

124 Liao, L.-S., Slusarek, W. K., Hatwar , T. K., Ricks , M. L., & Comfort , D. L. (2008). Tandem Organic Light-Emitting Diode using Hexaazatriphenylene Hexacarbonitrile in the Intermediate Connector. Advanced Materials, 20, 324-329. doi:10.1002/adma.200700454

125 Szu-Yi Chen, Ta-Ya Chu, Jenn-Fang Chen, Chien-Ying Su, Chin H. Chen, "Stable inverted bottom-emitting organic electroluminescent devices with molecular doping and morphology improvement," Appl. Phys. Lett. 89(5) (2006) 53518; doi: 10.1063/1.2335374

126 F. Li, H. Tang, J. Anderegg, J. Shinar, "Fabrication and electroluminescence of double-layered organic light-emitting diodes with the Al2O3/Al cathode," Appl. Phys. Lett. 70 (1997) 1233; doi: 10.1063/1.118539

127 Zilan Shen, Paul E. Burrows, Vladimir Bulović, Stephen R. Forrest, Mark E. Thompson, "Three-Color, Tunable, Organic Light-Emitting Devices," Science 276 (1997) 2009-2011; doi: 10.1126/science.276.5321.2009

128 G. Gu, G. Parthasarathy, P. Tian, P. E. Burrows, S. R. Forrest, ”Transparent stacked organic light emitting devices. I. Design principles and transparent compound electrodes,” J. Appl. Phys 86 (1999) 2009; doi: 10.1063/1.371331

129 Gufeng He, Carsten Rothe, Sven Murano, Ansgar Werner, Olaf Zeika, Jan Birnstock, “White stacked OLED with 38 lm/W and 100,000-hour lifetime at 1000 cd/m2 for display and lighting applications,” Journal of the SID 17/2 (2009) 159; doi:10.1889/JSID17.2.159

130 Tyler Fleetham and Jian Li, “Recent advances in white organic light-emitting diodes employing a single-emissive material,” Journal of Photonics for Energy 4 (2014) 040991-1; doi:10.1117/1.JPE.4.040991

131 Tianyou Zhang, Bei Chu, Wenlian Li, Zisheng Su, Qi Ming Peng, Bo Zhao, Yongshi Luo, Fangming Jin, Xingwu Yan, Yuan Gao, Hairuo Wu, Feng Zhang, Di Fan, and Junbo Wang, “Efficient Triplet Application in Exciplex Delayed-Fluorescence OLEDs Using a Reverse Intersystem Crossing Mechanism Based on a ΔES-T of around Zero,” ACS Appl. Mater. Interfaces 6(15) (2014) 11907-11914; doi: 10.1021/am501164s

132 Tianyou Zhang, Bo Zhao, Bei Chu, Wenlian Li, Zisheng Su, Xingwa Yan, Chengyan Liu, Hairuo Wu, Yuan Gao, Fangming Jin, Fuhua Hou, “Simple structured hybrid WOLEDs based on incomplete energy transfer mechanism: from blue exciplex to orange dopant,” Sci. Rep. 5 (2015) 10234; doi:10.1038/srep10234

133 D'Andrade, B. W., & Forrest , S. R. (2004). White organic light-emitting devices for solid-state lighting. Adv. Mater,, 16(18), 1585-1595. doi:10.1002/(ISSN)1521-4095

134 Qi Wang, Jungqiao Ding, Dongge Ma, Yanxiang Cheng, Lixiang Wang, Fosong Wang, “Manipulating Charges and Excitons within a Single-Host System to Accomplish Efficiency/CRI/Color-Stability Trade-off for High-Performance OWLEDs,” Adv. Mater. 21(23) (2009) 2397-2401; doi: 10.1002/adma.200803312

135 Kenichi Goushi, Kou Yoshida, Keigo Sato and Chihaya Adachi, “Organic light-emitting diodes employing efficient reverse intersystem crossing for triplet-to-singlet state conversion,” Nature Photonics 6 (2012) 253

136 Hiroki Uoyama, Kenichi Goushi, Katsuyuki Shizu, Hiroko Nomura, Chihaya Adachi, “Highly efficient organic light-emitting diodes from delayed fluorescence,” Nature 492 (2012) 234-238; doi: 10.1038/nature11687

137 Keigo Sato, Katsuyuki Shizu, Kazuaki Yoshimura, Atsushi Kawada, Hiroshi Miyazaki, and Chihaya Adachi, “Organic Luminescent Molecule with Energetically Equivalent Singlet and Triplet Excited States for Organic Light-Emitting Diodes,” Phys. Rev. Lett. 110 (2013) 247401; doi: 10.1103/PhysRevLett.110.247401

138 Takehiro Takahashi, Katsuyuki Shizu, Takuma Yasuda, Kazunori Togashi and Chihaya Adachi, "Donor-acceptor-structured 1,4-diazatriphenylene derivatives exhibiting thermally activated delayed fluorescence: design and synthesis, photophysical properties and OLED characteristics," Sci. Technol. Adv. Mater. 15(3) (2014) 034202; doi: 10.1088/1468-6996/15/3/034202

139 Yu Yang, Tai Peng, Kaiqi Ye, Ying Wu, Yu Liu, Yue Wang, "High-efficiency and high-quality white organic light-emitting diode employing fluorescent emitters," Organic Electronics 12(1) (2011) 29-33; doi: 10.1016/j.orgel.2010.10.006

140 Qi Wang, Junqiao Ding, Dongge Ma, Yanxiang Cheng, Lixiang Wang, Xiabin Jing, Fosong Wang, "Harvesting Excitons Via Two Parallel Channels for Efficient White Organic LEDs with Nearly 100% Internal Quantum Efficiency: Fabrication and Emission-Mechanism Analysis," Adv. Funct. Mater. 19(1) (2009) 84-95; doi: 10.1002/adfm.200800918

141 Young Jae Kim, Young Hoon Son and Jang Hyuk Kwon, "Highly efficient yellow phosphorescent organic light-emitting diodes for two-peak tandem white organic light-emitting diode applications," Journal of Information Display 14(3) (2013) 109-113; doi: 10.1080/15980316.2013.837106

142 Dongdong Zhang, Minghan Cai, Yunge Zhang, Deqiang Zhang, and Lian Duan, "Highly Efficient Simplified Single-Emitting-Layer Hybrid WOLEDs with Low Roll-Off and Good Color Stability through Enhanced Förster Energy Transfer," ACS Appl. Mater. Interfaces 7(51) (2015) 28693-28700; doi: 10.1021/acsami.5b10783

143 Zhongbin Wu, Jiajia Luo, Ning Sun, Liping Zhu, Hengda Sun, Ling Yu, Dezhi Lang, Xianfeng Qiao, Jiangshan Chen, Chuluo Yang, and Dongge Ma, "High-Performance Hybrid White Organic Light-Emitting Diodes with Superior Efficiency/Color Rendering Index/Color Stability and Low Efficiency Roll-Off Based on a Blue Thermally Activated Delayed Fluorescent Emitter," Advanced Functional Materials 26 (2016) 3306-3313; doi: 10.1002/adfm.201505602

144 Marrs, M. A., Moyer , C. D., Bawolek , E. J., Cordova , R. J., Trujillo , J., Raupp , G. B., & Vogt , B. D. (2011). Control of Threshold Voltage and Saturation Mobility Using Dual-Active-Layer Device Based on Amorphous Mixed Metal-Oxide-Semiconductor on Flexible Plastic Substrates. IEEE Transactions on Electron Devices, 58(10), 3428. doi:10.1109/TED.2011.2161764

145 Haq, J., Ageno , S., O'Rourke , S., Raupp , G. B., Vogt , B. D., & Loy , D. (2010). Temporary bond-debond process for manufacture of flexible electronics: Impact of adhesive and carrier properties on performance. J. Appl. Phys., 108(11), 114917.

146 Forrest, S. R., Bradley, D. D., & Thompson , M. E. (2003). Measuring the Efficiency of Organic Light-Emitting Diodes. Advanced Materials, 15(13), 1043. doi:10.1002.adma.200302151

147 Sun, Y., & Forrest , S. R. (2007). High-efficiency white organic light emitting devices with three separate phosphorescent emission layers. Appl. Phys. Lett., 91(28), 263503.

148 Park, Y. S., Kang , J. W., Kang , D. M., Park , J. w., Kim , Y. H., Kwon , S. K., & Kim , J. J. (2008). Efficient, Color Stable White Organic Light-Emitting Diode Based on High Energy Level Yellowish-Green Dopants. Adv. Mater., 20(10), 1957-1961.

149 http://www.chemicool.com/elements/iridium.html; accessed Sept 2016

150 Fleetham, T., Ecton , J., Wang , Z., Bakken , N., & Li , J. (2013). Single-Doped White Organic Light-Emitting Device with an External Quantum Efficiency Over 20%. Adv. Mater., 25(18), 2573-2576

151 Williams, E. L., Haavisto, K., Li, J., & Jabbour , G. E. (2007). Excimer-Based White Phosphorescent Organic Light-Emitting Diodes with Nearly 100% Internal Quantum Efficiency. Adv. Mater., 19(2), 197-202

152 Bei-Ping Yan, Cecil C. C. Cheung, Steven C. F. Kui, Hai-Feng Xiang, V. A. L. Roy, Shi-Jie Xu, and Chi-Ming Che, "Efficient White Organic Light-Emitting Devices Based on Phosphorescent Platinum(II)/Fluorescent Dual-Emitting Layers," Adv. Mater. 19 (2007) 3599-3603; doi:10.1002/adma.200602683

153 Fleetham, T., Wang , Z., & Li , J. (2012). Efficient deep blue electrophosphorescent devices based on platinum(II) bis(n-methyl-imidazolyl) benzene chloride. Org. Elect., 13(8), 1430-1435

154 Turner, E., Bakken , N., & Li , J. (2013). Cyclometalated Platinum Complexes with Luminescent Quantum Yields Approaching 100%. Inorg. Chem., 52(13), 7344-7351

155 Hang, X.-C., Fleetham , T., Turner , E., Brooks , J., & Li , J. (2013). Highly Efficient Blue-Emitting Cyclometalated Platinum(II) Complexes by Judicious Molecular Design. Angew. Chem. Int. Ed., 52, 6753-6756. doi:10.1002/anie.201302541

156 Fukagawa, H., Shimizu, T., Hanashima, H., Osada, Y., Suzuki, M., & Fujikake, H. (2012). Highly Efficient and Stable Red Phosphorescent Organic Light-Emitting Diodes Using Platinum Complexes. Advanced Materials, 24, 5099-5103. doi:10.1002/adma.201202167

157 J. A. Gareth Williams, Andrew Beeby, E. Stephen Davies, Julia A. Weinstein, Claire Wilson, "An Alternative Route to Highly Luminescent Platinum (II) Complexes:

Cyclometalation with N^C^N-Coordinating Dipyridylbenzene Ligands," Inorg Chem 42(26) (2003) 8609; doi: 10.1021/ic035083+

158 William B. Connick, David Geiger, and Richard Eisenberg, "Excited-State Self-Quenching Reactions of Square Planar Platinum(II) Diimine Complexes in Room-Temperature Fluid Solution," Inorg Chem 38(14) (1999) 3264-3265; doi: 10.1021/ic981387y

159 Millan M. Mdleleni, Jon S. Bridgewater, Richard J. Watts, Peter C. Ford, "Synthesis, Structure, and Spectroscopic Properties of Ortho-Metalated Platinum(II) Complexes," Inorg Chem 34(9) (1995) 2334-2342; doi: 10.1021/ic00113a013

160 Adamovich, V., Brooks, J., Tamayo, A., Alexander, A. M., Djurovich, P. I., & D'Andrade, B. W. (2002). High efficiency single dopant white electrophosphorescent light emitting diodes. New Journal of Chemistry, 26(9), 1171-1178. doi:10.1039/b204301g

161 M. Cocchi, J. Kalinowski, D. Virgili, V. Fattori, S. Devalay, J. A. G. Williams, "Single-dopant organic white electrophosphorescent diodes with very high efficiency and its reduced current density roll-off," Appl Phys Lett 90 (2007) 163508; doi: 1.1063/1.2722675

162 Brian W. D'Andrade and Stephen R. Forrest, "Effects of exciton and charge confinement on the performance of white organic p-i-n electrophosphorescent emissive excimer devices," J Appl Phys 94 (2003)3101; doi: 10.1063/1.1597942

163 Tyler Fleetham, Liang Huang, and Jian Li, "Tetradentate Platinum Complexes for Efficient and Stable Excimer-Based White OLEDs," Advanced Functional Materials 24 (2014) 6066-6073; doi: 10.1002/adfm.201401244

164 B. O'Brien, G. Li, T. Fleetham, and J. Li, "White Organic Light Emitting Diodes Using Pt-Based Red, Green and Blue Phosphorescent Layers," Proc. of SPIE, 8829, (2013) 882909-1; doi: 10.1117/12.2027143

165 Xiao, L., Su , S.-J., Agata , Y., Lan , H., & Kido , J. (2009). Nearly 100% internal quantum efficiency in an organic blue-light electro-phosphorescent device using a weak electron transporting material with a wide energy gap. Adv. Mater., 21(12), 1271-1274. doi:10.1002/adma.v21:12

166 Sasabe, H., Gonmori , E., Chiba , T., Li , Y.-J., Tanaka , D., Su , S.-J., . . . Kido , J. (2008). Wide-energy-gap electron-transport materials containing 3,5-dipyridyl-phenyl moieties for an ultra high efficiency blue organic light-emitting device. Chem. Mater., 20(19), 5951-5953. doi:10.1021/cm801727d

167 Guijie Li, Jeremy Ecton, Barry O'Brien, Jian Li, "Efficient and stable red organic light emitting devices from a tetradentate cyclometalate platinum complex," Organic Electronics 15 (2014) 1862-1867, doi: 10.1016/j.orgel.2014.04.020

168 Su, S.-J., Gonmori, E., Sasabe, H., & Kido, J. (2008). Highly Efficient Organic Blue- and White-Light-Emitting Devices Having a Carrier- and Exciton-Confining Structure for Reduced Efficiency Roll-Off. Advanced Materials. doi:10.1002/adma.200801375

169 J. Lee, N. Chopra, S. Eom, Y. Zheng, J. Xue, F. So, J. Shi, "Effects of triplet energies and properties of carrier transporting materials on blue phosphorescent organic light emitting devices," Appl. Phys. Lett. 93 (2008) 132206

170 T. Fleetham, Z. Wang, J. Li, "Efficient deep blue electrophosphorescent devices based on platinum(II) bis(n-methyl-imidazolyl)benzene chloride," Org. Electron. 13 (2012) 1430-1435

171 R. Kwong, M. Nugent, L. Michalski, T. Ngo, K. Rajan, "High operational stability of electrophosphorescent devices," Appl. Phys. Lett. 81 (2002) 162-164

172 I. Tanaka, Y. Tabata, S. Tokito, "Förster and Dexter energy-transfer processes in fluorescent BAlq films doped with phosphorescent Ir(ppy)3 molecules," J. Appl. Phys. 99 (2006) 073501

173 V. Adamovich, S. Cordero, P. Djurovich, A. Tamayo, M. Thompson, B. D'Andrade, S. Forrest, "New charge-carrier blocking materials for high efficiency OLEDs," Org. Electron. 4 (2003) 77-87

174 S. Ye, Y. Liu, C. Di, H. Xi, W. Wu, Y. Wen, K. Lu, C. Du, Y. Liu, G. Yu, "Wide-energy-gap host materials for blue phosphorescent organic light-emitting diodes," Chem. Mater. 21 (2009) 1333-1342,

175 C. Féry, B. Racine, D. Vaufrey, H. Doyeux, S. Cinà, "Physical mechanism responsible for the stretched exponential decay behavior of aging organic light-emitting diodes," Applied Physics Letters 87 (2005) 213502. Doi: 10.1063/1.2133922

176 Young Gu Lee, Ho-Nyeon Lee, Sung Kee Kang, Tae Sik Oh, Soonil Lee, Ken Ha Koh, "Fabrication of highly efficient and stable doped red organic light-emitting device using 2-methyl-9, 10-di(2-naphthyl)anthracene and tris (8-hydroxyquinolinato)aluminum as cohost materials," Appl. Phys. Lett. 89 (2006) 183515; doi: 10.1063/1.2374811

177 Neetu Chopra, James S. Swensen, Evgueni Polikarpov, Lelia Cosimbescu, Franky So, and Asanga B. Padmaperuma, "High efficiency and low roll-off blue

phosphorescent organic light-emitting devices using mixed host architecture," Appl. Phys. Lett 97 (2010) 033304; doi:10.1063/1.3464969

178 Sung Hyun Kim, Jyongsik Jang, Kyoung Soo Yook, Jun Yeob Lee, "Stable efficiency roll-off in phosphorescent organic light-emitting diodes," Appl. Phys. Lett. 92 (2008) 023513; doi: 10.1063/1.2836270

179 Jonghee Lee, Jeong-Ik Lee, Jun Yeob Lee, Hye Yong Chu, "Stable efficiency roll-off in blue phosphorescent organic light-emitting diodes by host layer engineering," Org Elect 10(8) (2009) 1529-1533; doi: 10.1016/j.orgel.2009.08.020

180 S. Pimputkar, J. S. Speck, S. P. DenBaars, and S. Nakamura, "Prospects for LED Lighting," Nature Photonics 3(4) (2009) 180-182; doi: 10.1038/nphoton.2009.32

181 A. Panahi, "Challenges and Opportunities in LED Based Lighting," Proc. SPIE 8720 (2013) 87200G; doi: 10.1117/12.2017987

182 Yersin, H., & Finkenzeller , W. J. (2008). Triplet Emitters for Organic Light-Emitting Diodes: Basic Properties. In H. Yersin (Ed.), Highly Efficient OLEDs with Phosphorescent Materials (pp. 1-97). WILEY-VCH Verlag.

183 J. A. Gareth Williams, S. Develay, D. L. Rochester, L. Murphy," Optimizing the luminescence of platinum(II) complexes and their application in organic light-emitting devices (OLEDs)," Coord Chem Rev 252(23-24) (2008) 2596-2611; doi: 10.1016/j.ccr.2008.03.014

184 O'Brien, B., Norby, G., Li, G., & Li , J. (2014). High efficiency white organic light emitting diodes employing blue and red platinum emitters. Journal of Photonics for Energy, 4, 043597. doi:10.1117/1.JPE.4.043597

185 Ho, C. L., Wong, W.-Y., Gao, Z.-Q., Chen, C.-H., Cheah, K.-W., Yao, B., . . . Lin, Z. (2008). Red-light-emitting iridium complexes with hole-transporting 9-arylcarbazole moieties for electrophosphorescence efficiency/color purity trade-off optimization. *Adv. Funct. Mater., 18*(2), 319-331. doi:10.1002/(ISSN)1616-3028

186 H. Sasabe and J. Kido, "Development of high performance OLEDs for general lighting," Journal of Materials Chemistry C.1 (2013) 1699; doi: 10.1039/c2tc00584k

187 H. Sasabe, J. Kido, "Recent Progress in Phosphorescent Light-Emitting Devices," Eur. J. Org. Chem. (2013) 7653-7663; doi: 10.1002/ejoc.201300544

188 Reineke, S., Lindner, F., Schwartz, G., Seidler, N., Walzer, K., Lüssem, B., & Leo, K. (2009). White organic light-emitting diodes with fluorescent tube efficiency. Nature, 459, 234. doi:10.1038/nature08003

189 Commission Internationale de l'Eclairage, Colour Rendering (TC 1-33 closing remarks), Vienna (Austria): CIE, Publication No. 135/2:1999

190 Commission Internationale de l'Eclairage, Method of Measuring and Specifying Color Rendering Properties of Light Sources, CIE, Vienna (Austria), 1995, p. 16. Publication No. 13.3:1995

191 Kido, J., Kimura, M., & Nagai, K. (1995). Multilayer White Light-Emitting Organic Electroluminescent Device. Science, 267, 1332.

192 Gather, M. C., Köhnen, A., Falcou, A., Becker, H., & Meerholz, K. (2007). Solution-Processed Full-Color Polymer Organic Light-Emitting Diode Displays Fabricated by Direct Photolithography. Advanced Functional Materials, 17, 191-200. doi:10.1002/adfm.200600651

193 Kido, J., Hongawa, K., Okuyama, K., & Nagai, K. (1994). White light-emitting organic electroluminescent devices using the poly(N-vinylcarbazole) emitter layer doped with three fluorescent dyes. Applied Physics Letters, 65, 815.

194 Adamovich, V., Brooks, J., Tamayo, A., Alexander, A. M., Djurovich, P. I., & D'Andrade, B. W. (2002). High efficiency single dopant white electrophosphorescent light emitting diodes. New Journal of Chemistry, 26, 1171-1178. doi:10.1039/b204301g

195 Chang, Y.-L., & Lu, Z.-H. (2013). White Organic Light-Emitting Diodes for Solid-State Lighting. Journal of Display Technology, 9, 459-468. doi:10.1109/JDT.2013.2248698

196 J. K. Bin, N. S. Cho, J. -I. Hong, "New Host Material for High-Performance Blue Phosphorescent Organic Electroluminescent Devices," Advanced Materials 24 (2012) 2911-2915; doi:10.1002/adma.201200972

197 D. Volz, M. Wallesch, C. Fléchon, M. Danz, A. Verma, J. M. Navarro, D. M. Zink, S. Bräse and T. Baumann, "From iridium and platinum to copper and carbon: new avenues for more sustainability in organic light-emitting diodes," Green Chem. 17 (2015) 1988-2011; doi: 10.1039/C4GC02195A

198 Kalinowski, J., Di Marco, P., Cocchi, M., Fattori, V., Camaioni, N., & Duff, J. (1996). Voltage-tunable-color multilayer organic light emitting diode. Applied Physics Letters, 68, 2317. doi:10.1063/1.115843

199 A. Poloek, C.-T. Chen, C.-T. Chen, High performance hybrid white and multi-colour electroluminescence from a new host material for a heteroleptic naphthyridinolate

platinum complex dopant, Journal of Materials Chemistry C. 2 (2014) 1376. doi:10.1039/c3tc32394c;

200 D. F. O'Brien, M. A. Baldo, M. E. Thompson, and S. R. Forrest, "Improved energy transfer in electrophosphorescent devices," Applied Physics Letters 74 (1999), 442; doi: 10.1063/1.123055

201 H. Cao, H. Sun, Y. Yin, X. Wen, G. Shan, Z. Su, et al., Iridium (iii) complexes adopting 1, 2-diphenyl-1 H-benzoimidazole ligands for highly efficient organic light-emitting diodes with low efficiency roll-off and non-doped feature, Journal of Materials Chemistry C. 2 (2014) 2150–2159

202 Andreas F. Rausch, Herbert H. H. Homeier, and Hatmut Yersin, "Organometallic Pt(II) and Ir(III) Triplet Emitters for OLED Applications and the Role of Spin-Orbit Coupling: A Study Based on High-Resolution Optical Spectroscopy," Top. Organomet. Chem. 29 (2010) 193; doi: 10.1007/3418_2009_6

203 Andreas F. Rausch, Mark E. Thompson, Hartmut Yersin, "Triplet state relaxation processes of the OLED emitter Pt(4,6-dFppy)(acac)," Chem. Phys. Lett 468(1-3) (2009) 46-51; doi: 10.1016/j.cplett.2008.11.075

204 Jason Brooks, Yelizaveta Babayan, Sergey Lamansky, Peter I. Djurovich, Irina Tsyba, Robert Bau, and Mark E. Thompson, "Synthesis and Characterization of Phosphorescent Cyclometalated Platinum Complexes," Inorg. Chem. 41(12) (2002) 3055-3066; doi: 10.1021/ic0255508

205 J. Kalinowski, V. Fattori, M. Cocchi, J. A. G. Williams, "Light-emitting devices based on organometallic platinum complexes as emitters," Coord. Chem. Rev. 255 (2011) 2401-2425

206 H. Fukagawa, T. Shimizu, H. Hanashima, Y. Osada, M. Suzuki, H. Fujikake, "Highly efficient and stable red phosphorescent organic light-emitting diodes using platinum complexes," Adv. Mater. 24 (2012) 5099-5103

207 K. Li, G. Cheng, C. Ma, X. Guan, W. -M. Kwok, Y. Chen, et al. "Light-emitting platinum(ii) complexes supported by tetradentate dianionic bis(N-heterocyclic carbine) ligands: towards robust blue electrophosphors," Chem. Sci. 4 (2013) 2630

208 Gregory Norby, Choong-Do Park, Barry O'Brien, Guijie Li, Liang Huang, Jian Li, "Efficient white OLEDs employing red, green, and blue tetradentate platinum phosphorescent emitters," Organic Electronics 37 (2016) 163-168; doi: 10.1016/j.orgel.2016.06.007

209 K. Kanakarajan, A.W. Czarnik, Synthesis and some reactions of hexaazatriphenylenehexanitrile, a hydrogen-free polyfunctional heterocycle with D3h symmetry, The Journal of Organic Chemistry. 51 (1986) 5241–5243

210 N. Chopra, J.S. Swensen, E. Polikarpov, L. Cosimbescu, F. So, A.B. Padmaperuma, High efficiency and low roll-off blue phosphorescent organic light-emitting devices using mixed host architecture, Applied Physics Letters. 97 (2010) 033304. doi:10.1063/1.3464969

211 Y. Ohno, Spectral design considerations for white LED color rendering, Optical Engineering. 44 (2005) 111302. doi:10.1117/1.2130694

212 H. Ries, I. Leike, J. Muschaweck, Optimized additive mixing of colored light-emitting diode sources, Optical Engineering. 43 (2004) 1531–1536.

213 R.G. Kepler, J.C. Caris, P. Avakian, E. Abramson, Triplet excitons and Delayed Fluorescence in anthracene crystals., Phys. Rev. Lett. 10 (1963) 400–402

214 http://spectrum.ieee.org/green-tech/conservation/led-streetlights-are-giving-neighborhoods-the-blues; accessed 11/2016

215 http://www.oled-info.com/lg-chem-plans-build-gen-5-oled-lighting-fab-2015-reduce-costs-95; accessed 11/2106

216 http://www.oled-info.com/gjm-developed-roll-roll-oled-deposition-system; http://www.oled-info.com/itri-building-flexible-oled-lighting-roll-roll-pilot-line; accessed 11/2016

217 http://www.automotive-eetimes.com/news/flexible-oled-starting-blocks-automotive-lighting; http://www.electronics-eetimes.com/news/bmws-fastest-production-road-car-premieres-oled-technology; http://www.electronics-eetimes.com/news/audi-demo-oled-exterior-lighting-iaa

218 Kim, S., & Young , B. (2012). Display Week 2012 Review: OLEDs. Information Display(July-August), 29.

219 Zardetto, V., Brown, T. M., Reale, A., & Di Carlo, A. (2011). Substrates for Flexible Electronics: A Practical Investigation of the Electrical, Film Flexibility, Optical, Temperature and Solvent Resistance Properties. Journal of Polymer Science Part B: Polymer Physics, 49, 638-648.

220 Shawn M. O'Rourke, Sameer M. Venugopal, Gregory B Raupp, David R. Allee, Scott Ageno, Edward J. Bawolek, Douglas E. Loy, Jann P Kaminski, Curt Moyer, Barry O'Brien, Ke Long, Michael Marrs, Dirk Bottesch, Jeff Dailey, Jovan Trujillo, Rita Cordova, Mark Richards, Daniel Toy & Nicholas Colaneri, "Active Matrix

Electrophoretic Displays on Temporary Bonded Stainless Steel Substrates with 180 °C a-Si:H TFTs," SID Digest (2008) 422-424

221 Kuo, Y. (Ed.). (2004). Thin Film Transistors: Materials and Processes (Vol. 1). Boston: Kluwer Academic Publishers.

222 Parsons, G. N. (2000). Surface reactions in very low temperature (<150C) hydrogenated amorphous silicon deposition, and applications to thin film transistors. Journal of Non-Crystalline Solids, 266-269, 23-30.

223 Sazonov, A., & Nathan, A. (2000). 120C fabrication technology for a-Si:H thin film transistors on flexible polyimide substrates. J. Vac. Sci. Technol. A, 18(2), 780-782.

224 Nomura, K., Ohta, H., Takagi, A., Kamiya, T., Hirano, M., & Hosono, H. (2004). Room Temperature Fabrication of Transparent Flexible Thin-Film Transistors using Amorphous Oxide Semiconductors. Nature, 488

225 Hosono, H. (2006). Ionic amorphous oxide semiconductors: Material design, carrier transport, and device application. Journal of Non-Crystalline Solids, 352, 851-858

226 Kaftanoglu, K., Venugopal, S. M., Marrs, M., Dey, A., Bawolek, E. J., Allee, D. R., & Loy, D. (2011). Stability of IZO and a-Si:H TFTs Processed at Low Temperature (200^{o}C). Journal of Display Technology, 7(6), 339. doi:10.1109/JDT.2011.2107879

227 http://www.oled-info.com/sharp-announced-worlds-highest-density-display-4k-55-806ppi-igzo-lcd-panel; http://www.oled-info.com/sharp-demonstrated-igzo-lcd-curved-corner-display; http://www.oled-info.com/japan-display-co-develop-next-gen-caac-igzo-backplane-tech-sel

228 http://www.sharp-world.com/igzo/; http://www.sharpusa.com/AboutSharp/NewsAndEvents/PressReleases/2016/March/SHARP-TO-PREVIEW-NEW-8K-DISPLAY-DURING-DIGITAL-SIGNAGE-EXPO-2016.aspx; http://www.oled-info.com/sharp-begins-produce-oxide-tft-igzo-based-lcds

229 Marrs, M. A., Moyer , C. D., Bawolek , E. J., Cordova , R. J., Trujillo , J., Raupp , G. B., & Vogt , B. D. (2011). Control of Threshold Voltage and Saturation Mobility Using Dual-Active-Layer Device Based on Amorphous Mixed Metal-Oxide-Semiconductor on Flexible Plastic Substrates. *IEEE Transactions on Electron Devices*, *58*(10), 3428. doi:10.1109/TED.2011.2161764

230 O'Brien, B., Lee, Y. K., Marrs, M., Smith, J., Strnad, M., Forsythe, E., & Morton, D. (2013). 14.7" Active Matrix PHOLED Displays on Temporary Bonded PEN Substrates with Low Temperature IGZO TFTs. SID 2013 Digest, (pp. 447-450)

231 Sarma, K. (2003). AMOLED using 150C a-Si TFT on Flex Plastic. Proc SPIE, 5080, 180.

232 Doug Loy, Yong Kyun Lee, Cynthia Bell, Mark Richards, Ed Bawolek, Scott Ageno, Curt Moyer, Michael Marrs, Sameer M. Venugopal, Jann Kaminski, Nick Colaneri, Shawn M. O'Rourke, Jeff Silvernail, Kamala Rajan, Ruiqing Ma, Michael Hack, and Julie Brown, Eric Forsythe, David Morton, "Active Matrix PHOLED Displays on Temporary Bonded Polyethylene Naphthalate Substrates with 180 °C a-Si:H TFTs," SID 09 Digest (2009) 988-991

233 Haq, J., Ageno , S., O'Rourke , S., Raupp , G. B., Vogt , B. D., & Loy , D. (2010). Temporary bond-debond process for manufacture of flexible electronics: Impact of adhesive and carrier properties on performance. J. Appl. Phys., 108(11), 114917

234 Kagan, C. R., & Andry, P. (Eds.). (2003). Thin-Film Transistors. Marcel Dekker

235 Xiaofan Ren, Jian Li, Russell J. Holmes, Peter I. Djurovich, Stephen R. Forrest, and Mark E. Thompson, "Ultrahigh Energy Gap Hosts in Deep Blue Organic Electrophosphorescent Devices," Chem. Mater. 16 (2004) 4743-4747; doi: 10.1021/cm049402m

236 Marina E. Kondakova, Thomas D. Pawlik, Ralph H. Young, David J. Giesen, Denis Y. Kondakov, Christopher T. Brown, Joseph C. Deaton, Jerome R. Lenhard, and Kevin P. Klubek, "High-efficiency, low-voltage phosphorescent organic light-emitting diode devices with mixed host," Journal of Applied Physics 104 (2008) 094501; doi: 10.1063/1.3000046

237 Sergey Lamansky, Peter Djurovich, Drew Murphy, Feras Abdel-Razzaq, Hae-Eun Lee, Chihaya Adachi, Paul E. Burrows, Stephen R. Forrest, and Mark E. Thompson, Highly Phosphorescent Bis-Cyclometalated Iridium Complexes: Synthesis, Photophysical Characterization, and Use in Organic Light-Emitting Diodes," J. Am. Chem. Soc. 123(18) (2001) 4304-4312; doi: 10.1021/ja003693s

238 R. J. Holmes, S. R. Forrest, Y.-J. Tung, R. C. Kwong, J. J. Brown, S. Garon, M. E. Thompson, "Blue organic electrophosphorescence using exothermic host-guest energy transfer," Appl. Phys. Lett. 82 (2003) 2422; doi: 10.1063/1/1568146

239 Young Hoon Son, Shin Hye Kim and Jang Hyuk Kwon, "All-phosphorescent three-color two-stack tandem white organic light emitting diodes with high-color-rendering index values," Journal of Information Display 15(4) (2014) 185-189, doi:10.1080/15980316.2014.963715

240 Hany Aziz and Zoran D. Popovic, “Degradation Phenomena in Small-Molecule Organic Light-Emitting Devices,” Chem Mater 16(23) (2004) 4522-4532; doi: 10.1021/cm040081o

241 Franky So and Denis Kondakov, “Degradation Mechanisms in Small-Molecule and Polymer Organic Light-Emitting Diodes,” Adv Matls 22 (2010) 3762; doi: 10.1002/adma.200902624

242 N. C. Giebink, B. W. D’Andrade, M. S. Weaver, P. B. Mackenzie, J. J. Brown, M. E. Thompson and S. R. Forrest, “Intrinsic luminance loss in phosphorescent small-molecule organic light emitting devices due to bimolecular annihilation reactions,” Journal of Applied Physics 103 (2008) 044509

243 Gregor Schwartz, Sebastian Reineke, Thomas Conrad Rosenow, Karsten Walzer and Karl Leo, “Triplet Harvesting in Hybrid White Organic Light-Emitting Diodes,” Advanced Functional Materials 19 (2009) 1319-1333, doi: 10.1002/adfm.200801503

244 Meerheim, R., Scholz, S., Olthof, S., Schwartz, G., Reineke, S., & Walzer, K. (2008). Influence of charge balance and exciton distribution on efficiency and lifetime of phosphorescent organic light-emitting devices. Journal of Applied Physics, 104, 014510. doi:10.1063/1.2951960

245 Sebastian Scholz, Cathrin Corten, Karsten Walzer, Dirk Kuckling, Karl Leo, “Photochemical reactions in organic semiconductor thin films,” Org Elect 8(6) (2007) 709-717; doi: 10.1016/j.orgel.2007.06.002

246 Red and green phosphorescent emitters, host, hole blocker, electron transport and electron injection materials were obtained from Universal Display Corporation and other recommended suppliers. Fluorescent blue emitter and host materials were obtained from Sun Fine Chemicals.

247 Shi-Jian Su, Hisahiro Sasabe, Takashi Takeda and Junji Kido, “Pyridine-Containing Bipolar Host Materials for Highly Efficient Blue Phosphorescent OLEDs,” Chem Mater 20(5) (2008) 1691-1693; doi: 10.1021/cm703682q

248 https://en.wikipedia.org/wiki/NTSC#Colorimetry, accessed 5/21/2016

249 http://www.oled-info.com/ubi-oled-lcd-market-smartphone-2020

250 http://www.oled-info.com/ubi-sees-flexible-amoled-market-growing-over-40-billion-2020

251 http://www.oled-info.com/displaysearch-flexible-oled-market-could-reach-20-billion-2020

252 LG Display, “LG Display OLED Lighting Catalog,” 2016. [online]. http://www.lgoledlight.com/resources/LG_Display_OLED_light_Catalogue.pdf.

APPENDIX A

CO-AUTHOR PERMISSIONS

All co-authors of the following publications have granted their permissions to incorporate these results into this dissertation.

1. B. O'Brien, G. Li, T. Fleetham, and J. Li, "White Organic Light Emitting Diodes Using Pt-Based Red, Green and Blue Phosphorescent Layers," Proc. of SPIE, 8829, (2013) 882909-1; doi: 10.1117/12.2027143

2. O'Brien, B., Norby, G., Li, G., & Li , J. (2014). High efficiency white organic light emitting diodes employing blue and red platinum emitters. *Journal of Photonics for Energy, 4*, 043597. doi:10.1117/1.JPE.4.043597

3. Gregory Norby, Choong-Do Park, Barry O'Brien, Guijie Li, Liang Huang, Jian Li, "Efficient white OLEDs employing red, green, and blue tetradentate platinum phosphorescent emitters," Organic Electronics 37 (2016) 163-168; doi: 10.1016/j.orgel.2016.06.007

4. O'Brien, B., Lee, Y. K., Marrs, M., Smith, J., Strnad, M., Forsythe, E., & Morton, D. (2013). 14.7" Active Matrix PHOLED Displays on Temporary Bonded PEN Substrates with Low Temperature IGZO TFTs. *SID 2013 Digest*, (pp. 447-450)

APPENDIX B

FULL CHEMICAL NAMES FOR MATERIAL ABBREVIATIONS

Material	IUPAC Chemical Name
26mCPy	2,6-bis(*N*-carbazolyl)pyridine
Ag	Silver
Al	Aluminum
Alq3	tris(8-quinolinolato)aluminum(III)
BAlq	4-biphenyloxolatoaluminum(III)bis(2-methyl-8-quinolinato)4-phenylphenolate
BCP	2,9-dimethyl-4,7-diphenyl-1,10-phenanthroline
BCP	2,9-dimethyl-4,7-diphenyl-1,10-phenanthroline
BmPyPB	1,3-bis(3,5-dipyrid-3-yl-phenyl)benzene
BPhen	4,7-diphenyl-1,10-phenanthroline
CBP	N,N'-dicarbazolyl-4–4'-biphenyl
DPPS	diphenyl-bis[4-(pyridin-3-yl)phenyl]silane
FIrpic	iridium(III) bis(4,6-(difluorophenyl)pyridinato-N,C20)picolinate
HAT-CN	hexaazatriphenylene hexacarbonitrile
Ir(btp)2(acac)	bis[2-(2'-benzothienyl)pyridinato-N,C3'(acetylacetonato)iridium(III)
Ir(ppy)2(acac)	bis(2-phenylpyridine)(acetylacetonate)iridium(III)
Ir(ppy)3	fac-tris(2-phenylpyridinato)iridium(III) (Ir(ppy)3)
ITO	Indium-Tin Oxide
LiF	lithium fluoride
Liq	8-hydroxyquinolinolato-lithium
mCBP	3,3-di(9H-carbazol-9-yl)biphenyl
mCP	1,3-bis(N-carbazolyl)benzene
MgAg	magnesium-silver alloy
NPB	4-4'-bis[N-(1-naphthyl)-N-phenyl-amino]biphenyl
PEDOT:PSS	Poly(3,4-ethylene-dioxythiophene):poly(styrene sulfonic acid)
PQIr	iridium(III) bis(2-phenyl quinolyl-N,$C^{2'}$)acetylacentonate
TAPC	1,1-bis[(di-4-tolylamino)phenyl]cyclohexane
TCTA	tris(4-carbazolyl-9-ylphenyl)amine

APPENDIX C

PUBLICATIONS

1. Barry O'Brien, Guijie Li, Tyler Fleetham, and Jian Li, "White Organic Light Emitting Diodes Using Pt-Based Red, Green and Blue Phosphorescent Layers," Proc. of SPIE, 8829, (2013) 882909-1; doi: 10.1117/12.2027143

2. Barry O'Brien, Greg Norby, Guijie Li, & Jian Li, "High efficiency white organic light emitting diodes employing blue and red platinum emitters. Journal of Photonics for Energy 4 (2014) 043597. doi:10.1117/1.JPE.4.043597

3. Gregory Norby, Choong-Do Park, Barry O'Brien, Guijie Li, Liang Huang, Jian Li, "Efficient white OLEDs employing red, green, and blue tetradentate platinum phosphorescent emitters," Organic Electronics 37 (2016) 163-168; doi: 10.1016/j.orgel.2016.06.007

4. Barry O'Brien, Yong Kyun Lee, Michael Marrs, Joseph Smith, Mark Strnad, Eric Forsythe, and David Morton, "14.7" Active Matrix PHOLED Displays on Temporary Bonded PEN Substrates with Low Temperature IGZO TFTs," SID 2013 Digest, pp. 447

5. Michael A. Marrs, Edward J. Bawolek, Barry P. O'Brien, Joseph T. Smith, Mark Strnad, David C. Morton, "Flexible Amorphous Silicon PIN Diode Sensor Array Process Compatible with Indium Gallium Zinc Oxide Transistors," SID 2013 Digest, pp 455

6. Tyler Fleetham, Barry O'Brien, John P. Mudrick, Jiangeng Xue, Jian Li, "Efficiency enhancement in small molecular organic photovoltaic devices employing dual anode interfacial layers," Proc SPIE 8830 (2013) 883009-1; doi: 10.1117.12.2023679

7. Joseph T. Smith, Barry O'Brien, Yong-Kyun Lee, Edward J. Bawolek, and Jennifer Blain Christen, "Application of Flexible OLED Display Technology for Electro-Optical Stimulation and/or Silencing of Neural Activity," IEEE Journal of Display Technology 10(6) (2014) 514; doi: 10.1109/JDT.2014.2308436

8. Vivek Sharma, Adam Bailey, Bill Dauksher, Clarence Tracy, Stuart Bowden and Barry O'Brien, "Characterization and comparison of silicon nitride films deposited using two novel processes," J Vac Sci Tech A 30(2) (2012) 021201-1; doi: 10.1116/1.3687423

9. Bryan D. Vogt, Barry O'Brien, David R. Allee, Doug Loy, Bulent Akgun, Sushil K. Satija, "Distribution of hydrogen in low temperature passivated amorphous silicon (a-Si:H) films from neutron reflectivity," J Non-Crystalline Solids 357 (2011) 1114; doi: 10.1016/j.noncrysol.2010.11.030

10. U. S. Patent disclosure, “Manufacturing flat panel digital x-ray detectors using low cost commercial flexible organic light emitting diode (OLED) display technology,” Joseph T. Smith, YK Lee, Barry O’Brien, submitted April 10, 2016

11. U. S. Patent 6,424,083 B1, “Field Emission Device Having an Improved Ballast Resistor,” Gordon Tam, Ganming Qin, Barry P. O’Brien